UNIVERSITÀ DELLA CALABRIA
Dottorato di Ricerca in
Ingegneria dei Sistemi e Informatica

XIX ciclo

Tesi di Dottorato

Unified approach for measurement on digital modulated signals

Domenico Luca Carnì

Coordinatore
Prof. Domenico Talia

Supervisore
Prof. Domenico Grimaldi

DIPARTIMENTO DI ELETTRONICA, INFORMATICA E SISTEMISTICA
Settore Scientifico Disciplinare: ING-INF/07

To my parents

Acknowledgements

First of all, I would like to express my sincere gratitude to Prof. Domenico Grimaldi, my PhD thesis tutor. His wise guide, supervision and his suggestions was fundamentals for the good accomplishment of my PhD thesis.

I would like to thank to all the L.E.I.M. group: Ing. Guglielmelli, Ing. Lamonaca, Ing. Aiello and Ing. Serratore, we have spent several time in laboratory.

Many thanks to the professors of measurement group of the university of Sannio prof. Pasquale Daponte and Sergio Rapuano, for their suggestions, and Ing. Eulalia Balestrieri for her precious contributions and help.

I would like to acknowledge all my friends and especially : Antonio, Rocco, Monia, Adele that support me in these years.

I want to especially thank Ing. Laura Tomaciello for her help, support, encourage and patience during the writing of this thesis.

This thesis is dedicated to my parents, they always encouraged and believed in me.

Introduction

As a consequence of the large diffusion of the telecommunication systems, great interest is devoted to develop an intelligent instrument able to characterize the signal quality whichever digital modulation is used.

Such instrument has important role in electronic surveillance systems, in military communications, in emitters intercepting, in signal quality assessment, and in interference identification.

In that direction, the first step to be performed is the set-up of an automatic modulation classifier that identifies the modulation type of the received signal, without the preventive knowledge of some parameters.

The information furnisched by the modulation classifier concern both the modulation schemes and the level number among:

- the amplitude modulated signals:
  - M-ary Quadrature Amplitude Modulation (M-QAM),
  - M-ary Amplitude Shift Keying (M-ASK),
- the angle modulated signals:
  - M-ary Phase Shift Keying (M-PSK),
  - M-ary Frequency Shift Keying (M-FSK).

After the identification of the modulation type, the successive step is to estimate all the parameters characterizing the modulation. Indeed, these parameters are used for signal demodulation, signal decoding and signal quality assessment.

The methods presented in literature for measurement all parameters of the digital modulated signal are not able to work by using only the information arising from the classifier. Moreover, each of these methods are able to work on one modulation scheme at time, only.

In this scenario the measurement method able to operate with only the information furnished by the modulation classifier on all the modulation schemes is of fundamental importance.

Therefore, the idea of the unified approach for measurement on modulated signals with reduced starting information is both very attractive and promising way to address the research.

On the basis of this consideration, the research activities given in this thesis are devoted to pointed out a method based on unified approach able to operate on the modulation schemes:

- M-QAM,
- M-ASK,
- M-PSK,
- M-FSK.

By looking at the implementation of this measurement method on measurement instrument, the following aspect are taken into account, also:

1. the needs to operate on signal affected by noise and distortion beyond the limits of International Recommendations,
2. the design characteristic of the hardware structure.

The investigation about the first aspect addresses the interest towards the new demodulator based on Artificial Neural Network in order to overcome the working limits of that conventional.

The analysis of the trend of the practical realization of the hardware for application in the field of telecommunication systems directs the interest towards the architecture of the Software Radio (SR).

As a consequence, the content of the thesis is organised in three parts.

The first part, after the overview on the measurement on digital modulation signal, is devoted to illustrate the unified approach for measurement on digital modulated signals. The limits of the methods reported in literature are made in evidence and the method based on the unified approach is described in dept.

The unified approach permits to design specific methods to be integrated in the modular structure of the automatic classifier presented in [1] in order to performe the measurement of:

- the carrier frequency,
- the carrier phase offset,
- the phase noise,
- the amplitude noise,
- the symbol timing,

for a number of single carrier digital modulations.

In particular, the carrier frequency parameter evaluation uses the mean value of the instantaneous frequencies as an incorrect evaluation of the carrier frequency. In order to determine the error of the estimation two different procedures are pointed out. The former is used in the case of the M-FSK modulation, the latter in the case of M-ASK, M-PSK and M-QAM modulations,

according to their different characteristic properties. For M-FSK modulation, in the histogram the M central frequencies are selected. For M-ASK, M-PSK and M-QAM the corrective factor is evaluated by the trend of the straight line obtained with an elaboration of the base-band signal. The result of numerical and experimental tests confirm the robustness of the method.

For the phase offset parameter estimation the grid G is created on the basis of the theoretical constellation to be examined. The grid is rotated and the number of the points included into the grid is evaluated. The rotation angle, corresponding to the maximum number of the points in the grid proximity, is the phase offset.

The amplitude and phase noise parameter estimation method, is based on the creation of the Virtual Symbol (VS) from the knowledge of the theoretical modulation scheme of the input signal. The amplitude and the phase noise are estimated with the excursion of the module and the phase of the VS respect to the theoretical point, respectively.

The last parameter estimated is the symbol time. To perform this measure the input signal is demodulated using a very short symbol timing that is the measurement unit. After this operation, the consecutive repetition length is determined and the histogram of this length is computed. The maximum value of the occurrences permits to select the length of the symbol time respect to the measurement unit taken into account.

The second part of the thesis is devoted to the design and test of an innovative demodulator for digital modulated signal. In fact, for the parameters measurement on telecommunication signal, the demodulation process is important step. If the input signal is affected by high level of noise and distortion, it's possible that the traditional demodulators don't recognize the real information transmitted. This error decreases the accuracy of the measure.

To overcome this problem is introduced the use of the Artificial Neural Networks (ANN) . They can be used to efficiently process the input signals affected by high level of both noise and distortion that characterize the telecommunication networks. In particular, the analysis and the developing of a demodulator for UMTS signal based on ANNs is the topic of the sixth chapter.

In the third part of the thesis the analysis of the hardware structure able to implement the proposed method is given. Particular interest is devoted to the SR hardware architecture. The benefits of this approach consist in using single general-purpose platform to perform different functions by simply running different programs. This permits to obtain an architecture with both flexibility and adaptability characteristics that can efficiently implement the method pointed out for the characterization of digital modulated signals.

In the SR architecture the acquisition component plays a fundamental role. Different structure can be used, with different performances. In the thesis is shown as the $\Sigma\Delta$ converter is the Analogue to Digital Converter that permit to have a light hardware structure with the best performances of the method.

Contents

List of Tables

List of Figures

1

Different characteristics of the digital modulated signals for telecommunication

Communication systems are designed to transmit information [2] and they may be described by the block diagram shown in Fig. 1.1. Three main subsystems can be highlighted: the transmitter, the channel and the receiver. A digital information source produce a finite set of possible messages, there are a finite number of characters that can be emitted by this source. The message could be an audio, a video signal, or an image signal acquired. Into a digital communication system the message produced by the source is converted into a binary value. The bits number in the binary representation is chosen to reduce the redundancies, and the process that convert the message into the binary sequence is the source coder.

The channel coder introduce redundancies in the binary sequence. In fact, it is possible that noise and impulsive interferences can modify the transmitted signal, and errors are present in the received signal. The redundancies permit at the receiver to detect and to correct the error in the signal acquired.

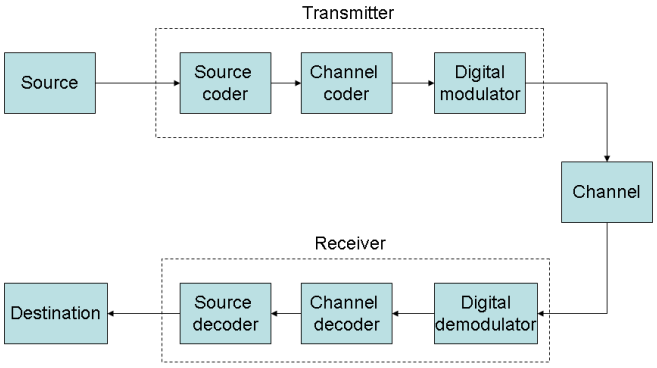

Fig. 1.1. Transmission and reception system

The sequence binary characters is transmitted by the channel, that can be a wireless channel or a wired channel. So it is necessary to convert this sequence into a waveform that the channel is capable to transmit. The device that implement this operation is the digital modulator. A simple digital modulator links to a 0 binary value a waveform $s_1(t)$, and to a 1 binary value the waveform $s_2(t)$, so every bit of the sequence can be transmitted.

For the receiver, the digital demodulator processes the received waveform, with the deteriorations of the channel, and estimate the coded symbol in every waveform. For example, if a binary modulation is used, the demodulator have to process the waveform received and choose if the bit transmitted is 0 or 1.

The channel decoder, process the demodulated sequence, and determine if the received code is correct. This block try to detect and to correct the errors in the demodulation operator.

The source decoder delete the redundancy introduced by the source coder.

1.1 Digital modulations

The move to digital modulation provides more information capacity, compatibility with digital data services, higher data security, better quality communication, and quicker system availability. Developers of communications systems face these constraints:

- available bandwidth
- permissible power
- inherent system noise level

Over the past few years a major transition has occurred from simple analog Amplitude Modulation (AM) and Frequency/Phase Modulation (FM/PM) to new digital modulation techniques. Examples of digital modulation include:

- Phase Shift Keying (PSK);
- Amplitude Shift Keying (ASK);
- Frequency Shift Keying (FSK);
- Minimum Shift Keying (MSK);
- Quadrature Amplitude Modulation (QAM);

Fundamental layer is constituted by the multiplexing. Two principal types of multiplexing (or "multiple access") are Time Division Multiple Access (TDMA) and Code Division Multiple Access (CDMA). These are two different ways to separate a signal from one another.

An ideal channel permits to the receiver to obtain the same signal transmitted [3]. The transmission channel can be modelled with a system that introduce, on the signal, three kinds of distortion: attenuation, delay, noise.

The attenuation is a energy loss into the signal propagation from the source to the destination. The value of energy loss is a function of the frequency.

The delay distortion in a waveform consisting of two or more wave components at different frequencies, distortion caused by the difference in arrival times of the frequency components at the output of a transmission system. When a bit component arrives in different time is increased the probability of a bit wrong detection.

The noise is energy not provided by the transmitter, that is superimposed to the signal transmitted.

1.1.1 Polar display

A simple way to view amplitude and phase of a signal is with the polar diagram. The carrier becomes a frequency and phase reference and the signal is interpreted relative to the carrier. The signal can be expressed in polar form as a magnitude and a phase, like is shown in Fig.1.2. The phase is relative to a reference signal. The magnitude is either an absolute or relative value. Both are used in digital communication systems. Polar diagrams are the basis of many displays used in digital communications, although it is common to describe the signal vector by its rectangular coordinates of In-phase (I) and Quadrature (Q).

Fig.1.3 shows different forms of modulation in polar form. Magnitude is represented as the distance from the center and phase is represented as the angle.

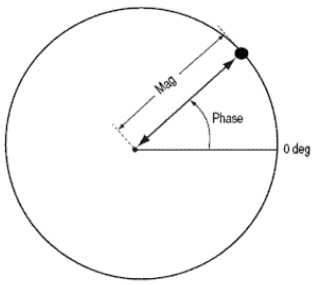

Fig. 1.2. Polar Display - Magnitude and Phase represented together

1.1.2 I/Q format

In digital communications, modulation is often expressed in terms of I and Q. This is a rectangular representation of the polar diagram. On a polar diagram, the I axis lies on the zero degree phase reference, and the Q axis is rotated by 90 degrees. The signal vector's projection onto the I axis is its "I" component and the projection onto the Q axis is its "Q" component, like is shown in Fig.1.4.

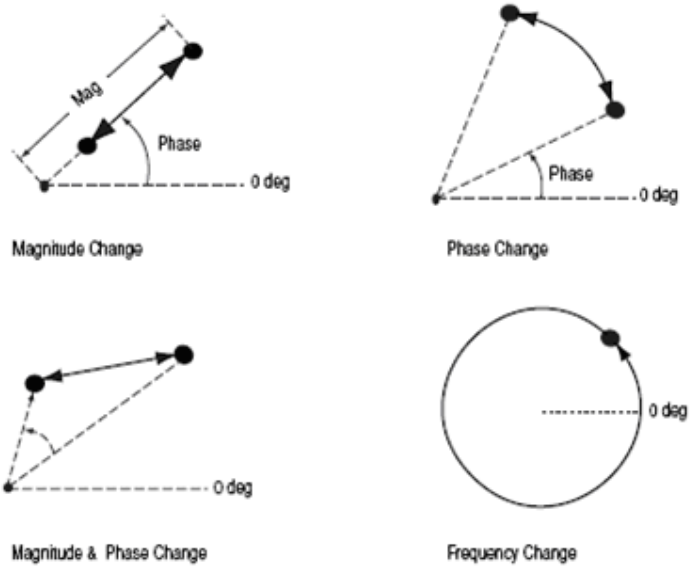

Fig. 1.3. Polar Display - Signal changes or modifications

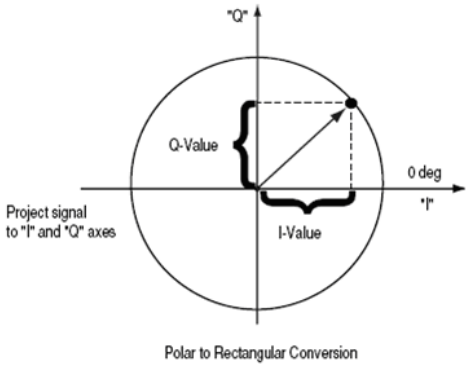

Fig. 1.4. IQ format

Digital modulation is easy to accomplish with I/Q modulators. Most digital modulation maps the data to a number of discrete points on the I/Q plane. These are known as constellation points. As the signal moves from one point to another, simultaneous amplitude and phase modulation usually results. To accomplish this with an amplitude modulator and a phase modulator is difficult and complex. It is also impossible with a conventional phase modulator. The signal may, in principle, circle the origin in one direction forever, necessitating infinite phase shifting capability. Alternatively, simultaneous Amplitude and

Phase Modulation is easy with an I/Q modulator. The I and Q control signals are bounded, but infinite phase wrap is possible by properly phasing the I and Q signals.

1.1.3 Amplitude Shift Keying

In the Amplitude Shift Keying (ASK) the modulator codes the information into a finite amplitude set. The signal waveform can be represented as:

$$S_m(t) = Re\left[A_m u(t) e^{j2\pi f_c t}\right] \qquad m = 1, 2, ..., M \;\; and \;\; t \in [0, Tb], \tag{1.1}$$

Where A_m, m=1,2,...,M are the M possible amplitude of the symbols, T_b are the symbol time and u(t) is an impulsive waveform. An example of ASK modulated signal is shown in Fig.1.5

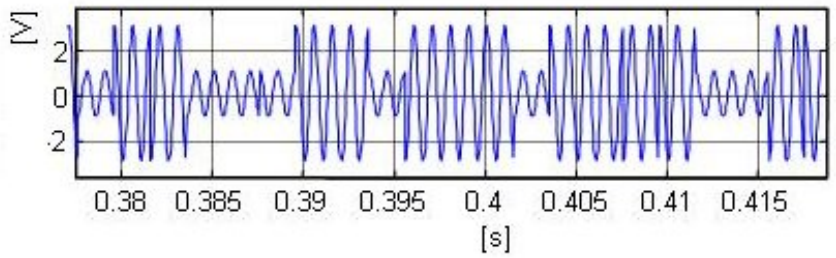

Fig. 1.5. 2-ASK modulation

1.1.4 Phase Shift Keying

One of the simplest forms of digital modulation is binary or Binary-Phase Shift Keying (BPSK). On an I and Q diagram, the I state has two different values. There are two possible locations in the state diagram, so a binary one or zero can be sent. A M-PSK signal is generated assigning to a set of M possible symbols one of the possible phase value $\theta_m = 2\pi(m-1)/M$, m=1,2,...,M. so the waveform produced are expressed as:

$$S_m(t) = Re\left[A_m u(t) e^{j\theta_m} e^{j2\pi f_c t}\right] = u(t) cos\left[2\pi f_c + \frac{2\pi}{M}(m-1)\right]$$

$$m = 1, 2, ..., M \, and \, t \in [0, Tb], \tag{1.2}$$

An example of the constellation obtained for a 4 PSK signal is shown in Fig.1.6 and in Fig.1.7 is shown a 2-PSK modulated signal.

A more common type of phase modulation is Quadrature Phase Shift Keying (QPSK). It is used extensively in applications including Code Division Multiple Access (CDMA) cellular service, wireless local loop, Iridium (a voice/data satellite system) and Digital Video Broadcasting - Satellite (DVB-S).

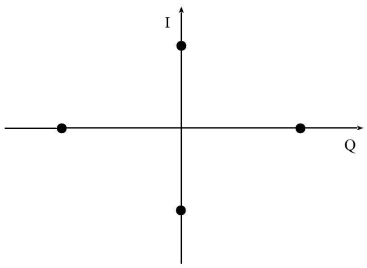

Fig. 1.6. 4-Phase Shift Keying constellation

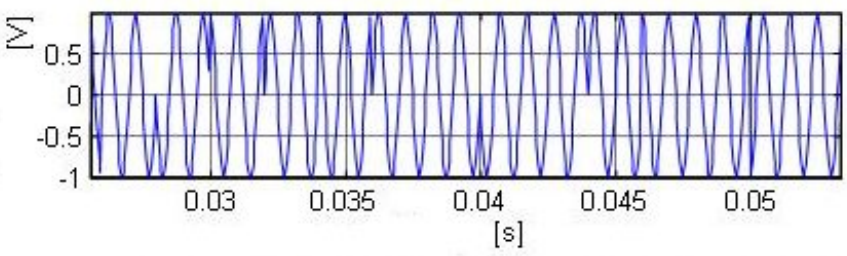

Fig. 1.7. 2-PSK modulation

Quadrature means that the signal shifts between phase states which are separated by 90 degrees. The signal shifts in increments of 90 degrees from 45 to 135, -45, or -135 degrees. These points are chosen as they can be easily implemented by using an I/Q modulator. Only two I values and two Q values are needed and this gives two bits per symbol.

1.1.5 Frequency Shift Keying

Frequency and phase modulation are closely related. A static frequency shift of +1 Hz means that the phase is constantly advancing at the rate of 360 degrees per second (2 π rad/s), relative to the phase of the unshifted signal.

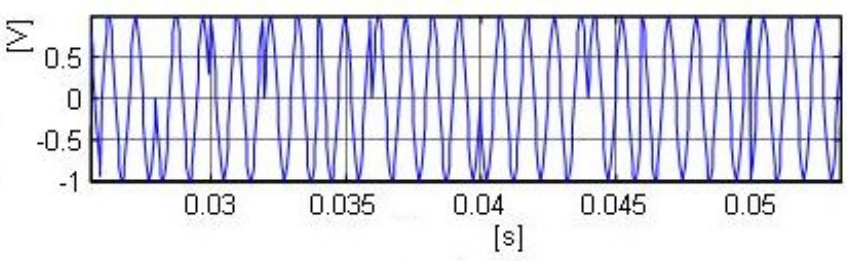

Fig. 1.8. 2-FSK modulation

Frequency Shift Keying (FSK) is used in many applications including cordless and paging systems. Some of the cordless systems include Digital Enhanced Cordless Telephone (DECT) and Cordless Telephone 2 (CT2).

In FSK, the carrier frequency is changed as a function of the modulating signal (data) being transmitted as is shown in Fig.1.8. Amplitude remains unchanged. In binary FSK (BFSK or 2-FSK), a "1" is represented by one frequency and a "0" is represented by another frequency. A M-FSK signal can be expressed as:

$$S_m(t) = Re\left[A_m u(t) e^{j\Delta f_m t} e^{j2\pi f_c t}\right] = u(t) cos\left[2\pi\left(f_c + \frac{2m - M - 1}{2}\right)t\right]$$

$$m = 1, 2, ..., M \, and \, t \in [0, Tb], \tag{1.3}$$

Where Δf if the frequency interval between the symbols. If $\Delta f = 1/\mathrm{Tb}$ the FSK modulation is orthogonal [4].

1.1.6 Minimum Shift Keying

Since a frequency shift produces an advancing or retarding phase, frequency shifts can be detected by sampling phase at each symbol period. Phase shifts of $(2N + 1)\pi/2$ radians are easily detected with an I/Q demodulator. At even numbered symbols, the polarity of the I channel conveys the transmitted data, while at odd numbered symbols the polarity of the Q channel conveys the data.

This orthogonally between I and Q simplifies detection algorithms and hence reduces power consumption in a mobile receiver. The minimum frequency shift which yields orthogonality of I and Q is that which results in a phase shift of $\pi/2$ radians per symbol (90 degrees per symbol). FSK with this deviation is called MSK (Minimum Shift Keying). The deviation must be accurate in order to generate repeatable 90 degree phase shifts. MSK is used in the GSM (Global System for Mobile Communications) cellular standard.

A phase shift of +90 degrees represents a data bit equal to "1", while -90 degrees represents a "0". The peak-to peak frequency shift of an MSK signal is equal to one-half of the bit rate.

FSK and MSK produce constant envelope carrier signals, which have no amplitude variations. This is desirable characteristic for improving of the power transmitters efficiency. Amplitude variations can exercise nonlinearities in an amplifier's amplitude-transfer function, generating spectral regrowth, and components in adjacent channel power.

MSK has a narrower spectrum than wider deviation forms of FSK. The width of the spectrum is also influenced by the waveforms causing the frequency shift. If those waveforms have fast transitions or high slew rate, then the spectrum of the transmitter will be broad. In practice, the waveforms are filtered with a Gaussian filter, resulting in a narrow spectrum. In addition, the Gaussian filter has no time-domain overshoot, which would broaden the spectrum by increasing the peak deviation. MSK with a Gaussian filter is termed GMSK (Gaussian MSK) shown in Fig.1.9 and in Fig.1.10.

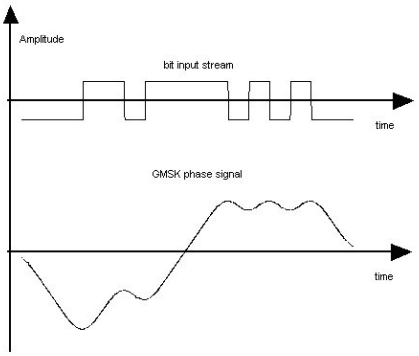

Fig. 1.9. GMSK phase signal and corresponding bit input strem.

1.1.7 Quadrature Amplitude Modulation

The Quadrature Amplitude Modulation (QAM) is used in applications including microwave digital radio, DVB-C (Digital Video Broadcasting-Cable), and modems.

It is more efficient than BPSK, QPSK, or 8-PSK. The current practical limits are approximately 256-QAM, though work is underway to extend the limits to 512 or 1024 QAM. A 256-QAM system uses 16 I-values and 16 Q-values, giving 256 possible states. However, the symbols are very close together and are thus more subject to errors due to noise and distortion. Such a signal may have to be transmitted with extra power (to effectively spread the

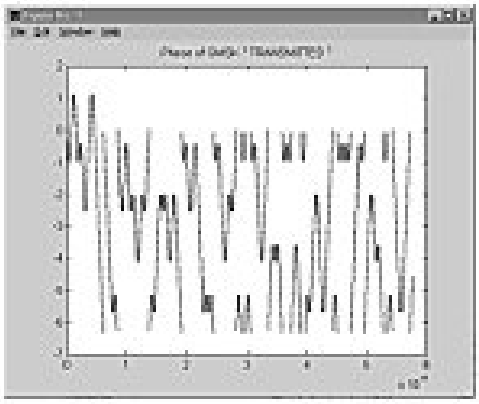

Fig. 1.10. GMSK modulated signal.

symbols out more) and this reduces power efficiency as compared to simpler schemes. The M-QAM waveform can be expressed as:

$$S_m(t) = Re\left[(A_{mc} + jA_{ms})\, u(t) e^{j2\pi f_c t}\right] =$$

$$A_{mc} u(t) cos\,(2\pi f_c t) - A_{ms} u(t) sin\,(2\pi f_c t) \tag{1.4}$$

$$S_m(t) = Re\left[V_m e^{j\theta_m} u(t) e^{j2\pi f_c t}\right] = V_m u(t) cos\,(2\pi f_c t + \theta_m) \tag{1.5}$$

$$V_m = \sqrt{A_{mc}^2 + A_{ms}^2} \qquad \theta_m = tan^{-1}\,(A_{ms}/A_{mc}) \qquad t \in [0, Tb] \tag{1.6}$$

Where A_{mc} is the amplitude of the signal for the information coded into the cosine waveform, and A_{ms} is the amplitude of the signal for the information coded into the sine waveform. An example of 32-QAM constellation is shown in Fig.1.11and in Fig.1.12 is shown a QAM modulated signal.

The 256-QAM system enables the same amount of information to be sent as BPSK using only one eighth of the bandwidth. It is eight times more bandwidth efficient. However, there is a trade-off. The radio becomes more complex and it is more susceptible to errors caused by noise and distortion.

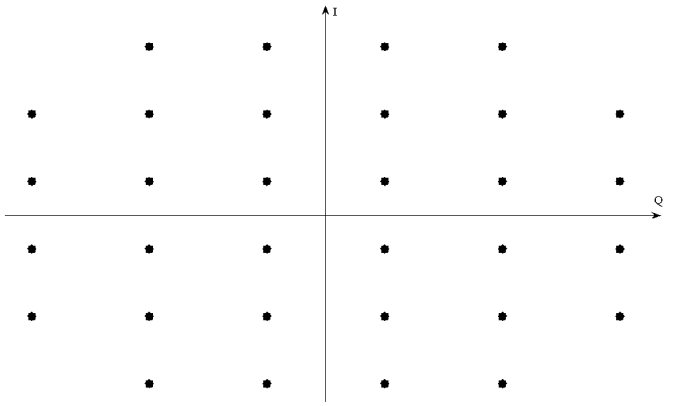

Fig. 1.11. Constellation of 32-Quadrature Amplitude Modulation

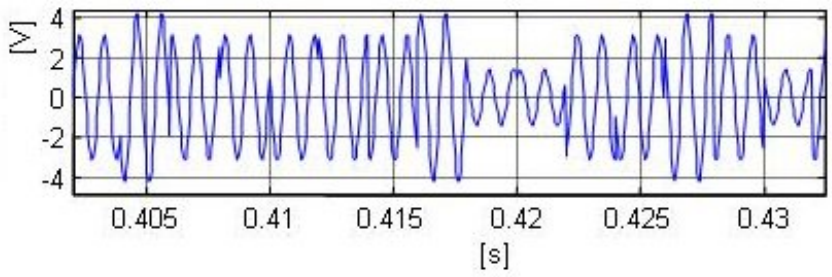

Fig. 1.12. 16-QAM modulated signal

1.1.8 Theoretical bandwidth efficiency limits

Bandwidth efficiency describes how efficiently the allocated bandwidth is utilized or the ability of a modulation scheme to accommodate data, within a limited bandwidth. The Tab.1.1 shows the theoretical bandwidth efficiency limits for the main modulation types. In practical, the radios require perfect modulators, demodulators, filter, and transmission paths. If the radio had a perfect (rectangular in the frequency domain) filter, then the occupied bandwidth could be made equal to the symbol rate. Techniques for maximizing spectral efficiency include the following:

- Relate the data rate to the frequency shift (as in GSM).
- Use premodulation filtering to reduce the occupied bandwidth. Raised cosine filters, as used in NADC, PDC, and PHS, give the best spectral efficiency.
- Restrict the transition types.

Table 1.1. Theoretical bandwidth performance limit for digital modulation

Modulation format	Theoretical bandwidth efficency limits
MSK	1 bit/s/Hz
BPSK	1 bit/s/Hz
QPSK	2 bit/s/Hz
8PSK	3 bit/s/Hz
16QAM	4 bit/s/Hz
32QAM	5 bit/s/Hz
64QAM	6 bit/s/Hz
256QAM	8 bit/s/Hz

1.1.9 I/Q modulation

The digital modulation schemes outlined are fundamental blocks for many communication systems, but the new communication systems have introduced some variation of these. There are three main variations on these basic building blocks that are used in communication systems: I/Q offset modulation, differential modulation and constant envelope modulation.

The first variation is offset modulation. One example of this is Offset QPSK (OQPSK). This is used in the cellular CDMA system for the reverse (mobile to base) link.

In QPSK, the I and Q bit streams are switched at the same time. The symbol clocks, or the I and Q digital signal clocks, are synchronized. In Offset QPSK (OQPSK), the I and Q bit streams are offset in their relative alignment by one bit period (one half of a symbol period). This is shown in the Fig.1.13.

Since the transitions of I and Q are offset, at any given time only one of the two bit streams can change values. This creates a dramatically different constellation, even though there are still just two I/Q values. This has power efficiency advantages. In OQPSK the signal trajectories are modified by the symbol clock offset so that the carrier amplitude does not go through or near zero (the center of the constellation). The spectral efficiency is the same with two I states and two Q states. The reduced amplitude variations allow a more power-efficient, less linear RF power amplifier to be used.

The second variation is differential modulation as used in Differential QPSK (DQPSK) and Differential 16-QAM (D16QAM). Differential means that the information is not carried by the absolute state, it is carried by the transitions between states. In some cases there are also restrictions on allowable transitions. This occurs in $\pi/4$ DQPSK where the carrier trajectory does not go through the origin. A DQPSK transmission system can transition from any symbol position to any other symbol position. The $\pi/4$ DQPSK modulation format is widely used in many applications including:

- North American Digital Cellular IS-54 (NADC) -Pacific Digital Cellular (PDC)

- cordless
  - Personal Handyphone System (PHS)
- trunked radio
  - Trans European Trunked Radio (TETRA)

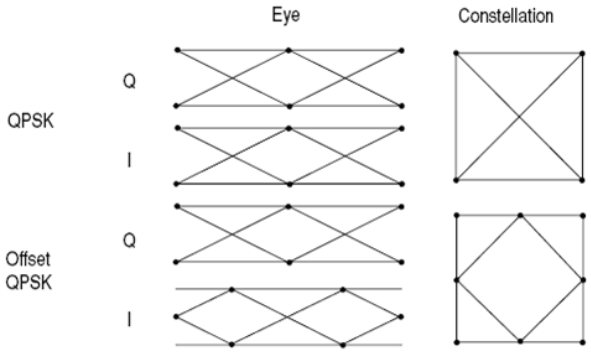

Fig. 1.13. IQ offset modulation.

The $\pi/4$ DQPSK modulation format uses two QPSK constellations offset by 45 degrees ($\pi/4$ radians) that is shown in Fig.1.14. Transitions must occur from one constellation to the other. This guarantees that there is always a change in phase for each symbol, making clock recovery easier. The data is encoded in the magnitude and direction of the phase shift, not in the absolute position on the constellation. One advantage of $\pi/4$ DQPSK is that the signal trajectory does not pass through the origin, thus simplifying transmitter design. Another is that $\pi/4$ DQPSK, with root raised cosine filtering, has better spectral efficiency than GMSK, the other common cellular modulation type.

The third variation is constant-envelope modulation. GSM uses a variation of constant amplitude modulation format called 0.3 GMSK . In constant-envelope modulation the amplitude of the carrier is constant, regardless of the variation in the modulating signal. It is a power-efficient scheme. However, constant-envelope modulation techniques occupy a larger bandwidth than schemes which are linear. In linear schemes, the amplitude of the transmitted signal varies with the modulating digital signal as in BPSK or QPSK, like is shown in Fig.1.14. MSK is a special type of FSK where the peak-to-peak frequency deviation is equal to half of the bit rate.

Gaussion MSK (GMSK)is a derivative of MSK where the bandwidth required is further reduced by passing the modulating waveform through a Gaussian filter. The Gaussian filter minimizes the instantaneous frequency variations over time. GMSK is a spectrally efficient modulation scheme and is particularly useful in mobile radio systems. It has a constant envelope, spectral efficiency, good Bit Error Rate (BER) performance, and is self-synchronizing.

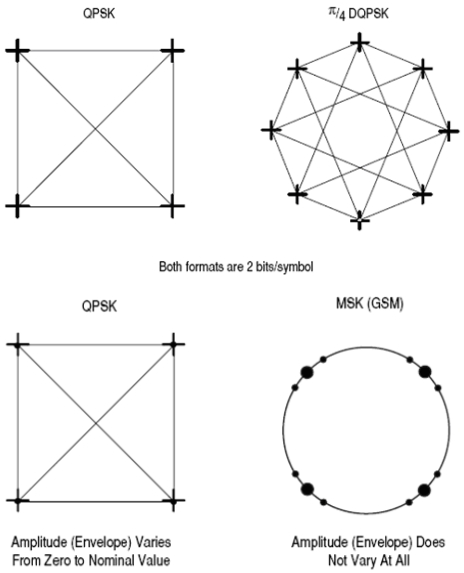

Fig. 1.14. IQ and MSK Modulation

1.2 Filtering

Filtering allows the transmitted bandwidth to be significantly reduced without losing the content of the digital data. This improves the spectral efficiency of the signal. There are many different varieties of filtering. The most common are:

- raised cosine
- square-root raised cosine
- Gaussian filters

Any fast transition in a signal, whether it be amplitude, phase, or frequency, will require a wide occupied bandwidth. Any technique that helps to slow down these transitions will narrow the occupied bandwidth. Filtering serves to smooth these transitions (in I and Q). Filtering reduces interference because it reduces the tendency of one signal or one transmitter to interfere with another in a Frequency-Division-Multiple-Access (FDMA) system. On the receiver end, reduced bandwidth improves sensitivity because more noise and interference are rejected.

Of course some types of filtering cause the trajectory modification of the signal (the path of transitions between the states) to overshoot in many cases. This overshoot can occur in certain types of filters such as Nyquist. This overshoot path represents carrier power and phase. For the carrier to take on these values it requires more output power from the transmitter amplifiers. It

requires more power than would be necessary to transmit the actual symbol itself. Carrier power cannot be clipped or limited (to reduce or eliminate the overshoot) without causing the spectrum to spread out again. Other tradeoffs are that filtering makes the radios more complex and can make them larger, especially if performed in an analog fashion. Filtering can also create Inter-Symbol Interference (ISI). This occurs when the signal is filtered enough so that the symbols blur together and each symbol affects those around it. This is determined by the time domain response or impulse response of the filter.

1.2.1 Nyquist or raised cosine filter

Nyquist filters have the property that their impulse response rings at the symbol rate. Fig.1.15 shows the impulse or time-domain response of a raised cosine filter, one class of Nyquist filter. The filter is chosen to ring, or have the filter impulse response cross through zero, at the symbol clock frequency.

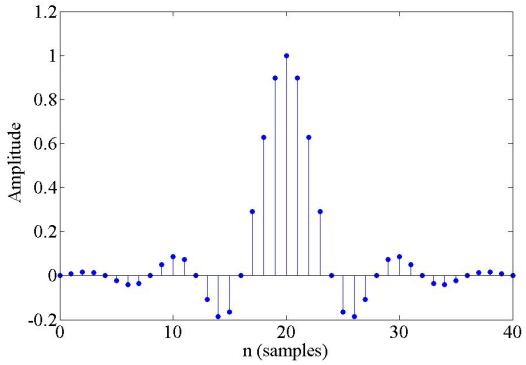

Fig. 1.15. Inpulse responce of a Raised cosine filter

The filter time response goes through zero with a period that exactly corresponds to the symbol spacing. Adjacent symbols do not interfere with each other at the symbol times because the response equals zero at all symbol times except the centre one.

Nyquist filters heavily filter the signal without blurring the symbols together at the symbol times. This is important for transmitting information without errors caused by ISI. Note that ISI exists at all times except the symbol times. Usually the filter is split, half being in the transmit path and half in the receiver path. In this case root Nyquist filters (commonly called root raised cosine) are used in each part, so that their combined response is that of a Nyquist filter.

1.2.2 Gaussian filter

In contrast, a GSM signal will have a small blurring of symbols on each of the four states because the Gaussian filter used in GSM does not have zero Inter-Symbol Interference. The phase states vary somewhat causing a blurring of the symbols, as shown in Fig.1.16. Wireless system architects must decide just how much of the ISI can be tolerated in the system and combine that with noise and interference. Gaussian filters are used in GSM for their advantages in carrier power, occupied bandwidth, and symbol-clock recovery. The Gaussian filter is a Gaussian shape in both the time and frequency domain, and it does not ring like done the raised cosine filters. Its effects in the time domain are relatively short and each symbol interacts significantly (or causes ISI) with only the preceding and succeeding symbols. This reduces the tendency for particular sequences of symbols to interact which makes amplifiers easier to build and more efficient.

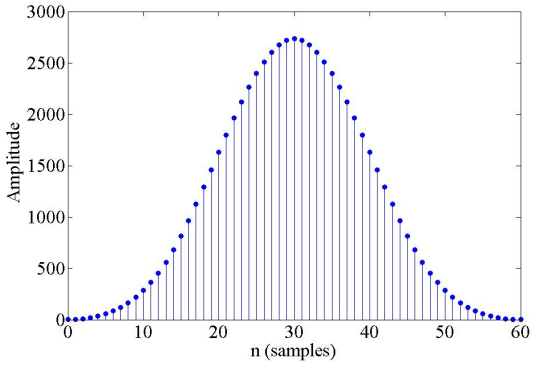

Fig. 1.16. Inpulse responce of a Gaussian filter

1.2.3 Filter bandwidth parameter alpha

Alpha (α) is defined as "excess bandwidth factor" and it indicates the amount of occupied bandwidth that will be required in excess of the ideal occupied bandwidth (which would be the same as the symbol rate). At the other extreme, take a broader filter with an alpha of one, which is easier to implement.

The sharpness of a raised cosine filter is described by α like is shown in Fig.1.17. Alpha gives a direct measure of the occupied bandwidth of the system and is calculated as:

- occupied bandwidth = symbol rate $X(1 + \alpha)$.

If the filter had a perfect characteristic with sharp transitions and an α of zero, the occupied bandwidth would be:

- for $\alpha = 0$, occupied bandwidth = symbol rate X (1 + 0) = symbol rate.

In a perfect world, the occupied bandwidth would be the same as the symbol rate, but this is not practical. An α of zero is impossible to implement.

The occupied bandwidth will be:

- for $\alpha = 1$, occupied bandwidth = symbol rate X (1 + 1) = 2 X symbol rate.

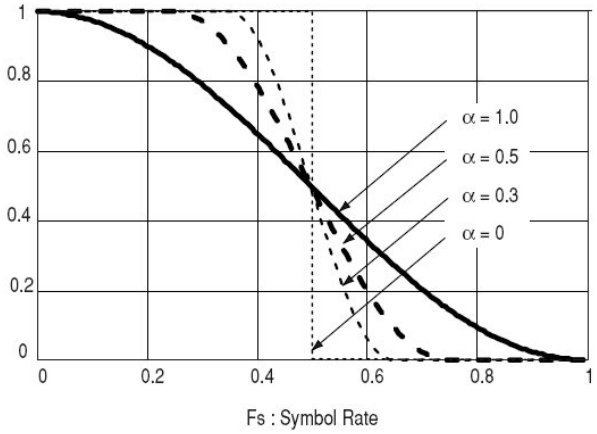

Fig. 1.17. Filter bandwidth parameters α

An α of one uses twice as much bandwidth as an alpha of zero. In practice, it is possible to implement an α below 0.2 and make good, compact, practical radios. Typical values range from 0.35 to 0.5, though some video systems use an α as low as 0.11. The corresponding term for a Gaussian filter is BT (Bandwidth Time product). Occupied bandwidth cannot be stated in terms of BT because a Gaussian filter's frequency response does not go identically to zero, as does a raised cosine. Common values for BT are 0.3 to 0.5.

1.3 Telecommunication signal analysis

The signal analysis is necessary for different reasons. During the project developing phase of a transmitter is necessary to follow rigours tests to determine if the project is robustness; different tests permit to verify that the project respect the limits imposed by the standards, and to determine the behaviour of the systems in the presence of other sub-systems.

When a telecommunication system is in use, the signal analysis permits to verify the presence of anomalies in the system and the causes of this anomalies.

Indeed, in security applications the signal analysis permits to detect hackers presence in the system also in the presence of legal communications. The signal can be analysed in different domain. Every domain can make in evidence different signal characteristics. The different domains that furnish information about the signal are: the time domain, the frequency domain, and the modulation domain. For an accurate analysis is necessary to have an instrument that can operate in every of the three domain.

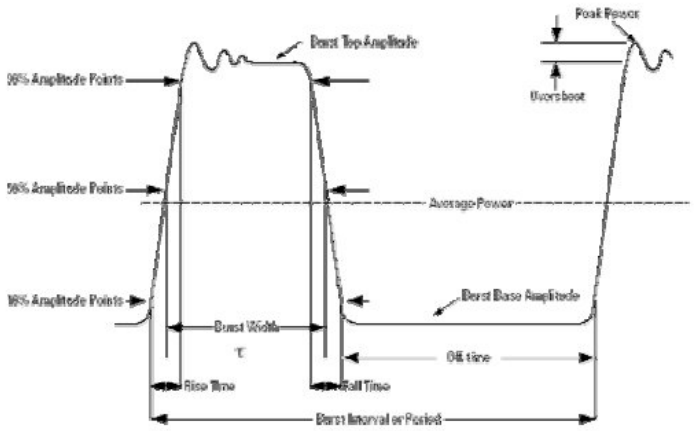

Fig. 1.18. Typical time measure

1.3.1 Time domain

The traditional instrument used to analyse the time evaluation of an electric signal is the oscilloscope. Another important instrument is the Vector Signal Analyser (VSA), that translate the signal in baseband from the radio frequency, and sample the IQ component. The samples are shown in different modality (Amplitude-Time, Phase-Time, IQ-Time, IQ Polar). The analysis in the time domain is more important for the modulation schemes based on TDMA. For this modulation scheme are necessary measure of the shape and of the time of a burst.

Timing measurement

Timing measurements are made most often in pulsed or burst systems. As is shown in Fig.1.18, measurements include pulse repetition intervals, on-time, off-time, duty cycle, and time between bit errors. Turn-on and turn-off times also involve power measurements. Power measurements include carrier power and associated measurements of amplifiers gain and insertion loss of filters

and attenuators. Signals used in digital modulation are noise-like. Bandpower (power integrated over a certain band of frequencies) or Power Spectral Density (PSD) measurements are often made. PSD measurements normalize power to a certain bandwidth, usually 1 Hz.

1.3.2 Frequency domain

The analysis in the time domain is not sufficient to characterize a telecommunication signal. In fact, is necessary to observe the spectral component. For the frequency domain measurement can be used both the spectral analyser and the VSA. The VSA permit to obtain the spectral measurement with the execution of a Fast Fourier Transform (FFT). The principal parameter estimated from the frequency domain are: occupied band-width, and adjacent power channel.

Frequency measurements

Frequency measurements are often more complex in digital systems since factors other than pure tones must be considered. Occupied bandwidth is an important measurement. It ensures that operators are staying within the bandwidth that they have been allocated. Adjacent channel power is also used to detect the effects one user has on other users in nearby channels.

Adjacent channel power

Adjacent channel power is a measure of interference created by one user that effects other users in nearby channels. This test quantifies the energy of a digitally modulated RF signal that spills from the intended communication channel into an adjacent channel. The measurement result is the ratio (in dB) of the power measured in the adjacent channel to the total transmitted power. A similar measurement is alternate channel power which looks at the same ratio two channels away from the intended communication channel.

For pulsed systems (such as TDMA), power measurements have a time component and may have a frequency component, too. Burst power profile (power versus time) or turn-on and turn-off times may be measured. Another measurement is average power when the carrier is on or averaged over many on/off cycles.

Occupied bandwidth

Occupied bandwidth (BW) is a measure of how much frequency spectrum is covered by the signal in question. The units are in Hz, and measurement of occupied BW generally implies a power percent age or ratio. Typically, a portion of the total power in a signal to be measured is specified. A common

percentage used is 99%. A measurement of power versus frequency (such as integrated band power) is used to add up the power to reach the specified percentage. For example, a possible definition is the "99% of the power in this signal is contained in a bandwidth of 30 kHz,". Another definition is: "The occupied bandwidth of this signal is 30 kHz if the desired power ratio of 99% was known".

1.3.3 Modulation Domain

Modulation accuracy measurements involve measuring how close either the constellation states or the signal trajectory is relative to a reference (ideal) signal trajectory. The received signal is demodulated and compared with a reference signal. The main signal is subtracted and what is left is the difference or residual. Modulation accuracy is a residual measurement. Modulation accuracy measurements usually involve precision demodulation of a signal and comparison of this demodulated signal with a (mathematically generated) ideal or "reference" signal. The difference between the two is the modulation error, and it can be expressed in a variety of ways including:

- IQ constellation diagram,
- Error Vector Magnitude (EVM),
- Phase error, magnitude error, frequency error, offset IQ;
- Amplitude of the error vector versus time, spectrum of the error vector;
- Trellis diagram and eye diagram;
- Symbol table and code domain analysis.

The reference signal is subtracted from the demodulated signal, leaving a residual error signal. Residual measurements are very powerful for troubleshooting. Once the reference signal has been subtracted, it is easier to see small errors that may have been swamped or obscured by the modulation itself. The error signal itself can be examined in many ways; in the time domain or (since it is a vector quantity) in terms of its I/Q or magnitude/ phase components. A frequency transformation can also be performed and the spectral composition of the error signal alone can be viewed.

Error Vector Magnitude (EVM)

Digital bits occupies any one of several unique locations on the I versus Q plane. Each location encodes a specific data symbol, which consists of one or more data bits. A constellation diagram shows the valid locations for all permitted symbols of which there must be 2^n, given n bits transmitted per symbol. To demodulate the incoming data, the exact magnitude and phase of the received signal for each clock transition must be accurately determined. The layout of the constellation diagram and its ideal symbol location is determined generically by the modulation format chosen. The trajectory taken

by the signal from one symbol location to another is a function of the specific system implementation, but is readily calculated nonetheless. At any moment, the signal's magnitude and phase can be measured. These values define the actual or "measured" phasor. At the same time, a corresponding ideal or "reference" phasor can be calculated, given knowledge of the transmitted data stream, the symbol-clock timing, baseband filtering parameters, etc. The differences between these two phasors form are the basis for the EVM measurements.

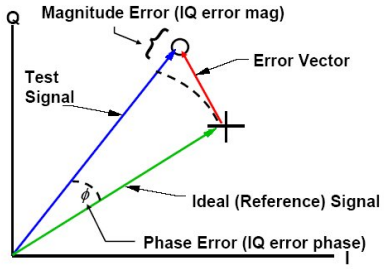

Fig. 1.19. Error Vector Magnitude

As shown in Fig.1.19, EVM is the scalar distance between the two phasor end points, it is the magnitude of the difference vector. Expressed another way, it is the residual noise and distortion remaining after an ideal version of the signal has been stripped away.

In the NADC-TDMA (IS-54) standard, EVM is defined as a percentage of the signal voltage at the symbols. In the $\pi/4$ DQPSK modulation format, these symbols all have the same voltage level, though this is not true of all formats. IS-54 is currently the only standard that explicitly defines EVM, so EVM could be defined differently for other modulation formats. In a format such as 64-QAM, for example, the symbols represent a variety of voltage levels. EVM could be defined by the average voltage level of all the symbols (a value close to the average signal level) or by the voltage of the outermost (highest voltage) four symbols. While the error vector has a phase value associated with it, this angle generally turns out to be random because it is a function of both the error itself and the position of the data symbol on the constellation. A more useful angle is measured between the actual and ideal phasors (I/Q phase error), which contains information useful in troubleshooting signal problems. Likewise, I/Q magnitude error shows the magnitude difference between the actual and ideal signals. EVM, as specified in the standard, is the Root-Mean-Square (RMS) value of the error values at the instant of the symbol-clock transition. Trajectory errors between symbols are ignored. Measurements of error vector magnitude and related quantities can, when properly applied,

provide much insight into the quality of a digitally modulated signal. They can also pinpoint the causes for any problems uncovered by identifying exactly the type of degradation present in a signal and even help identify their sources.

Phase Error

Phase error is the instantaneous angle difference between the measured signal and the ideal reference signal. When viewed as a function of time (or symbol), it shows the modulating waveform of any residual or interfering PM signal. Sinewaves or other regular waveforms indicate an interfering signal. Uniform noise is a sign of some form of phase noise (random jitter, residual PM/FM, etc.).

Eye diagram

The eye diagram is an oscilloscope display of a digital signal, repetitively sampled to get a good representation of its behavior. In a radio system, the point of measurement may be prior to the modulator in a transmitter, or following the demodulator in a receiver, depending on which portion of the system requires examination. The eye diagram can also be used to examine signal integrity in a purely digital system-such as fiber optic transmission, network cables or on a circuit board.

The following information can be obtained from an eye diagram:

- Jitter is a measure of signal quality and is defined as the measure of variance in signal characteristics. A zero jitter measurement indicates that the signal transition occurs at exactly the same point in time for each transition. The wide superimposed transitions in the eye pattern diagram is the result of high jitter associated with the signals, implying that the signals are not consistently transitioning at the required time. Small eye width implies a large variance in signal transition time;
- Transition time is the rise and fall time that is associated with the signals. Transition times can be measured using the slope of the transitioning signals in the eye diagram. A 90 degree slope implies a rise and fall time of 0 ns. In reality, however, there is a certain transition time associated with rising and falling signals. The closer the slope is to 90 degrees, the smaller the transition time. A smaller transition time indicates that the signal is valid for a longer time at the next time period.

Code domain power

Code domain power (CDP) is an analysis of the distribution of signal power projected on a code-space of a particular dimension, normalized to the total signal power. To analyze the composite waveform, each channel is decoded using a code-correlation algorithm. This algorithm determines the correlation

coefficient for each code. Once the channels are decoded, the power in each code channel is determined.

Code domain error (CDE) measurements are made by sampling the down-converted input signal, then applying DSP (Digital Signal Processing) techniques to determine the original data input to the UE transmitter's OVSF code spreading function for each channel. The DSP uses the original data and coding to generate a representation of the original waveform. This is the reference waveform for the code domain error measurements.

CDE is determined by comparing the reference waveform with the waveform being measured to determine the error vector. The error vector is projected onto the code domain at the same spreading factor used to determine CDP. The error vector for each power code is defined as the ratio to the mean power of the reference waveform expressed in dB.

1.4 Conclusion

The different digital modulation schemes used in the telecommunication systems and some parameters to characterize the signal are presented. These parameters have an important role to establish the quality and to identify the causes of the problem in the communication.

All the methods to measure this parameters operate on the signal with the knowledge of a lot of a priori information about the input signal. Among these information there are the modulation scheme, the carrier frequency, the symbol time, or the particular telecommunication standard used. This is a limits of the actual measurement methods.

In order to overcome these limits, the goal of the thesis is the setting-up of a measurement method that needs reduced information about the modulated signal. As a consequence of the reduced information needed, the method must be characterised by an unified approach to the measurement of the parameters of the digital modulated signals without a priori knowledge of the modulation scheme.

2

Towards the unified approach for measurement on digital modulated signals

The estimate of the parameters characterizing the modulated signals are used for signal demodulation, signal decoding and signal quality assessment. The parameters characterizing the digital modulations that must be taken into account and that play a leading role [5] are:

1. the carrier frequency,
2. the carrier phase offset between the transmitter and the receiver,
3. the phase noise,
4. the amplitude noise,
5. the symbol timing.

Most of the methods proposed in literature operate in the particular contexts and are devoted to solve specific problems [6]-[23].

In [6] the carrier and phase estimation problem is analysed only for a QAM signal.

In [7]-[10] solutions are presented for the phase offset estimation for the QAM signal.

In [11] the carrier and phase offset estimation problem is considered for the PSK signal.

In [14]-[18] the methods able to operate only on sinusoidal signal are proposed for the amplitude and phase noise measurement.

In [19] a cyclostationary statistics are used to determine the symbol-rate for the symbol timing estimation.

Moreover, in [20] a feedforward, block processing, symbol timing recovery method based on the theory of maximum likelihood estimation is presented.

In [22] new nondata-aided feedforward symbol timing estimator is proposed, which can be applied to two samples per symbol.

In this scenario, a new idea consists on point out a measurement method based on an unified approach that permit to measure the same parameter without taking into account the particular modulation. The method must work with a priori knowledge of few parameters of the modulated signal. In

particular, the information to be used by the method are that furnished by the modulation classifier of the digital modulated signal.

2.1 Modulation classifier

In literature methods for modulation classification purpose have been presented. They are able to recognize the modulation type with the minimum a priori knowledge [1], [24]-[32].

Most of the classifiers proposed in literature identifies only few modulation schemes, such as M-PSK or M-QAM, or requires the knowledge of some parameters of signal. The methods that use statistical approach are particularly interesting, but they require the knowledge of the symbol rate. Other methods use neural network or time frequency representation achieving better result but requiring more complexity. Another classification strategy uses the zero crossing technique in computing the instantaneous frequency and its variations. These last are used to classify and to explore the properties of the modulated signal. Fig.2.1 shows the connection between the different modulation classifier proposed in literature.

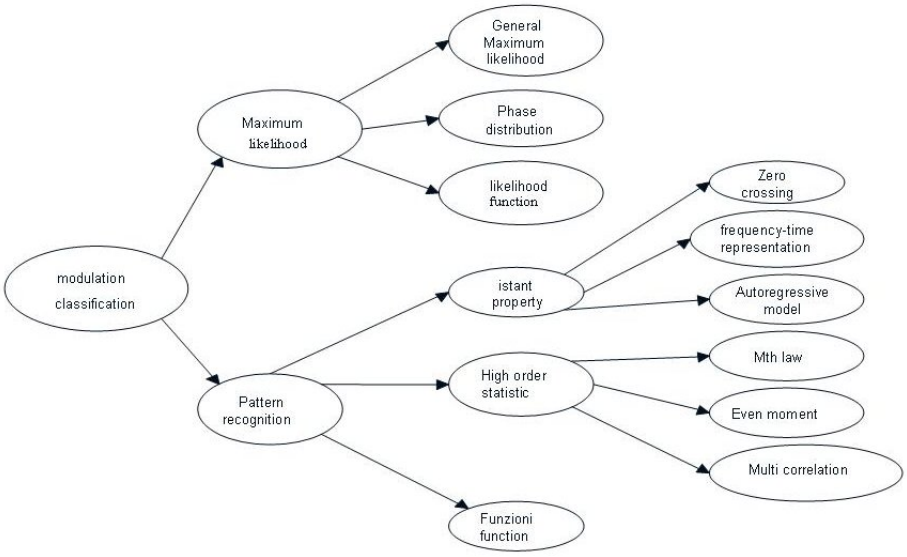

Fig. 2.1. Representation of the connection between the different modulation classifier proposed in literature.

The modulation classification, considered as basic step before the parameters measurement by means of the method based on the unified approach, is

based on a tree decisional structure shown in Fig.2.2 [1]. Every node of the tree executes a specific test. Therefore, the problem is divided in a number of steps. The first performs the selection of the modulation between Single Carrier (SC) and Multiple Carrier (MC). In order to realize this selection a test based on the fourth order cumulants is utilized. In fact, the MC signal can be considered formed by a great number of independent, identically distributed random variables, and the amplitude distribution of the samples can be approximated by Gaussian distribution. The fourth order cumulants are used like normality test.

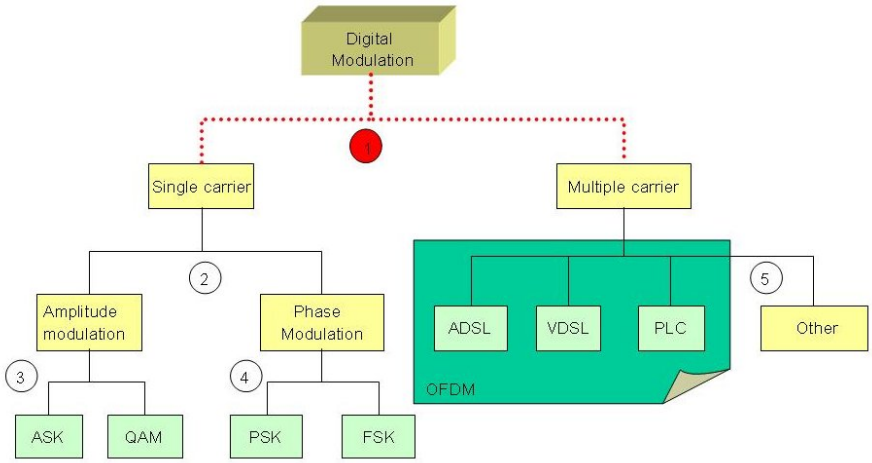

Fig. 2.2. Digital modulation classifier decisional structure.

For the SC modulation the successive step is the discrimination between the amplitude and phase modulation. The test is based on the analysis of the instantaneous amplitude. The angle modulated signals are characterized by quite constant amplitude versus time, so it is possible to determine a threshold value to discriminate between the two modulations. For the amplitude modulation the successive step is to discriminate between the QAM and ASK modulation. In order to resolve this problem the evaluation of instantaneous amplitude is used. For the ASK signal the probability density function of the instantaneous amplitude is uniform and it is centred around the value 0.5, for QAM signal it is not symmetric and has a lower mean value. The classification between the angle-modulation PSK and FSK is made by using the time intervals between two subsequence zero-crossing. This sequence has different trends for the two modulations. In particular, it is constant and equal to $1/2f_c$, where fc is the carrier frequency, inside each symbol for the PSK signals. The sequence for FSK signal is constant inside each symbol, but it is different from one symbol to another one. As a consequence, the classification

between the angle-modulated signal can be made analyzing the shape of the zero-crossing sequence. The method for the level number estimation depends by the particular modulation. For the PSK modulation, the histogram of the measured phase deviation is compared with the theoretical one. For the FSK modulation the histogram of the frequency is computed and the number of the different levels is counted. For the ASK and QAM modulations the method for the PSK modulation is utilized. The histogram is computed from the centred and normalized amplitude sequence.

2.2 The idea of the method based on the unified approach

The modulation classifier furnishs the minimum a priori information to be used by the method for the digital modulated signal characterization. In the research an unified approach is presented in [12], [33] and [34] for measurement purpose of

- the carrier frequency,
- the carrier phase offset,
- the phase noise,
- the amplitude noise,
- the symbol timing,

for a number of single carrier digital modulations.

The knowledge of this parameters guaranty the possibility to determine the symbol transmitted and the causes of a non accurate reception of the signal.

The approach proposed permits to design specific methods to be integrated in the modular structure of the automatic classifier presented in [1]. It is able to operate once received the information concerning the modulation scheme and the level number among:

- M-ary Quadrature Amplitude Modulation (M-QAM),
- M-ary Amplitude Shift Keying (M-ASK),
- M-ary Phase Shif Keying (M-PSK),
- M-ary Frequency Shift Keying (M-FSK).

2.2.1 Carrier frequency measurement

In order to evaluate the carrier frequency, the mean value of the instantaneous frequencies is evaluated on the basis of the time interval between two consecutive zero-crossing. This is an incorrect evaluation of the carrier frequency. In order to overcome this inconvenient, two different procedures are pointed out. The former is used in the case of the M-FSK modulation, the later in the

case of M-ASK, M-PSK and M-QAM modulations, according to their different characteristic properties. For M-FSK modulation, in the histogram the M central frequencies are selected. For M-ASK, M-PSK and M-QAM modulations the initial trial frequency is detected, successively the corrective factor is evaluated. This is evaluated from the base-band signal.

2.2.2 Carrier phase offset measurement

If the phase offset occurs, the constellation is uniformly rotated of the angle ψ. Moreover, the superimposed noise to the signal is rotated, too. The measurement procedure creates a grid G on the basis of the theoretical constellation to be examined. The grid is rotated and the number of the input point included into the grid is evaluated. The rotation angle, corresponding to the maximum number of the input points in the grid proximity, is the phase offset.

2.2.3 Amplitude and Phase noise measurement

The amplitude and phase noise estimation can be done by means of the transformation operator applied to the input signal symbols in the IQ plane. In fact, they can be grouped in only one, named Virtual Symbol (VS), in order to reduce the number of samples to be acquired by the Analog-to-Digital Converter (ADC). With the use of the VS, the phase noise is measured by evaluating on the VS the peak of the angle fluctuations around the ideal symbol. The amplitude noise is measured by evaluating the RMS of the module fluctuation around the ideal symbol.

2.2.4 Symbol time measurement

The symbol time measurement is based on the demodulation of the input signal with a very short symbol timing that is the measurement unit. The histogram is determined of the consecutive repetition length of a symbol after the demodulation. In the histogram of the occurrences small length, generated by the passage from a symbol to another in the demodulated signal, are not considered. The maximum value of the occurrences permits to select the length of the symbol time respect to the measurement unit taken into account.

2.2.5 Performance increasing of the method

To implement this method in a real instrument and to increase the performance respect to the usually telecommunication measurement instruments, two fundamental step must to be taken into account:

- the definition of a demodulation process able to operate on the input signal in presence of high value of noise and distortion;

- the definition of the hardware structure able to acquire the input signal and to implement the method.

By refering to the first step, it is necessary to use the method in presence of noise value greater than the noise value reported in the telecommunication standard for the correct reception of the signal. This is the limit noise value guarantying the correct reception by the usually demodulator.

The second step is devoted to determine the architecture scheme that permits to implement the method and to be used with the actual and the future standard of telecommunication signals.

2.3 Artificial Neural Network for the Modulation quality assessment

The demodulation is important process for the parameter measurement of telecommunication signals. Different measurement methods require to demodulate the input signal to compare it with the ideal signal transmitted. If the input signal is affected by high level of noise and distortion, it's possible that the demodulator doesn't recognize the real information transmitted. This error decreases the accuracy of the measure. To overcome this problem it's possible to use the Artificial Neural Networks (ANNs), that show interesting properties to efficiently process the input signals affected by high level of both noise and distortion characterizing the telecommunication networks.

ANNs are adaptive models that can learn from the data and generalize things learned. They extract the essential characteristics from the numerical data as opposed to memorizing all of it. This offers a convenient way to reduce the amount of data as well as to form a implicit model without having to form a traditional, physical model of the underlying phenomenon.

Learning in ANNs is done in terms of adaptation of the network parameters. Network parameters are changed according to pre-defined equations called the learning rules. The learning rules may be derived from pre-defined error measures or may be inspired by biological systems. The information-processing abilities of biological neural systems must follow from highly parallel processes operating on representations that are distributed over many neurons. One motivation for ANN systems is to capture this kind of highly parallel computation based on distributed architecture.

In conclusion, the parallel architecture of the ANNs permits:

- to process the signals in very fast way,
- to overcome the limits of the traditional approach to the signal processing.

2.4 The new proposed architecture

The hardware architecture that best fit the characteristics of the method based on the unified approach for measurement on digital modulated signal is the

Software Radio (SR) architecture. The benefits of this architecture consist in using single general-purpose platform to perform different functions by simply running different program. The main effort is to get the hardware architecture able to support the proposed measurement method, by taking into account the strong diversity of existing and future communication systems. This permits to obtain both flexible and adaptable architecture that can efficiently implement the method pointed out for the characterization of digital modulated signals.

In the SR architecture the incoming signal is translated into the digital domain by the Analog to Digital Converter (ADC) and is demodulated by using software techniques [35] in the elaboration unit.

As it is shown in Fig.2.3, into the unit for the control and elaboration is implemented the method for the parameters estimation and the modulation classifier. This last is necessary to furnish at the measurement method the minimum quantity of information without the user setting.

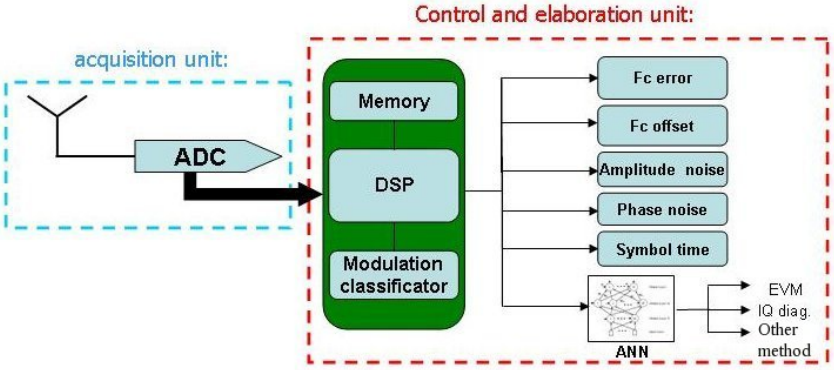

Fig. 2.3. Hardware architecture to acquire and process the signals by means of the proposed measurement method.

Fundamental is the selection of the ADC that permits to obtain good performance with the measurement method. Between the different ADC architectures proposed in literature, the Band Pass $\Sigma\Delta$ ADCs shows the better solution to obtain the minimum performance required by the method in a very simple way.

The Band Pass (BP) $\Sigma\Delta$ ADC represent a subgroup from more general group of the unconventional ADCs. The BP $\Sigma\Delta$ ADCs are mostly embedded into digital communication systems in various applications. Their main task is to provide a frequency down conversion along with narrowband filtering and the conversion of chosen parameters of analog signal into digit.

These converters are analog front end digital communication systems like SR, UMTS, GSM and GPS systems.

2.5 Conclusion

To overcome the necessity of the measurement methods for the digital modulated signal characterization to have a lot of a priory information about the signal to analyse, the new method is introduced. In particular, this method is based on a unified approach for parameter measurement of digital modulated signals. It can be integrated into a measurement instrument with a modulation classifier. The unified approach is able to operate on the single carrier digital modulated signals of the schemes M-ASK, M-QAM, M-FSK and M-PSK. The parameters that can be evaluated are:

- Carrier frequency measurement;
- Phase offset Measurement;
- Phase noise;
- Amplitude noise;
- Symbol time.

To increase the possibility of the method to operate with high level distorted signals, new demodulator architecture based on ANN is introduced.

The functional block architecture, obtained from the SR architecture, is selected for the hardware implementation of the measurement method. It is based on the cascade of the acquisition unit, and the control and elaboration unit.

For the acquisition unit more important is the Analog to Digital Converter (ADC), that has to be analysed and included in the structure.

3

Carrier frequency and phase offset measurement for single carrier digital modulations

If the communication channel exhibits very low signal-to-noise ratio (SNR) values, it can introduce large frequency shifts, due to the Doppler and other effects, while multipath propagation is generally negligible. In such conditions a critical operation in the receiver is the estimation of the carrier frequency in order to perform an accurate compensation in the demodulation process.

In literature different methods are presented to estimate the carrier frequency shift from the expected one. Most of these methods are based on maximumlikelihood (ML) [36]. A periodic sequence of training bits is recursively passed through a bank of bandpass filters (implemented in the form of a discrete Fourier transform) whose frequency spacing is varied so as to achieve an accurate estimate of the frequency at which the input signal spectrum peaks. Nevertheless, they are limited to specific standard applications.

In [6] and [37] the carrier and phase estimation problem is analysed for a Quadrature Amplitude Modulation (QAM) and Phase Shif Keying (PSK) signals. In [7]-[10] solution is presented for the phase offset estimation of the QAM signal. In [11] and [36] only the PSK signal is considered.

In [6] a Cramr-Rao lower bounds is presented for the estimation of phase offset for common QAM, PSK, and Pulse Amplitude Modulation (PAM) signals in Additive White Gaussian Noise (AWGN) channels.

In the following, the measurement method is presented for measurement purpose of the carrier frequency and the carrier phase offset.

It is able to operate once received the information concerning the modulation scheme and the level number.

Successively, both the performance and the accuracy of the implemented method is presented by considering the results of the experimental tests carried out on actual digital modulated signals according to the international recommendations [38]-[40].

3.1 Carrier frequency measurement

In order to evaluate the carrier frequency the proposed method [12] determines the mean value of the instantaneous frequencies. The instantaneous frequency is defined on the basis of the time interval between two consecutive zero crossing. Because both the noise and the carried information interfere with the zero crossing time instants, the semi-period of the modulated signal can be approximately determined and the incorrect evaluation of the carrier frequency can occur. In order to overcome this inconvenient, two different procedures are pointed out. The former is used in the case of the M-FSK modulation, the latter in the case of M-ASK, M-PSK and M-QAM modulations, according to their different characteristic properties. Indeed, characteristic property of the M-FSK modulation, in the case of same symbol time, is that: the occurrences of high values of the instantaneous frequencies are greater than those at low values. Therefore, the mean time interval computation gives the distorted evaluation of the carrier frequency. The accurate evaluation of the carrier frequency can be given on the basis of the following criteria:

- for M-FSK modulation, the histogram of the period time estimated by the zero crossing is considered. In the histogram the M central frequencies are selected on the basis of M greater values of the occurrences. The mean value of the M-selected central frequencies is computed, because it is the better estimation of the carrier frequency;
- for M-ASK, M-PSK and M-QAM modulations the initial trial frequency is detected, successively the corrective factor is evaluated. This is evaluated from the base-band signal.

By denoting with f_{sh} the shift frequency consequently to the incorrect carrier frequency evaluated by computing the mean value of the instantaneous frequencies, the demodulated signal s_d(t) is:

$$s_d(t) = \sum_k A_k e^{j(2\pi f_{sh}+\psi)} g(t - kT_s) \tag{3.1}$$

$$arg(s_d(t)) = 2\pi f_{sh} + \psi + \varphi_i \tag{3.2}$$

where: A_k, maps the transmitted symbols, ψ is the carrier phase offset, T_s is the symbol time, and g(t) is the finite energy signal with T_s duration, φ_i=cost for M-ASK, $\varphi_i = 2\pi i/M$ for M-PSK, and $\varphi_i = atan(b_k/a_k)$ for M-QAM.

By taking into account the shape of $arg(s_d(t))$ it is possible to distinguish the effects on $s_d(t)$ between that caused by the symbol changing (φ_i) and that caused by the residual carrier frequency f_{sh}. As it is shown in Fig.3.1, the trend of $arg(s_d(t))$ is characterized by the straight line with superimposed steps caused by symbol changing phase φ_i. The slope of the straight line furnishes the correcting factor of the carrier frequency previously given by computing the mean value of the instantaneous frequencies.

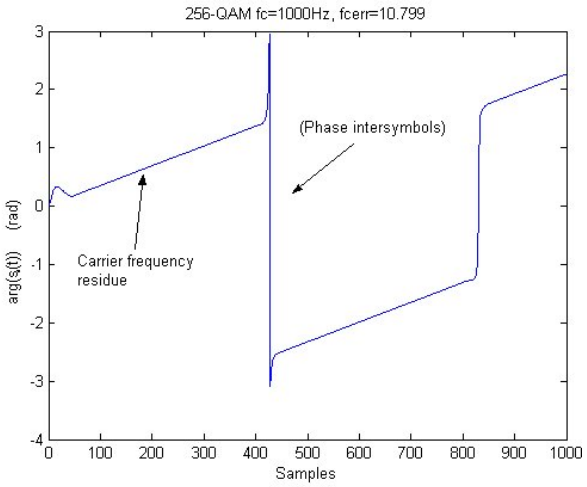

Fig. 3.1. Trend of $s_d(t)$ argument for the 256-QAM with carrier frequency shift equal to 10.799Hz.

To increase the method performance with signal affected by distortion and noise a pre processing block is used after the phase symbols compensation. In fact, the phase of the signal affected by noise is distorted and decreases the method performance. The preprocessing block is shown in Fig.3.2. The method steps are:

- the interpolation line is estimated from the phase distorted of the input signal with symbol phase compensation;
- the interpolation line is decimated in order to increase the measure accuracy;
- the estimation of the frequency is obtained from the slope of the decimated interpolation line.

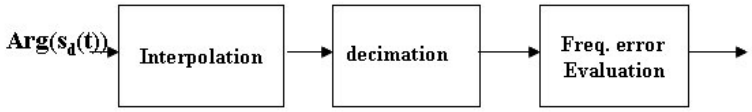

Fig. 3.2. Procedure modifications in presence of noise and distortion.

Some modifications of the method are needed in the case of M-PSK modulated signals of the Universal Mobil Telecommunication System (UMTS) standard [40]. The UMTS standard imposes the scrambling code in order

to realize the transmission by means of the frame Wide-band Code Division Multiple Access (W-CDMA). The scrambling code consists of multiplying the modulated signal by a pseudo-casual sequence of +1, 0 and -1. It can be requested to measure the carrier frequency in two situations, after and before the descrambling decoding. In the former, the M-PSK modulated signal can be processed on the basis of the procedure previous taken into account. In the latter, before the descrambling decoding, the modulated signal is far different from that processed on the basis of the procedure previous taken into account. In this situation the carrier frequency measurement is interesting, because permit light analysis. The scrambling operation modifies the phase component as shown in Fig.3.3a and does not permit to evaluate the carrier frequency error directly with the method proposed. To resolve this inconvenient only the peaks of the phase trend in a sub-interval must to be considered. The slope of the peak envelope indicates the presence of a residual of the carrier frequency in the base band signal, as shown in Fig.3.3b. It can be noted the similarity between the portraits shown in Fig.3.1 and Fig.3.3b. In order to minimize the size of the time interval where to examine the signal, it is assessed by numerical tests that the time interval corresponding to ten chips is adequate.

In order to reduce the noise influence a proper procedure is get ready.
The steps are:

1. the interpolation line of the peaks detected as previously described is determined;
2. the standard deviation of the absolute value of the distance between the interpolation line and the peaks is evaluated;
3. all the peaks whose distance from the interpolation line is greater than the standard deviation are eliminated;
4. the procedure stops if the standard deviation is less of the established threshold;
5. the interpolation line of the resulting peaks is determined and the frequency error is evaluated.

In this manner, a good estimation of the carrier frequency up to the value of SNR equal to 10dB is achievable.

3.1.1 Numerical tests

Numerical tests were performed preliminary in Matlab environmental in order to validate the characteristics of the method, and to detect the influence of the UMTS codes on the method accuracy. It was assumed:

1. carrier frequency fc=2kHz,
2. symbol frequency fsymb=100 symbol/s,
3. sampling frequency fs=20kHz.

The tests were performed by examining:

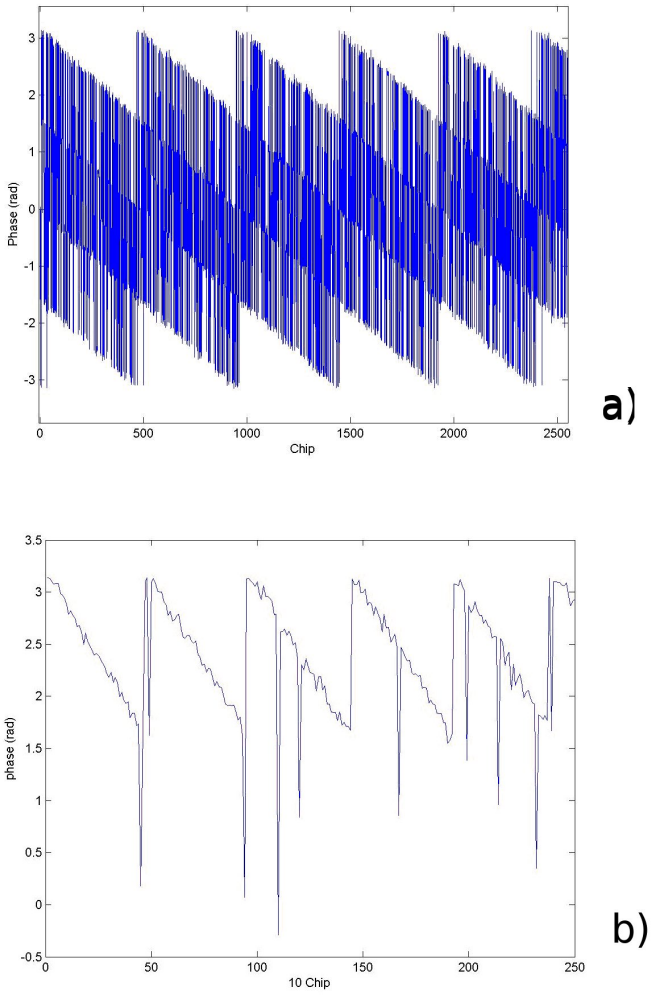

Fig. 3.3. Phase portrait of the UMTS modulated signal before the descrambling decoding (a), and the peaks envelope (b).

- 100 different test signals for each digital modulation,
- 30 ksamples for each test signal.

Tab.3.1 furnishes the standard deviation from the assigned value of the carrier frequency in the case of modulated signal without superimposed noise. The trend of the maximum error of the frequency measurement versus the SNR is shown in Fig.3.4. These results support the theoretical developments

and denote that the proposed technique is particularly attractive and robust for low SNRs, too.

Table 3.1. Standard deviation of the carrier frequency measurement without noise.

Modulation	Standard deviation [ppm]
2-FSK	58
4-FSK	108
8-FSK	123
4-ASK	3,73E-02
8-ASK	1,87E-02
16-QAM	4,10E-02
256-QAM	15,85E-01
2-PSK	8,35E-04
4-PSK	33,55E-03
8-PSK	43,70E-02

Other numerical tests were performed by simulating the modulated signals according to the UMTS [40]. All tests were performed by examinating of 100 different test signals each one constituted by burst of 2560 chips. The carrier frequency was set to 38.46MHz and the sampling frequency equal to 153.84MHz.

Before the descrambling decoding, the values of both the average error and the standard deviation are given in Tab.3.2, the trend of the maximum error versus the SNR is shown in Fig.3.5.

After the descrambling decoding, the values of both the average error and the standard deviation are given in Tab.3.3, the trend of the maximum error versus the SNR is shown in Fig.3.6.

Table 3.2. Average error and standard deviation of the carrier frequency measurement for UMTS signals before the descrambling decoding.

SNR [db]	Average error [ppm]	Standard deviation [ppm]
10	2,38	3,57
20	7,36E-1	2,11
30	2,93E-1	4,95E-1
40	5,18E-2	1,65E-1
50	7,48E-2	1,83E-1
60	7,33E-2	1,33E-1

It can be noted that the application of the method after the descrambling decoding increases the measurement accuracy.

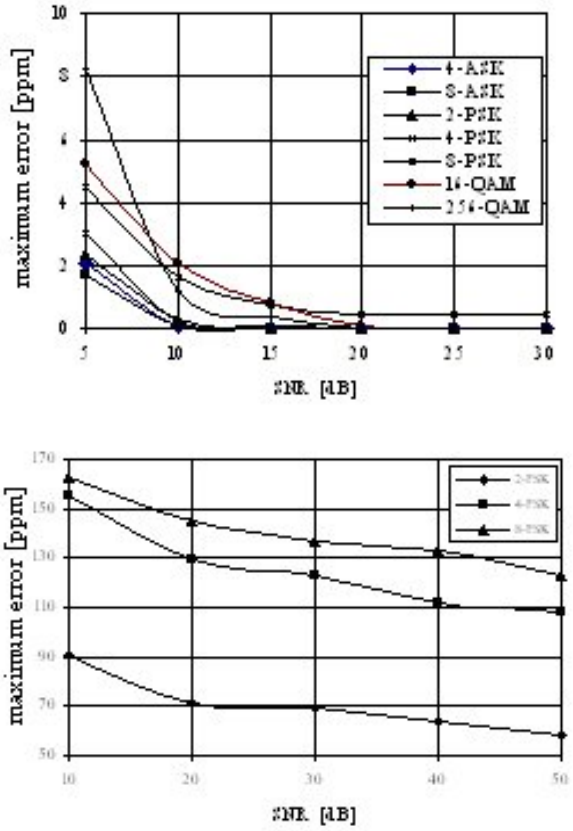

Fig. 3.4. Maximum error of the carrier frequency measurement versus the SNR for FSK, ASK, PSK and QAM modulations.

Table 3.3. Average error and standard deviation of the carrier frequency measurement for UMTS signals after the descrambling decoding.

SNR [db]	Average error [ppm]	Standard deviation [ppm]
10	1,20E-1	3,25E-1
20	6,16E-2	7,72E-1
30	4,88E-2	7,52E-2
40	4,94E-2	7,32E-2
50	4,49E-2	9,42E-2
60	5,00E-2	7,98E-2

3.2 Experimental tests on carrier frequency measurement

In order to validate the proposed method in presence of actual signals, experimental tests were carried out in two different conditions:

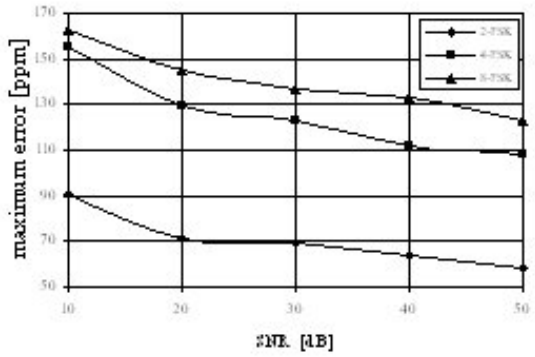

Fig. 3.5. Trend of the maximum error of the frequency measurement versus the SNR for the UMTS signal before the descrambling decoding.

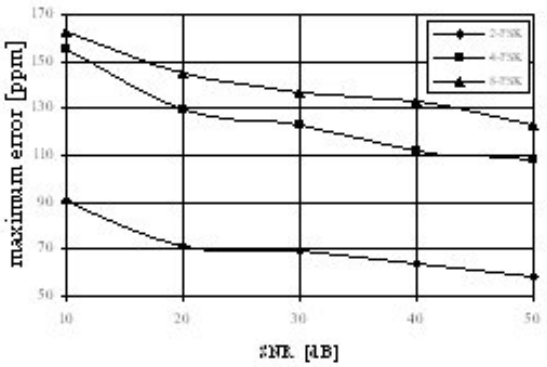

Fig. 3.6. Trend of the maximum error of the frequency measurement versus the SNR for the UMTS signal after the descrambling decoding.

- the digital modulated signals are generated in laboratory by programmable instruments according to the communication standards,
- the digital modulated signals are generated by programmable modems connected to the wired telecommunication network.

3.2.1 Digital modulated signals generated in laboratory

In order to generate in laboratory the digital modulated signals, the measurement station is shown in Fig.3.7 it is constituted by:

- Signal Generator (SG), Agilent E4435C,
- Data Acquisition board (DAQ), Signatec PDA 1000, on PCI bus,
- control and processing unit implemented on a Personal Computer (PC), Compaq Evo W4000 at 1.8 GHz,

- interconnecting interface bus IEEE 488.2 between the PC and the SG.

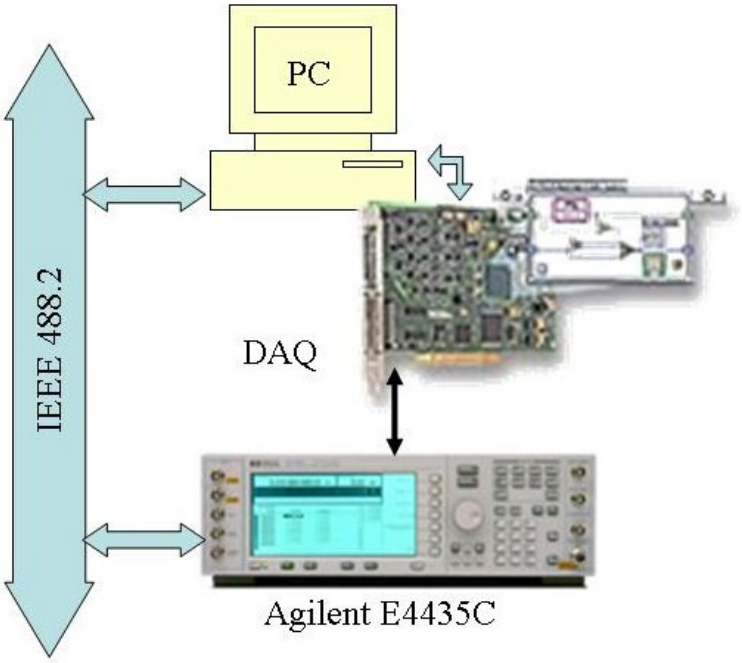

Fig. 3.7. Measurement station for experimental test on digital modulated signal.

The operating mode of the measurement station is:

1. the modulated signal is generated by the SG according to the specific standard under consideration, or, alternatively, is digitally synthesized, transferred to the local memory of the SG and given in output in the analogue form, in the case of specific requirements;
2. the DAQ digitises the analogue signal and passes the samples to the PC;
3. the PC implements the proposed method and controls the SG.

In order to assess the reliability and the efficacy of the technique, a number of tests have been carried out producing the same signals used in simulation. Successively, many experimental tests have been performed by considering

- the QAM signal produced according to the ETSI document TR 101 290 [38],
- the QPSK signal according to the ETSI document EN 300 421 [39].

The results of all these experimental tests show that:

- the proposed method is particularly robust,

- the measurement accuracy is slightly greater than that characterizing the numerical tests,
- the experimental standard deviation is contained in few percents.

Moreover, FSK modulated signals were considered with:

- carrier frequency equal to 25MHz,
- sampling frequency equal to 250MHz,
- symbol frequency equal to 12ksps.

For the carrier frequency measurement the maximum error of the method was equal to 178 ppm, the standard deviation from the ideal value is equal to 8.91 ppm. These values are compatible with the numerical tests.

Another test was produced for modulated signals according to the UMTS standard. The Downlink Dedicated Physical Channel (DPCH) was considered. The signal generated was characterised by

- the carrier frequency equal to 20.048MHz,
- the chip rate equal to 3.84Mcps.

This signal was digitalised at the sampling frequency equal to 250MHz. For the carrier frequency measurement the maximum error of the method was equal to 0.21 ppm, and the standard deviation from the ideal value equal to 0.06 ppm. These results confirm the validity of both the tests and the proposed method.

3.2.2 Digital modulated signals generated by programmable modems

Two modems U.S. Robotics Courier 56k Business Modem were used, both connected to the wired telecommunication public network as shown in Fig.3.8. One modem was programmed and controlled by Compaq Evo W4000 at 1.8 GHz and used as sender. Another was used as receiver able to negotiate the selected communication conditions according to the standard V.92 and V.90.

The processed digital modulated signals were acquired at the input of receiver modem where the signal is degraded by both the noise and the interferences of the network operating in actual conditions. Fig.3.9 a) shows the trend of the measured carrier frequency versus the sampling frequency fs, once the operating conditions at the sender are:

- 4-PSK modulated signal,
- carrier frequency equal to 1200Hz,
- symbol rate equal to 600 Symb/s.

Fig.3.9 b) shows the trend of the measured carrier frequency versus the sampling frequency fs, once the operating conditions at the sender are:

- 16-QAM modulated signal,
- carrier frequency equal to 2000Hz,

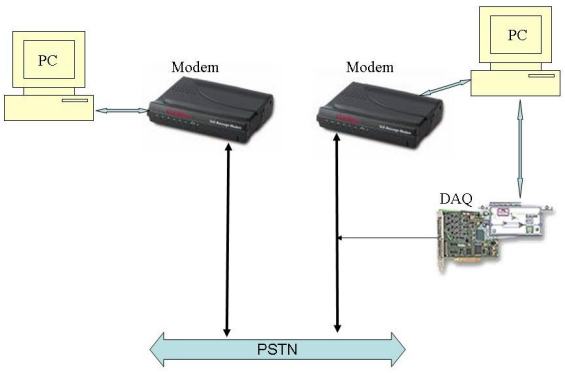

Fig. 3.8. Measurement station for experimental test on Modem signals.

- symbol rate equal to 8400 Symb/s.

These results highlight that the sampling frequency weakly influences the method accuracy.

3.3 Carrier phase offset measurement

Blind feedforward carrier synchronization of burst for M-PSK transmissions has received much attention in the literature. A generalized form of the maximum-likelihood feedforward (ML FF) method was originally proposed by A. J. Viterbi and A. M. Viterbi as a blind carrier phase estimator with improved performance at low and intermediate Signal-to-Noise Ratios (SNRs) [41], [42]. This carrier phase estimator [43], [44], [45], has been used to design blind frequency offset estimators for burst M-PSK modulations transmitted through AWGN channels [46] [47], [48].

An extensions of this estimator for flat Rayleigh and Ricean fading channels were reported in [49] and [50].

A different class of blind carrier frequency estimators that assume fractional sampling of the received signal is introducted in [43]. However, the statistical properties of the resulting estimators are partially analyzed based on certain approximations [43].

A quite general blind nonlinear least-squares (NLS) estimator for the carrier phase, frequency offset, and Doppler rate was proposed in [51]. However, the performance of the NLS-type estimator was not analyzed and exploited to develop carrier recovery methods with improved performance [51]. An alternative scheme proposed in [52] employs a sort of differential detector whose output is sampled at symbol rate and appropriately processed to remove modulation. In this manner a complex valued sequence of samples whose phase depends on the carrier frequency offset and not on data symbols is obtained.

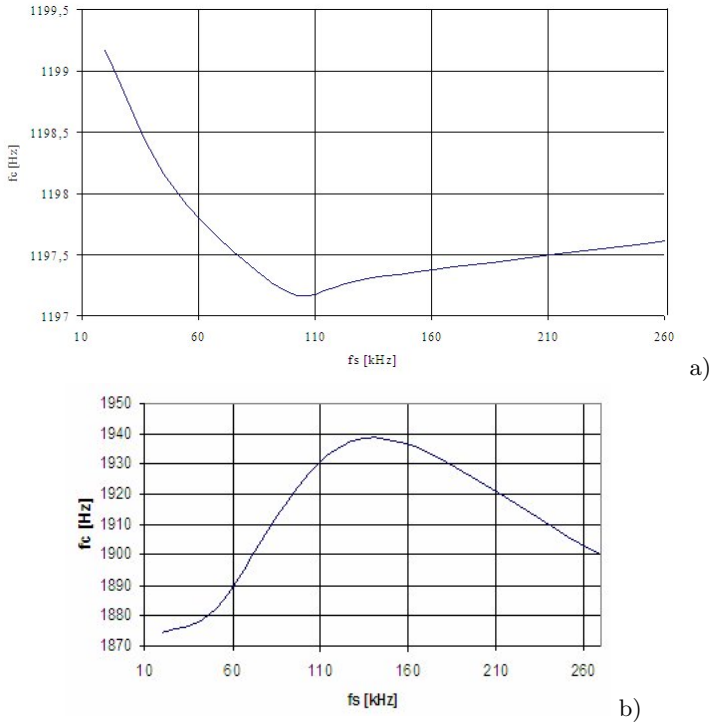

Fig. 3.9. Trend of the carrier frequency measurement versus the sampling frequency in the case modulated signals generated by modem: a) 4-PSK, carrier frequency equal to 1200 Hz, symbol rate equal to 600 Symb/s, and b) b 16-QAM, carrier frequency equal to 2000 Hz, symbol rate equal to 8400 Symb/s.

The limits of all this method are that they are able to operate only on QAM or PSK signals, and if is not possible to include other modulation schemes.

The unified approach for carrier phase offset measurement is proposed in [12]. In fact, once the carrier frequency is measured, the signal can be demodulated. The non correct synchronization during the demodulation causes the carrier phase offset. If the phase offset ψ occurs, the modulated signals obtained from 3.1 are:

$$s_d(t) = \sum_k A_k e^{j\psi} g(t - kT_s) \tag{3.3}$$

As it can be deduced from (3.3), the constellation is uniformly rotated of the angle ψ. Moreover, the superimposed noise to the signal is rotated, too. In order to evaluate the phase offset ψ, the following two properties of the constellations are taken into account:

- if ψ=0, the points are included in a circular round of ideal constellation diagram also when the noise occurs, as shown in Fig.3.10 for 16-QAM constellation,
- the previous property hold if ψ=0.

Therefore, the comparison between the ideal constellation rotated and the point of the constellation under examination is a simple way to establish how much the constellation must be rotated.

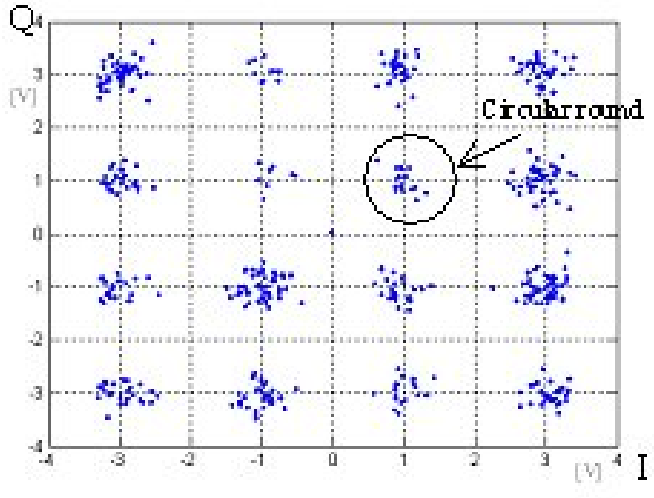

Fig. 3.10. Constellation of 16-QAM with SNR=10dB, without phase offset.

Then, the measurement procedure is organized with the following steps:

1. the input digital modulated signal is base-band translated and by using the I-Q components the signal constellation **G** is built;
2. the samples to be processed are decimated by eliminating the transition point between two different transmitted symbols. The vector X containing the complex values of the constellation is rearranged and the new decimated constellation **G'** is built;
3. the grid G is created on the basis of the theoretical constellation to be examined;
4. the grid is rotated of ψ producing $G' = Ge^{j\psi}$. The angle ψ corresponding to the maximum number of points of **G'** in the proximity of the constellation G', is the phase offset.

Fig.3.11 shows the constellation diagram of 16-QAM signal and SNR=1dB. In this case it is difficult to determine the transmitted symbol, but the contour shape is similar to that of the rotated constellation. The symmetry of

the constellation does not permit to recognize phase error over a threshold depending on both the digital modulation and the number of levels. For example, the maximum value of the phase offset that can be found in QAM and 4-PSK is 0.5π, in 8-PSK is 0.25π.

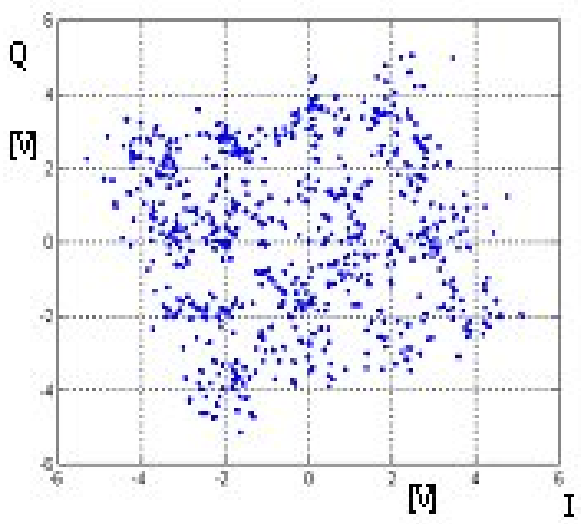

Fig. 3.11. Constellation of 16-QAM, SNR=1dB, $\psi = 0.1\pi$.

3.3.1 Numerical Tests

Numerical tests were performed preliminary in Matlab environment in order:

- to validate the characteristics of the method,
- to evaluate the effects and the propagation of the carrier frequency error on the phase offset evaluation.

It was assumed:

- carrier frequency fc=2kHz,
- symbol frequency fsymb=100 symbol/s,
- sampling frequency fs=20kHz.

The tests were performed by examining 100 different test signals for each digital modulation, and 30 ksamples for each test signal.

In the case of the carrier phase offset measurement, Tab.3.4 furnishes the standard deviation in the operating conditions characterised by the lower value of the SNR. These results support the theoretical developments and

denote that the proposed technique is particularly attractive and robust for low SNRs, too.

Table 3.4. Standard deviation of the carrier phase offset measurement.

Modulation	SNR [dB]	Standard deviation [ppm]
2-PSK	5	2,76
2-PSK	2	6,48
4-PSK	5	1,56
4-PSK	2	6,36
8-PSK	5	4,52
8-PSK	2	11,66
16-QAM	5	7,30
16-QAM	2	10,97
256-QAM		15 1,95
256-QAM	10	24,46

Other numerical tests were performed by simulating the modulated signals according to the UMTS [40]. All tests were performed by examination of 100 different test signals each one constituted by burst of 2560 chips. The carrier frequency was set to 38.46MHz and the sampling frequency equal to 153.84MHz. After the descrambling decoding, the values of the standard deviation are given in Tab.3.5.

Table 3.5. Standard deviation of the carrier phase offset measurement evaluated after the descrambling decoding.

SNR [dB]	Standard deviation [ppm]
10	7,2
20	4,1
30	1,2
40	0,7
50	0,4
60	0,4

The propagation of the error of the carrier frequency evaluation was taking into account and was analysed the influence on the correct phase offset evaluation. Fig.3.12 shows the trend of the error for the phase offset evaluation versus the carrier frequency error in the case of a) 8-PSK, b) 256 QAM, and c) UMTS signals. The stair shape of these curves highlight the low sensitivity and robustness of the proposed method.

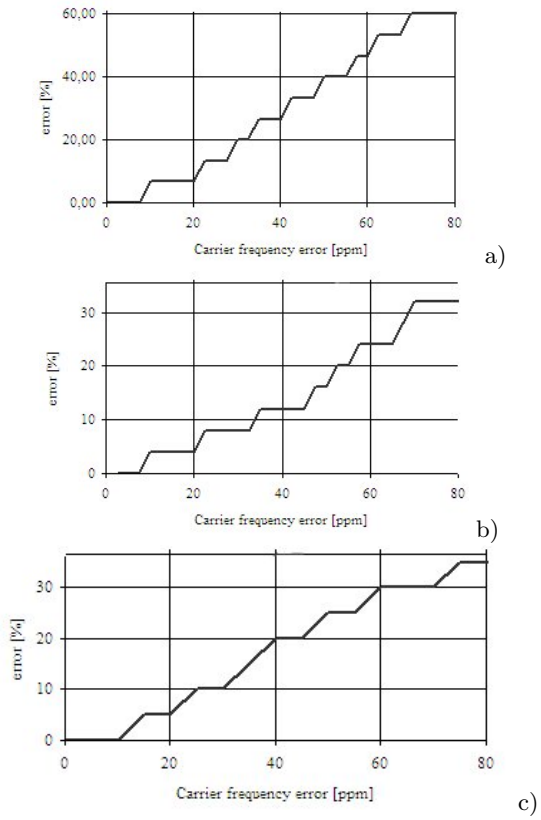

Fig. 3.12. Trend of the error for the phase offset evaluation versus the carrier frequency error in the case of a) 8-PSK, b) 256 QAM, and c) UMTS signals.

3.4 Experimental tests on phase offset measurement

In order to validate the proposed method in presence of actual signals, experimental tests were carried out in two different conditions:

- the digital modulated signals are generated in laboratory by programmable instruments according to the communication standards,
- the digital modulated signals are generated by programmable modems connected to the wired telecommunication network.

In order to generate in laboratory the digital modulated signals, the measurement station (Fig.3.13) is constituted by :

- the Signal Generator (SG), Agilent E4435C,
- the Data Acquisition board (DAQ), Signatec PDA 1000, on PCI bus,
- the control and processing unit implemented on a Personal Computer (PC), Compaq Evo W4000 at 1.8 GHz, and

- the interconnecting interface bus IEEE 488.2 between the PC and the SG.

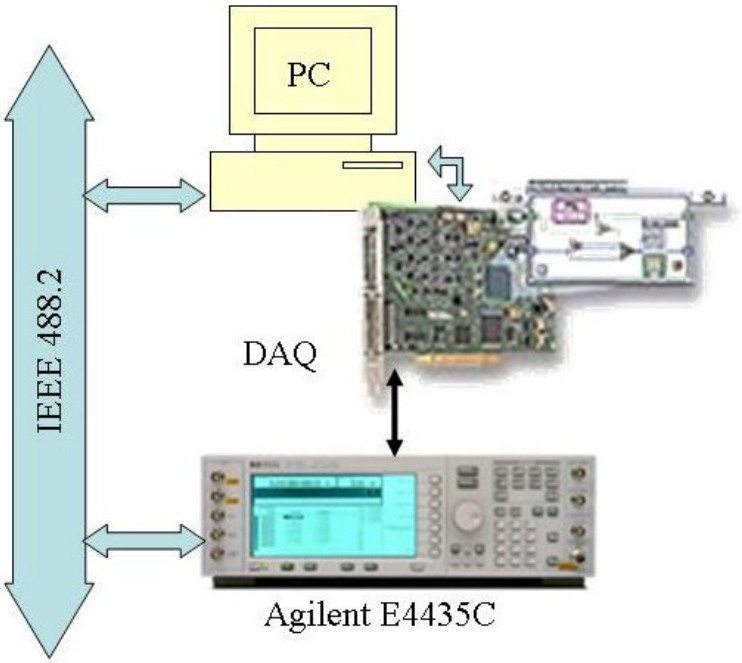

Fig. 3.13. Measurement station for experimental test on digital modulated signal.

The operating mode of the measurement station is:

1. the modulated signal is generated by the SG according to the specific standard under consideration, or, alternatively, is digitally synthesized, transferred to the local memory of the SG and given in output in the analogue form, in the case of specific requirements;
2. the DAQ digitises the analogue signal and passes the samples to the PC;
3. the PC implements the proposed method and controls the SG.

In order to assess the reliability and the efficacy of the technique, a number of tests have been carried out producing the same signals used in simulation. Successively, many experimental tests have been effectuated by considering the QAM signal produced according to the ETSI document TR 101 290 [38], and the QPSK signal according to the ETSI document EN 300 421 [39]. The results of all these experimental tests show that:

- the proposed method is particularly robust,
- the measurement accuracy is slightly greater than that characterizing the numerical tests,

- the experimental standard deviation is contained in few percents.

3.5 Conclusion

A general method is presented for measurement both the carrier frequency and the carrier phase offset for :

- the amplitude modulated signals:
  - M-ary Quadrature Amplitude Modulation
  - and M-ary Amplitude Shift Keying,
- the angle modulated signals:
  - M-ary Phase Shift Keying
  - M-ary Frequency Shift Keying.

Particular interest is devoted in developing the method to process the modulated signals of the UMTS standard.

By means of numerical tests the technique was validated and the measurement accuracy was evaluated versus different values of SNR.

Experimental tests are performed on actual signal generated according to:

- the UMTS standard,
- M-PSK and M-QAM according to V.92 and V.90 standards. These tests confirm the robustness and the accuracy of the method.

The method, the result of the numerical and experimental tests are published in the paper [12].

4

Amplitude and phase noise measurement for single carrier digital modulations

The amplitude and phase noise is of actual interest in the communication networks because degrades the quality of service and spoils the quality of the data transmission [53]-[56].

In literature, the methods for the amplitude and the phase noise measurement refer to sinusoidal signals without modulation. In particular, the amplitude noise is measured by analysing in the frequency domain:

- the power spectra obtained from the in phase (I) and in quadrature (Q) components [55],
- the two channel cross-correlation [56].

In [53] the phase noise measure is involved (L(fm)) directly on a spectrum analyzer. This measurement can be done as long as the analyzer has better phase noise than the measured source.

A second method uses a better source phase locked to the same frequency of the input signal with 90 of phase offset [53]. The mixed product of the unit under test and the reference signal is measured by using a FFT analyzer. The measurement of signal total power and calibration of the system is done by means of the premixing of input signal with a 1 kHz offset. This system has the best sensitivity in the range of -175 dBc/Hz. however, the reference synthetizer must be of supreme quality. The third method [54] uses a discriminator and compares the signal to itself delayed in time. This measurement is limited for close-in offsets, because a large part of close-in noise is canceled. The big advantage of this system is that it does not require an excellent reference.

Besides these methods, the phase noise can be measured by using a digital receiver. The sensitivity is limited with the dynamic range of the contemporary receivers, which is not higher than 150 dBFS/ $\sqrt{Hz}$. Also the frequency range is limited to the range of 100 MHz.

In all the methods for the phase noise measurement the signal is analysed in the time-domain [57] or in the frequency domain [58]-[61]. In the time-domain analysis, because the zero-crossing of the signal is taken into account,

the amplitude noise can influence the results. In the spectral analysis the results are greatly influenced by:

- the number of the processed samples,
- the shape of the noise taken into account.

In order to overcome these disadvantages, a new method to phase noise measurement is proposed in [33]. It is designed to measure the phase noise of the sinusoidal signal, and the single carrier digital modulated signal. In particular, the method concerns with the modulation that can be shown in the IQ plane as:

- the amplitude modulated signals:
  - M-ary Quadrature Amplitude Modulation (M-QAM),
  - and M-ary Amplitude Shift Keying (M-ASK),
- the angle modulated signals:
  - M-ary Phase Shift Keying (M-PSK).

This method requires the knowledge of both the carrier frequency and the carrier phase offset. These two parameters are previously evaluated on the basis of the approach shown in [1], [12] and discussed in Chapter 3.

In order to overcome the limitations and the difficulties of the previous considered measurement methods, it can be noted that in the IQ plane the shape of each symbol of the constellation is degraded from the theoretical one by the effect of both the amplitude noise and the phase noise, contemporaneously influencing the modulated signal. As shown in Fig.4.1, according to [62]:

- the phase noise is detectable by means of the angular excursion around the ideal symbol,
- the amplitude noise is detectable by means of the excursion of the module around the ideal symbol.

Therefore, in the IQ plane the complete information about the amplitude and phase noise can be detectable.

The extension of the method is proposed in [33] to measure both the phase and the amplitude noise on the sinusoidal signal, and the single carrier digital modulated signal. In this manner the limitation to operate only on the sinusoidal signal of the literature methods is overcame. Some features of the proposed method are:

- high measurement accuracy,
- amplitude noise and phase noise measured in separate way,
- unified approach for both sinusoidal signal and digital modulated signals corresponding to the schemes M-ASK, M-PSK, and M-QAM.

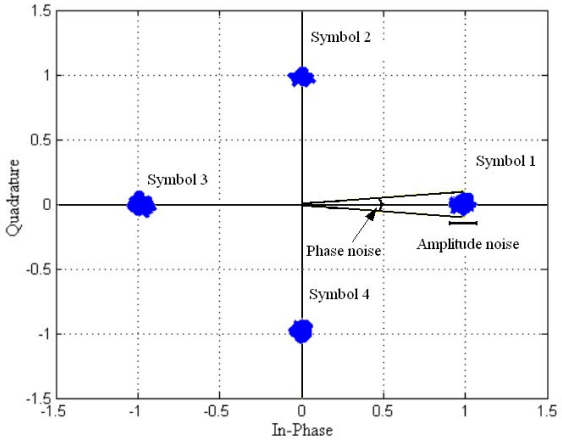

Fig. 4.1. Constellation of the 4-PSK modulated signal affected by amplitude and phase noise.

4.1 Amplitude and phase noise measurement

A unified approach for the amplitude and phase noise is proposed [33]. The method analyses the digital modulated signal affected by amplitude and phase offset down-converted in base-band. This one can be expressed as:

$$s_d(t) = \sum_k (A_k + \alpha_c(t)) e^{j[\phi_c(t)+\varphi_i]} g(t - kT_s) \tag{4.1}$$

where: φ_i is the phase angle characterizing the modulation scheme and it is well known, A_k maps the transmitted symbols, T_s is the symbol time, g(t) is the finite energy signal with the T_s duration, $\phi_c(t)$ is the instantaneous phase noise fluctuation of the transmitted carrier signal, $\alpha_c(t)$ is the instantaneous amplitude noise fluctuation of the input signal. The values of A_k for M-ASK, M-PSK and M-QAM modulations are given in chapter 3 and reported in Tab.4.1.

Table 4.1. Expression of the carried information A_k

Digital modulation	Carrier information A_k
M-ASK	$A_k = 2i - M - 1, \quad i = 0, 1, ..., M-1$
M-PSK	$A_k = e^{j\frac{2\pi i}{M}}, \quad i = 0, 1, ..., M-1$
M-QAM	$A_k = a_k + jb_k, \quad a_k, b_k = 2i - M - 1, \quad i = 0, 1, ..., M-1$

Moreover, the values of φ_i are: φ_i=cost for M-ASK, $\varphi_i = 2\pi i/M$ for M-PSK, $\varphi_i = atan(b_k/a_k)$ for M-QAM.

Because the signal is filtered in base-band, according to the scheme of Fig.4.3, $\alpha_c(t)$ and $\phi_c(t)$ could differ from that affecting the modulated signal at the transmission frequency. From 4.1 it is:

$$mod(s_d(t)) = A_k + \alpha_c(t) \tag{4.2}$$

$$arg(s_d(t)) = \phi_c(t) + \varphi_i \tag{4.3}$$

As it can be deduced from the (4.2) and (4.3), the amplitude and phase noise influence in the same manner all the transmitted symbols. As a consequence the following consideration holds:

- the modulated signal can be examined in the IQ plane in order to detect the amplitude and phase noise;
- all the symbols in the IQ plane can be grouped in only one, named Virtual Symbol (VS), as shown in Fig.4.2, in order to reduce the number of samples to be acquired by the Analog-to-Digital Converter (ADC).

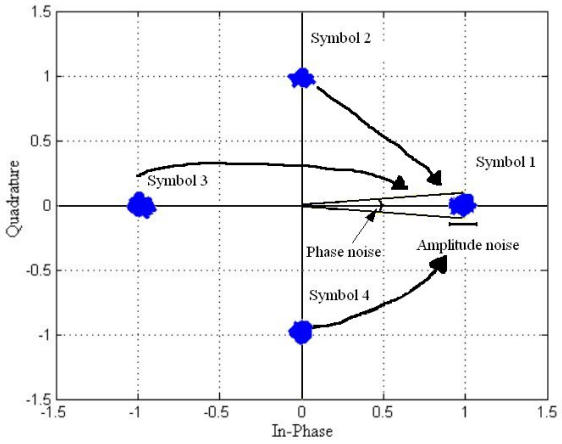

Fig. 4.2. Virtual Symbol creation with a 4-PSK constellation affected by amplitude and phase noise.

In order to reduce the real constellation to the VS, the rotation and translation operator must be determined. The proprieties of this operator are the following:

- all the real symbols in the neighbourhood of the ideal symbol must be translated and rotated of the same entity to avoid the real symbol alteration;
- the operator don't distort the signal;

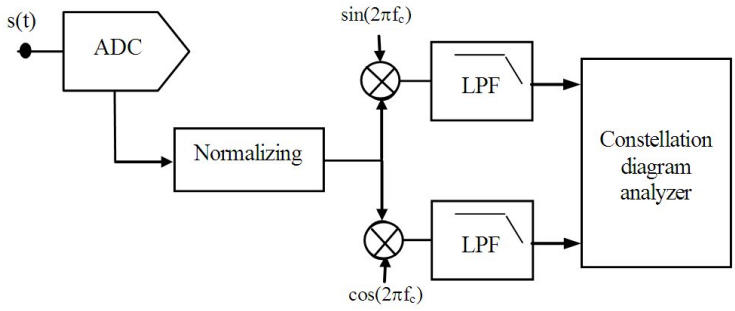

Fig. 4.3. Block diagram of the digital down conversion and the low pass filtering before the IQ plane analysis.

- the entity of the rotation and translation depend on:
  - the ideal symbol coordinate,
  - the virtual symbol coordinate.

Therefore, according to the M-ASK, M-PSK and M-QAM digital modulations taken into account, the rotation and translation operator is defined as:

$$\xi = \frac{1}{A_k e^{j\varphi_i}} \tag{4.4}$$

By applying the rotation and traslation operator only one symbol, the VS, is to be considered.

Numerical tests were performed to assess that the VS is not the deformed transformation of the real symbol. Results of the tests by referring to the amplitude noise are shown in Fig.4.4. In particular:

- Fig.4.4a shows the trend of the noise evaluated on the VS on the basis of the previous transformation;
- Fig.4.4b shows that the noise of Fig.4.4a has Gaussian distribution;
- Fig.4.4c shows that the difference between the noise distribution superimposed to the symbol of the input signal and the noise distribution evaluated on the VS is small.

Other numerical tests were performed in similar manner, by referring to the phase noise. Also these tests confirm that the VS can be used to amplitude and phase noise measurement. As a consequence, the VS is characterized by:

- high number of samples if compared with the original symbols,
- amplitude and phase noise distribution as on the original symbols.

On the basis of these results, the proposed method introduces the novelty to take into account and to use the VS, only. Therefore, the phase noise is measured by evaluating on the VS the peak of the angle fluctuations around

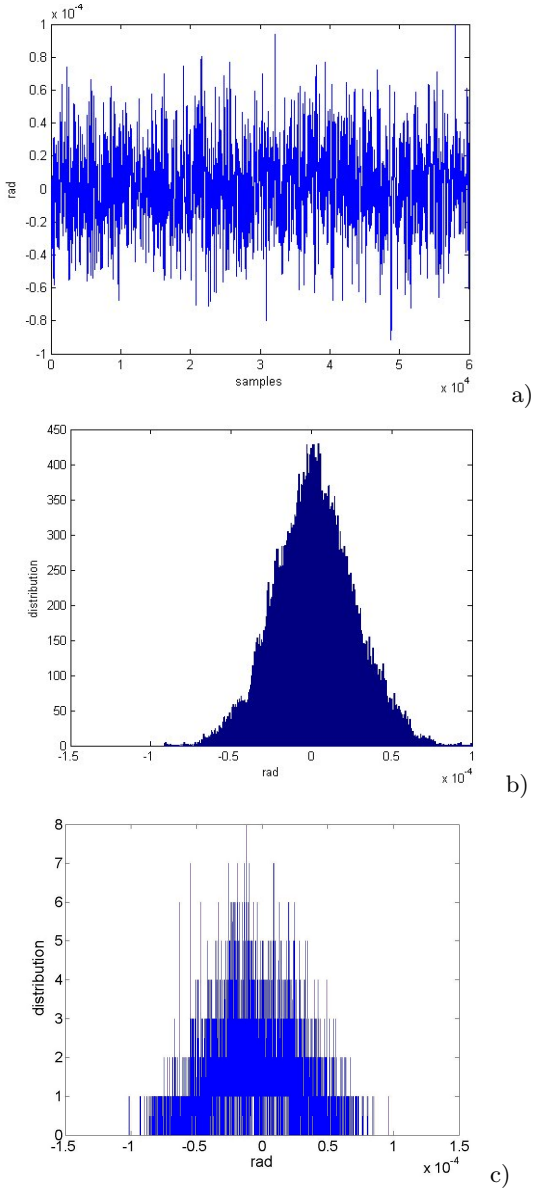

Fig. 4.4. a) Noise estimation performed on the virtual symbol; b) noise distribution evaluated on the virtual symbol, c) difference between the noise distributions on the symbol of the input signal and the noise distribution evaluated on the virtual symbol.

the ideal symbol. The amplitude noise is measured by evaluating on the VS the RMS of the module fluctuation around the ideal symbol.

In the case the carrier phase offset ψ occurs in the signal demodulation, each symbol in the constellation is rotated of the angle ψ from the ideal symbol [63]. The method can be always used, but it needs:

- the phase offset ψ to be detected according to the method shown in [63],
- to taken into account that the real symbol is rotated.

4.1.1 Phase and amplitude noise measurement on standard modulated signal

In order to perform the phase and amplitude noise measurement in the case of standard modulated signal, the pre-processing stage must be performed to separate and to extract the noise components from IQ plane representation. Indeed, the real digital signal transmitter uses the signal filter that limits the output signal band according to the transmission standard. This filter modifies both the amplitude and the phase trend in the time domain. In particular, Fig.4.5 shows the real signal according to the DVB standard [63]. As a consequence, the shape of the base-band signal representation into the IQ plane, Fig.4.6, is deformed and altered from that characterising the signal without the cosine rise filter. The links among the symbols in the IQ plane are a consequence of the band limiting filter. Therefore, the shape of all the symbols are deformed and the measurement of the phase and amplitude noise values by operating on the VS is not correct. The correct measurement can be achieved once the effects of the band limiting filter on the symbol shape are eliminated or reduced.

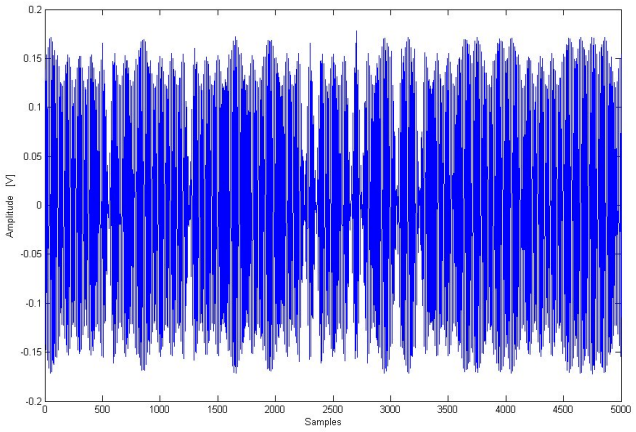

Fig. 4.5. Real DVB signal in the time domain.

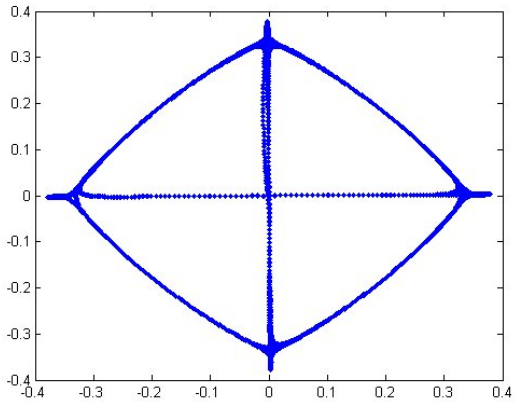

Fig. 4.6. IQ plane representation of the base-band translated real DVB signal.

According to the previous analysis, the procedure pointed out to separate and to extract the noise components from IQ plane representation can be based on the following steps:

- *signal decoding*: the input signal is decoded in order to determine the transmitted symbols. In this stage is important that the demodulator is robust and low sensitive to both distortion and noise. On the basis of the previous experience [64] the Artificial Neural Network based decoder can be conveniently used.
- *coded signal reconstruction*: according to the decoded symbols, the new coded signal is reconstructed. The same standard characterising the original signal is followed. In particular, attention is devoted to the filter defined in the standard recommendations.
- *VS building*: the VS is determined by subtracting to the IQ plane representation of the original coded signal the IQ plane representation of the coded signal reconstructed.

The properties of the resulting VS are:

- position near the origin of the IQ axis,
- high number of samples if compared with the original symbols,
- amplitude and phase noise distribution as on the original symbols,
- invariance of the amplitude noise and phase noise, if compared to that evaluated on the original symbols.

All these properties can be verified by numerical analysis. By excluding the first, all the remained properties are common to the VS determined as for the previous paragraph valid in the case the band limiting filter is not considered.

4.1.2 Numerical Tests

Numerical tests were performed in MATLAB environment in order to validate the method, and to asses the measurement accuracy. In all the tests it was assumed:

1. both the amplitude and the phase noise characterized by Gaussian distribution,
2. peak value of the phase noise in the range [10-4, 5*10-3] rad,
3. RMS value of the amplitude noise in the range [4*10-4 , 2.4*10-3]V,
4. carrier frequency f_c in the range [10, 50] kHz,
5. ratio between the sampling frequency f_s and f_c equal to 102.

In order to evaluate the measurement accuracy, the percentage error versus the assigned value was estimated.

The results for 4-PSK modulated signal are given. Fig.4.7 shows the trend of the percentage error of the phase noise estimation versus the assigned peak value of the phase noise. Fig.4.8 shows the trend of the percentage error of the RMS amplitude noise estimation versus the assigned RMS percentage of the amplitude noise.

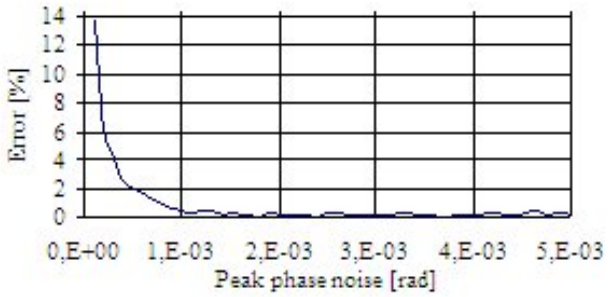

Fig. 4.7. Trend of the percentage error of the peak phase noise estimation versus the assigned peak value of the phase noise.

Moreover, the method accuracy is compared to that of the method based on the FFT analysis. It is assumed a sinusoidal signal, a ADC resolution equal to 16 bit, and 1024 samples for the FFT computation. Fig.4.9 shows the percentage error trend of the amplitude noise measurement in the case of the IQ based method and the FFT based for different RMS percentage values of the amplitude noise. Fig.4.10 shows the percentage error trend of the phase noise measurement in the case of the IQ based method and the FFT based for different values of the phase noise. The IQ based method is characterized by constant and very small error value. In the case of the FFT based method the error oscillates as the amplitude noise increases, and increases as the

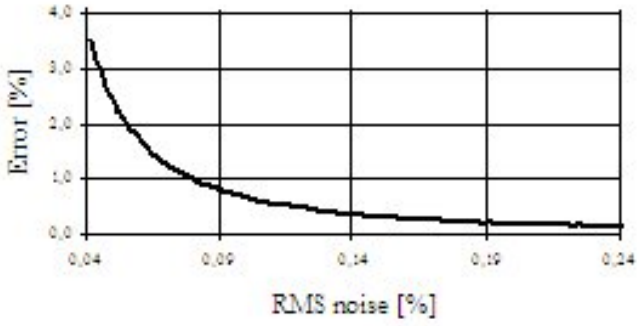

Fig. 4.8. Trend of the percentage error of the RMS amplitude noise estimation versus the assigned RMS percentage of the amplitude noise.

phase noise increases. Other tests confirm that only in the case of FFT the number of samples influence the error. The tests performed confirm that the method shows quite the same characteristics in the case of modulated signal and sinusoidal signal. In particular, for small values of the amplitude and phase noise the error increases for the modulated signal respect to the error in the case of sinusoidal signal.

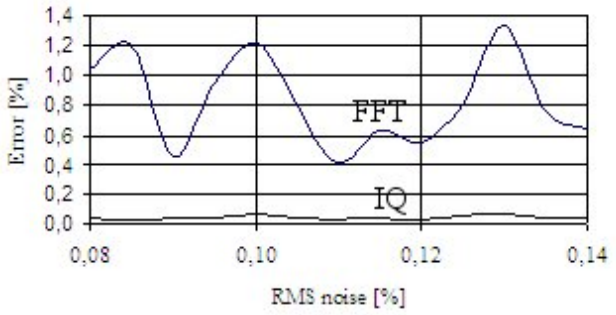

Fig. 4.9. Comparison between the percentage error trend in the case of the IQ based method and the FFT based method for different values of the amplitude noise.

Other tests are devoted to determine the influence of the phase noise on the amplitude noise measurement and vice versa. Fig.4.11 shows the trend of the ratio between the RMS value of the amplitude noise measured and the RMS value of the amplitude noise assigned in the case of sinusoidal signal affected by the phase noise with maximum amplitude equal to 0.001 rad and 0.002 rad, respectively.

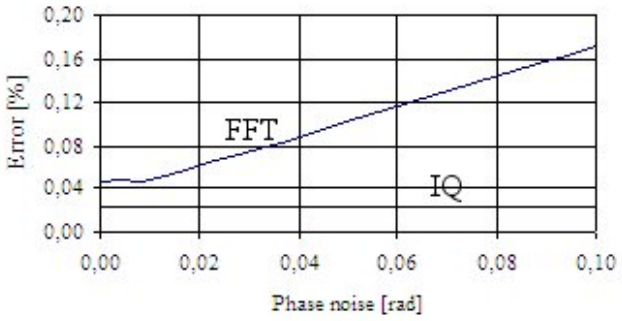

Fig. 4.10. Comparison between the percentage error trend in the case of the IQ based method and the FFT based method for different values of the phase noise. The FFT is computed on 1024 samples.

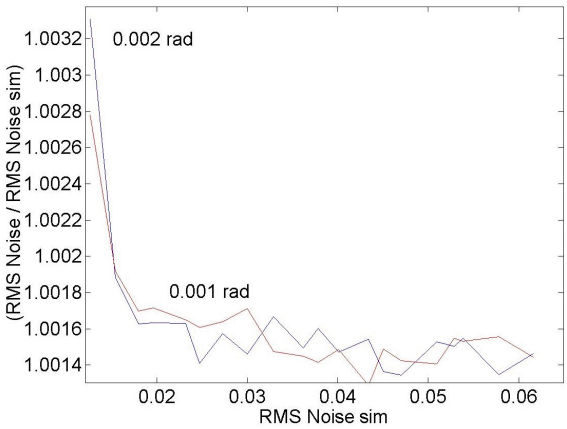

Fig. 4.11. Trend of the ratio between the RMS of the amplitude noise measured and the RMS of the noise assigned for sinusoidal signal corrupted by peak value of phase noise equal to 0.001 rad and 0.002 rad, respectively.

Other tests are performed to estimate the influences of the amplitude noise on the phase noise measurement. The results are shown in Fig.4.12.

The results shown in Fig.4.13 and Fig.4.14 include the effects of the ideal digital conversion performed by 8 bit ADC. As shown in Fig.4.13 the phase noise measurement error is lightly varying if 16 bit or 8 bit is considered. Lower ADC bit number influences both the amplitude and phase noise measurement.

4.1.3 Method performance

Measurement tests are developed to establish the performance of the method with the modulated input signal. In all the tests it was assumed amplitude

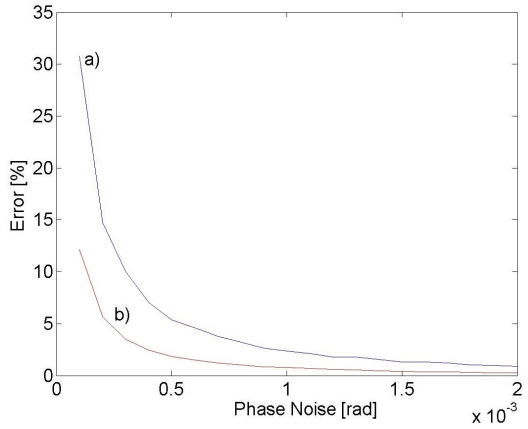

Fig. 4.12. Percentage error trend for the phase noise measurement in the case of sinusoidal signal corrupted by amplitude noise and RMS equal to a) 0.0126 [V] b) 0.00251 [V], respectively.

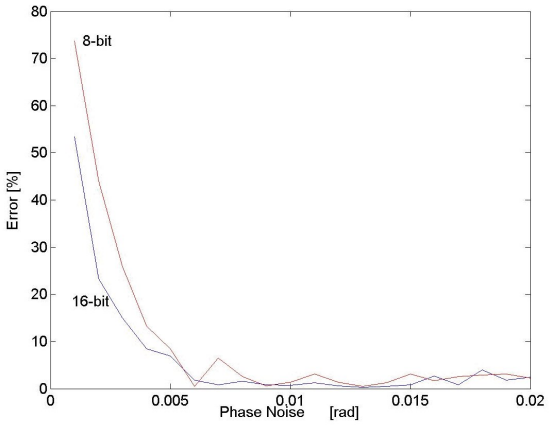

Fig. 4.13. Trend of the phase noise measurement error with sinusoidal signal and 16 bit and 8 bit ADC.

noise and phase noise influencing the signal simultaneously. Fig.4.14 shows the trend of the phase noise measurement error for the 4-ASK, 4-PSK and 16-QAM modulated signal affected by different values of the amplitude noise. It is evident that the error increases as the amplitude noise increases.

Fig.4.15 shows the trend of the amplitude noise measurement error for the previous modulated signal affected by different values of the phase noise. Also in this case the measurement error increases as the phase noise increases. All

the tests show that the percentage of measurement error decreases as the both amplitude and phase noise increase.

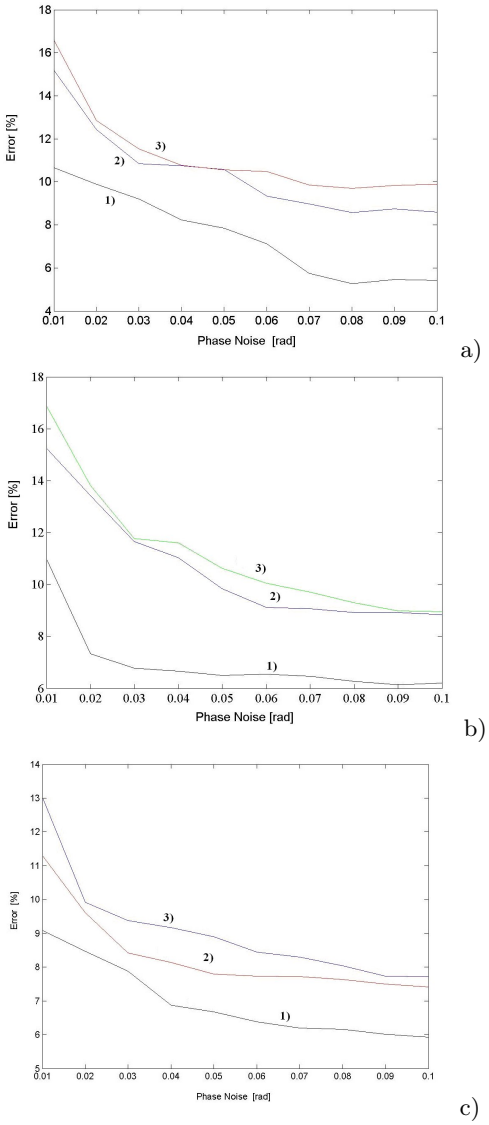

Fig. 4.14. Trend of the percentage error in the phase noise measurement for a a) 16-QAM., b) 4-ASK and c) 4-PSK signal with 8 bit ADC and the RMS amplitude noise equal to 1) 0 V, 2) 1e-5 V, and 3) 1e-4V, respectively.

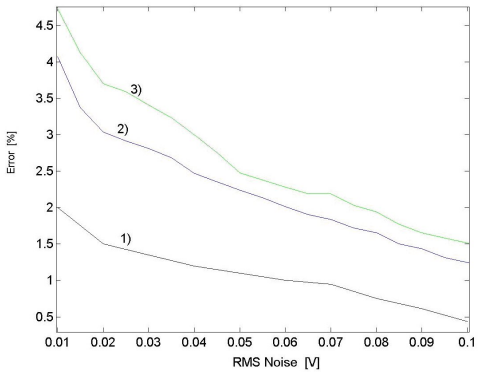

a)

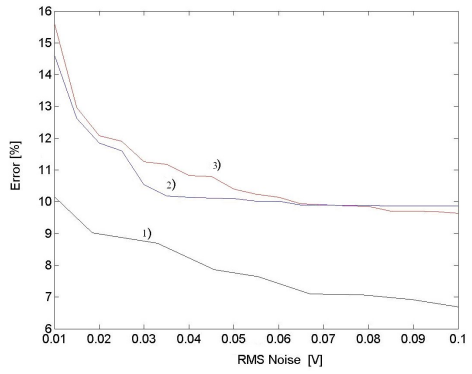

b)

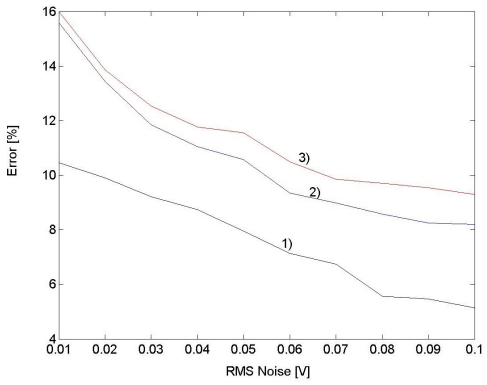

c)

Fig. 4.15. Trend of the percentage error in the amplitude noise measurement for a) 16-QAM, b) 4-ASK and c) 4-PSK signals with 8 bit ADC and phase noise amplitude equal to 1) 0 rad, 2) 5*10e-4 rad, and 3) 5*10*e-3 rad, respectively.

4.2 Experimental tests

Experiment tests was performed by using DVB standard signals [63]. The digital modulation is the QPSK, the filter defined into the standard is the cosine roll-off filter with roll-off factor equal to 0.35 [39].

The measurement station (Fig.4.16) is made up of:

- control and processing unit implemented on a Personal Computer (PC),
- vector signal generator Agilent e4438c esg,
- LeCroy sda 6000A serial data analyzer
- interconnecting interface bus realized by IEEE 488.2.

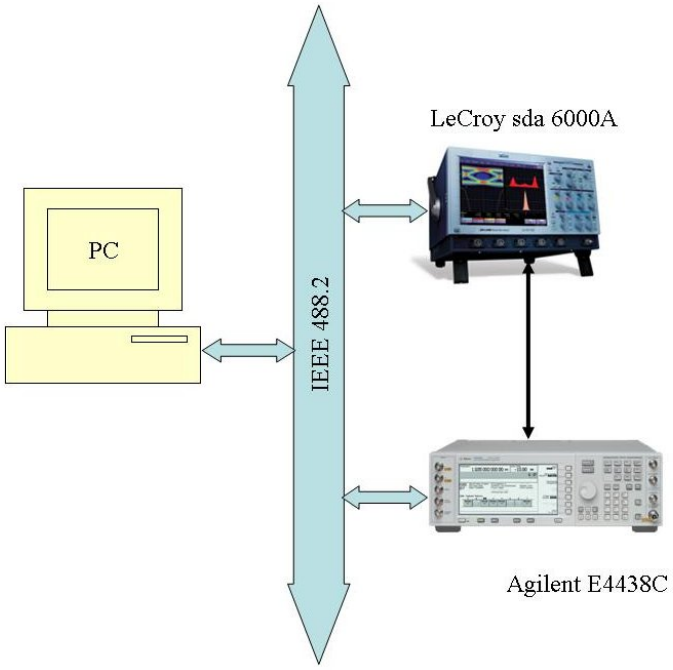

Fig. 4.16. Measurement station for experimental test on DVB signal.

Fig.4.17 shows the percentage error trend of the amplitude noise measurement versus the assigned RMS amplitude noise. The error is quite constant and lower of 6%.

Fig.4.18 shows the percentage error trend of the phase noise measurement versus the assigned phase noise. The error degreases as increases the assigned phase noise value.

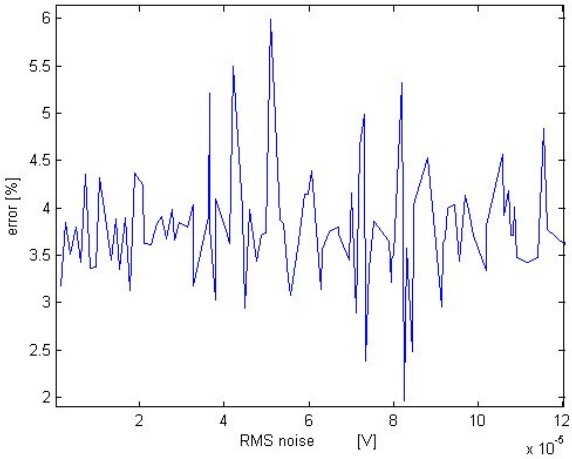

Fig. 4.17. Percentage error trend of the amplitude noise measurement versus the RMS amplitude noise value for the DVB standard signal.

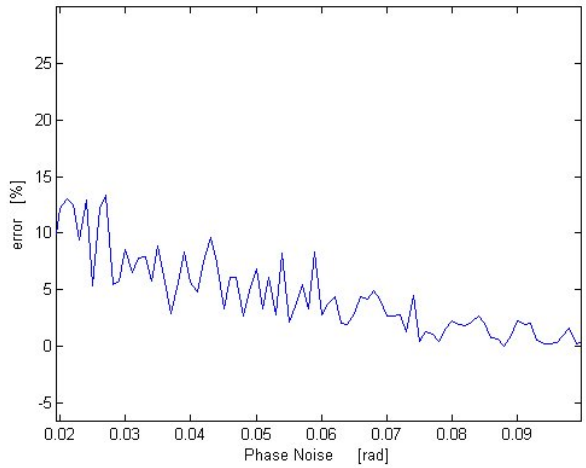

Fig. 4.18. Percentage error trend of the phase noise measurement versus the assigned phase noise value for the DVB standard signal.

4.3 Conclusion

The new method for both the phase and the amplitude noise measurement is proposed. It is able to operate on both the sinusoidal signal and the single carrier digital modulated signals of the modulation schemes M-ASK, M-QAM and M-PSK.

The method is based on the analysis in the IQ plane of the signal translated on base-band. The numerical tests support the theoretical developments. Moreover, these tests denote that the method is particularly attractive, robust, and accurate if compared with the method based on the frequency domain analysis.

The experimental results confirms the robustness and the accuracy of the proposed method.

To use the method with digital standard modulated signal some preliminary steps are necessary. The results of the tests confirm the possibility to use the same method for every standard taking into consideration.

The method, the results of the numerical and experimental tests are published in the paper [33].

5

Symbol timing measurement for single carrier digital modulations

The measurement of the symbol timing of the transmitted digital modulated signal is of actual interest in the communication networks. In fact, this measure is necessary to permit the receiver synchronization without transmitting the pilot sequence. Potential applications include blind synchronization of high speed communication networks, passive listening and automatic classification of digital modulations [65].

The approaches followed in literature to estimate the symbol timing are based on:

- the theory of maximum likelihood estimation,
- the second-order cyclostationary statistics.

The method based on the maximum likelihood estimation is presented in [66]. The performance of this method shows that it can be conveniently used for Binary Phase Shift Keying (B-PSK) modulation, with and without phase and small frequency offsets.

The cyclostationary statistic approach is applied in [65], [67] in order to blind estimate the symbol timing by over-sampling a sequence of unknown symbols. Moreover, in [68] and [69] it is assessed that using two samples per symbol the estimation accuracy of the new estimator is similar to that of the conventional estimator which requiring more samples per symbol. Nevertheless, the estimator convergence is greatly influenced by the sample number of the processed signal.

The new method is proposed [12] in order to overcome the convergence problems of the typical measurement method. It is designed:

- to measure the symbol timing by means of statistical analysis,
- to be used for several types of single carrier digital modulations,
- to be integrated in the intelligent measurement instrument able to characterize the signaling quality whichever digital modulation is used [1].

The method operates after a previous block that measure both the carrier frequency and the phase offset of the single carrier modulated signal. These parameters are evaluated on the basis of the approach shown in [12], [63].

The proposed method operates on the base band signal and it performs the symbol timing measurement by using the information coming out from these two previous blocks, in addition to the sampled modulated signal.

The approach followed is based on the statistical analysis of the digital modulated signal. The symbol timing is evaluated once the occurrences of the consecutive repetition of the virtual symbol are detected. This approach is particular convenient and permits to realise a very fast and reliable method.

In the following paragraph this method is described in dept.

5.1 Symbol time measurement

The model of the single carrier modulated signal under analysis, after the down conversion in the base band and the appropriate filtering, results:

$$y_n = e^{j[\theta(t)]} a_n + w_n \tag{5.1}$$

where $\theta(t) = 2\pi f_{err} t + \varphi$, with f_{err} the carrier frequency error and φ the phase offset error between the transmitted carrier signal and the received one occurred during the demodulation, a_n the transmitted symbol, and w_n the Gaussian noise. In the following, φ and f_{err} are assumed to be constant. This assumption is not restrictive and the results remain true if φ and f_{err} are assumed to be lightly variable.

The steps of the method for measuring the symbol timing (T_{Symb}) are [34]:

1. *Demodulate the input signal.* The modulated input signal is demodulated with a very short symbol timing $T_{Symbmin}$;
2. *Define a number of length.* The different virtual symbols, each one defined by the virtual symbol timing $T^V_{Symbmin}$, are detected on the demodulated signal. The length of the consecutive repetition of the virtual symbols define the symbol classes, each one identified by the parameter ρ equal to the length;
3. *Determinate the occurrences of each virtual symbol.* The vector Y containing the occurrences of each symbol class is determined;
4. *Evaluate the real symbol timing* (T_{Symb}). In the vector Y are eliminated the very small length, generated by the passage from a symbol to another in the demodulated signal. After the histogram of the occurrences versus the parameter ρ of the symbol classes stored is determined using Y. The maximum value of the occurrences permits to select ρ_{max}. Then, it is $T_{Symb} = \rho_{max} T_{Symbmin}$.

Some considerations need in the case of the M-PSK modulated signals of the UMTS standard [70]. The symbol timing must be measured after the descrambling decoding and before the despreading decoding.

In order to better exploit the method operation mode, in the following the symbol timing measurement in the case of 16-QAM modulation is taken into account. Fig.5.1a shows the demodulated 16-QAM signal with SNR=20dB and assigned symbol timing TSymb=20ms. Fig.5.1b shows the same signal demodulated with TSymbmin=0.5 ms. It can be noted that the symbols are varying at the same time, but it need to determinate when a symbol really terminates.

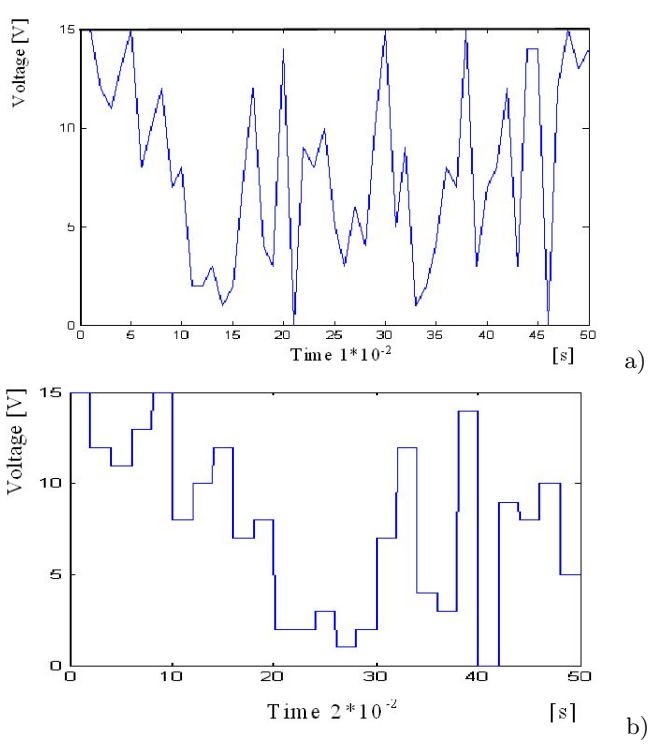

Fig. 5.1. Demodulated 16-QAM signal with SNR=20dB and (a) $T_{Symb} = 20ms$, and (b) $T_{Symbmin} = 0.5ms$.

In the case of the signal of Fig.5.1b, the Fig.5.2a shows the histogram of the occurrences of the symbol classes stored in the vector Y versus the parameter ρ. Then, it is $\rho_{max} = 40$ and, consequently, as expected, it is $T_{Symb} = 40 * 0.5ms = 20ms$.

The noise presence causes more variation in the demodulated signal. As a consequence, the number of the classes of virtual symbols increases. These new classes are characterized by the reduced number of occurrences. As an example, Fig.5.2b shows the histogram for 16-QAM modulated signal in the case of SNR=12dB, TSymb=20ms, and TSymbmin=0.5 ms. By means of

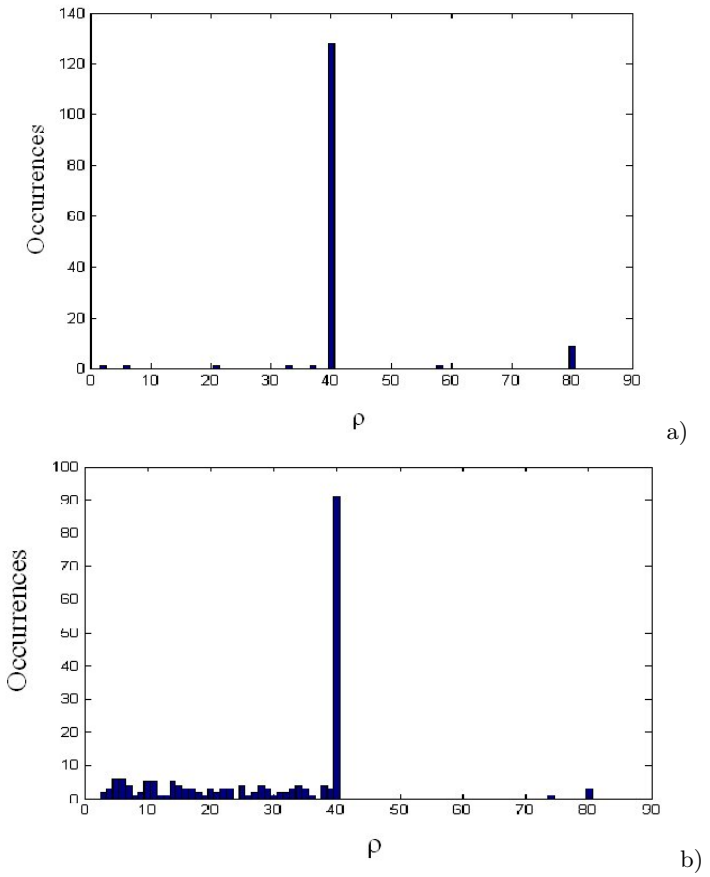

Fig. 5.2. Histogram of the virtual symbol occurrences versus the parameter ρ, for 16-QAM a) SNR=20dB, and b) SNR=12dB.

numerical tests it has been assessed that up to the limit value of SNR=10 dB the method is low sensitive to the noise in the case of the modulations M-ASK, M-FSK, M-PSK and M-QAM.

Some considerations need in the case of the M-PSK modulated signals of the Universal Mobil Telecommunication System (UMTS) standard [70]. The UMTS standard imposes:

- the scrambling code in order to realize the transmission with frame Wide-band Code Division Multiple Access (W-CDMA),
- the spreading code in order to realize the multi-user transmission.

The scrambling code consists of multiplying the modulated signal by a pseudo-casual sequence of +1, 0 and -1. It operates on the transmitted symbol so as to cover the symbol timing. Therefore, the symbol timing must be

measured after the descrambling decoding and before the despreading decoding. In this condition the modulated signal is similar to that previous taken into account. In the case the scrambling code are not known a priori, in the UMTS standard the generation key of the pseudo-casual scrambling code is well defined. Therefore, by means of the cross correlation operation it is possible to detect the scrambling code sequence.

5.2 Numerical tests

Numerical tests were performed preliminary in MATLAB environmental in order to validate the method with:

- superimposed noise to the signal,
- modulated signal according to the UMTS standard.

5.2.1 Modulated signal and superimposed noise

In all the tests it was assumed carrier frequency $f_c = 2kHz$ and a sampling frequency $f_s = 10kHz$. The tests were performed by examining:

- 100 different test signals for each digital modulation,
- 30 ksamples for each test signal.

In order to evaluate the measurement results, the influence of the oversampling period $T_{Symbmin}$, and the SNR was investigated. The modulations taken into account were: M-ASK, M-FSK, M-PSK and M-QAM. In the tests, the parameter ρ defined at step 2 of the method, was assumed to be integer values. Operating in this condition, the method furnishes the correct symbol timing or, alternatively, the inconsistent value. Tab.5.1 shows the success percentage for the correct symbol timing measurement for:

- the digital modulations taken into account,
- different values of both T_{Symb} and $T_{Symbmin}$,
- the limit value of SNR=12 dB.

The success percentage decreases as the SNR decreases.

The numerical tests support the theoretical developments and denote that the proposed method is particularly attractive and robust.

5.2.2 Modulated signal according to UMTS standard

Other numerical tests were performed by simulating the modulated signals according to the UMTS standard [40]. In the simulations were considered:

- the chip rate equal to 3,84Mcps,
- the carrier frequency equal to 10 times the chip rate,
- the sampling rate equal to 80 times the chip rate,

Table 5.1. Success percentage for the correct symbol timing measurement for different single carrier modulations and SNR=12dB.

Modulation	Tsymb [ms]	$T_{Symbmin}$ [ms]	Success [%]
4-ASK	40	2	99
8-ASK	40	2	98
8-ASK	50	0.5	95
8-ASK	50	1	91
8-ASK	50	2	95
16-QAM	40	20	100
16-QAM	50	1	100
16-QAM	50	2	100
256 QAM	50	2	67
2-PSK	50	1	98
2-PSK	50	2	93
4-PSK	50	1	100
4-PSK	50	2	100
8-PSK	50	1	100
2-FSK	50	1	96
2-FSK	50	2	97
4-FSK	50	1	100
4-FSK	50	2	100

- the burst constituted by 2560 chips.

Moreover, the Additive White Gaussian Noise (AWGN) was superimposed to the modulated signals.

In order to perform the symbol timing measurement, the modulated signal was considered after the descrambling decoding, but before the despreading decoding for some spreading code. The symbol timing was evaluated by counting the consecutive repetition of the chip into the symbol. The occurrences of the consecutive chip repetition for the UMTS signal with SNR=10 dB are shown in Fig.5.3. By referring to the maximum value of the occurrences equal to 128, the symbol timing is equal to $33.33\mu s$.

Further numerical tests were performed by analysing different sets of test signals, each set defined by 100 signals and different values of both the symbol time and the SNR. The success percentage for the symbol timing measurement versus different values of the SNR and the consecutive chip repetition per symbol is given in Tab.5.2. From Tab.5.2 it can be noted that the percentage of correct evaluation of the symbol timing with larger number of consecutive chip repetition is lower of the percentage of correct evaluation of the symbol timing with smaller number of consecutive chip repetition in presence of the signal degradation. In fact, if the number of spreading factor is low, less symbols are transmitted in the burst, so the incorrect chip recognition can exceed the correct chip recognition, as a consequence of the superimposed noise.

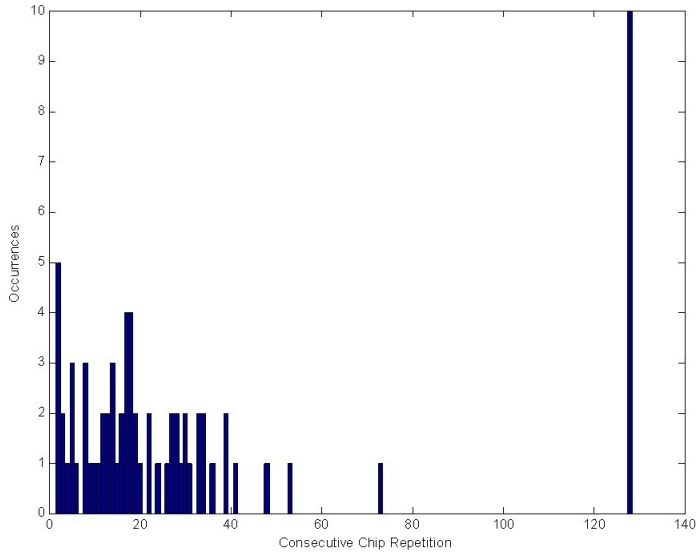

Fig. 5.3. Histogram of the consecutive chip repetition for the UMTS signal and SNR=10dB.

Table 5.2. Success percentage for the correct symbol timing measurement for UMTS signal and different value of the SNR and consecutive chip repetition.

Consecutive chip repetition per symbol 128	Consecutive chip repetition per symbol 64	consecutive chip repetition per symbol 32
29	89	100
53	100	100
98	100	100
100	100	100
100	100	100

5.3 Experimental tests

In order to validate the proposed method, experimental tests were carried out on actual signals. Two different sets of tests were performed. The first set is devoted to assess the reliability and the efficacy of the method, and the experimental tests were carried out producing the same signals used in simulation by means of an Arbitrary Waveform Generator (AWG).

The second set is devoted to assess the influence of the telecommunication standard on the method performance, and the experimental tests were carried out on:

- GMSK modulated signals of the GSM standard,

- 2-FSK modulated signals with not integer number of the carrier period per symbol,
- digital modulated signals generated by programmable modems connected to the wired telecommunication network.

5.3.1 Modulated signals by AWG

A suitable automatic measurement station was set up to assess the reliability, the efficacy and the accuracy of the method on processing the modulated signals digitised by means of an actual digitiser. The measurement station is shown in Fig.5.4 was constituted by:

- AWG Sony-Tektronix AWG 2021, working in base band,
- Digital Storage Oscilloscope (DSO) Tektronix TDS7154B,
- control and processing unit implemented on Personal Computer (PC), Compaq Evo W4000 at 1.8 GHz,
- interconnecting interface bus IEEE 488.2.

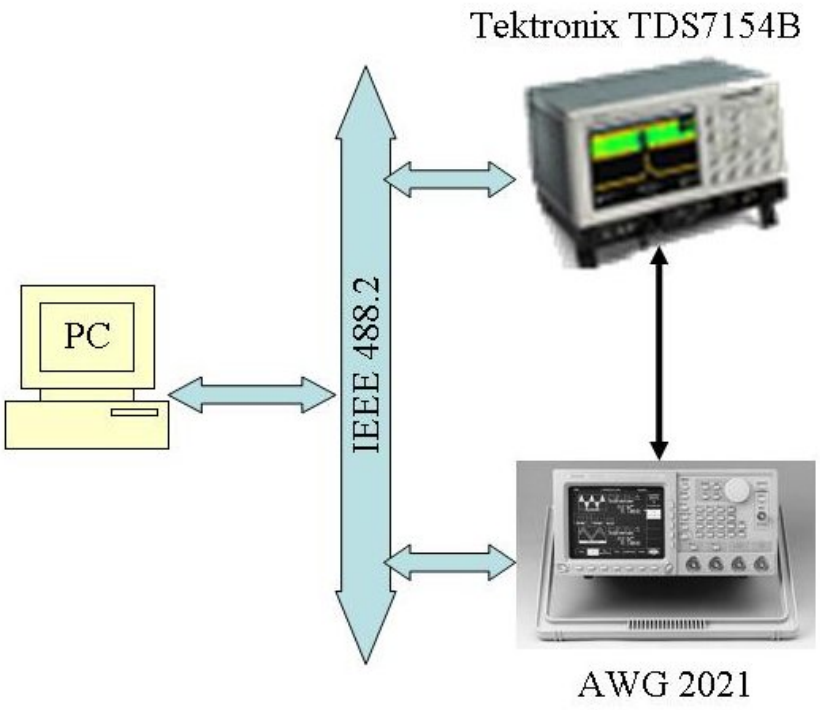

Fig. 5.4. Measurement station for experimental test on digital modulated signal by AWG.

The operating mode of the measurement station is:

1. the modulated signal digitally synthesized is transferred to the local memory of the AWG and given in output in the analogue form;
2. the DSO digitises the input analogue signal and transfers the samples to the PC by means of the IEEE 488.2 interface;
3. the PC implements the measurement method and controls the AWG.

Experimental tests were carried out by considering:

- the M-ASK, M-FSK, M-PSK modulated signals;
- the QAM signal produced according to the ETSI document TR 101 290 [38];
- the QPSK signal according to the ETSI document EN 300 421 [39].

The results of the experimental tests show that the method is particularly robust, the measurement uncertainty is slightly greater than that characterizing the numerical tests, and the experimental standard deviation is contained in few percents.

5.3.2 Modulated signals according to telecommunication standard

Suitable automatic measurement station was set up to analyse the modulated signal of the GSM standard. It was constituted by:

- RACAL 6113E GSM Signal Generator,
- Digital Scope Tektronix TDS154B,
- HP 8594E Spectrum Analyzer (SA),
- control and processing unit implemented on PC Compaq Evo W4000 at 1.8 GHz,
- interconnecting interface bus IEEE 488.2.

The generator worked at RF with carrier frequency equal to 908.2MHz and was able to generate the modulated signal according to the standard GSM 900 Burst. By using the SA the signal was down converted at the IF equal to 21.4 MHz. Successively, the signal was acquired at the sampling rate of 200MS/s, translated in the base band in digital way, and processed to extract the phase information. The phase trajectory was decimated by the factor 90, so the resulting sample rate of the signal was equal to 2,22 MS/s. At this sampling rate of the signal results 9 samples per bit.

Tests were carried out on:

- signal constituted by the sequence 0000,
- signal constituted by the sequence 1111,
- signal of the control channel.

By referring to the histograms of Fig.5.5a and Fig.5.5b the error for the symbol timing measurement was one sample for both the sequences 0000 and 1111

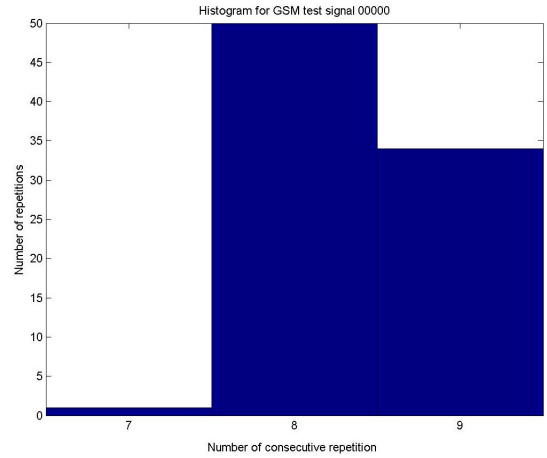

a)

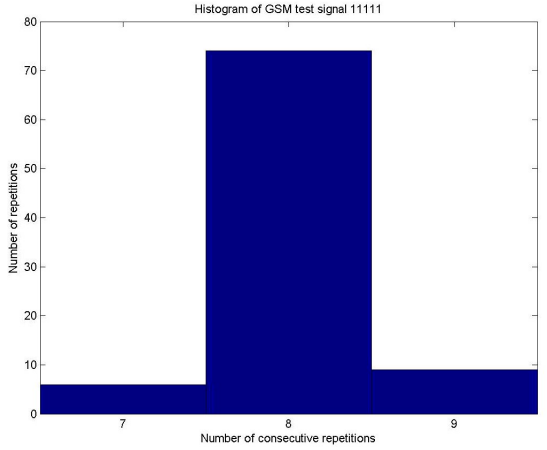

b)

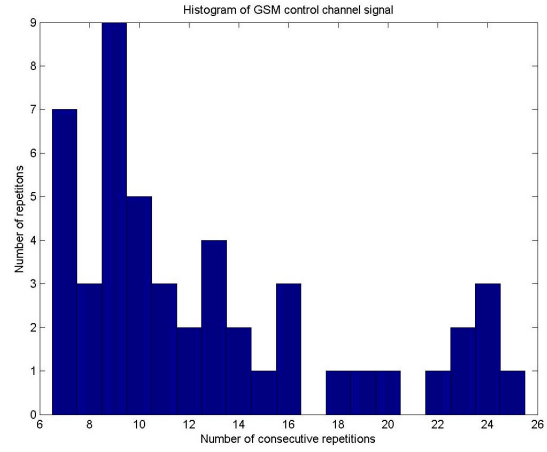

c)

Fig. 5.5. Histogram of the occurrences versus the number of the consecutive repetition of the virtual symbol for GSM signals: a) signal constituted by sequence 0000, b) signal constituted by sequence 1111, and c) signal of the control channel.

By referring to the histograms of Fig.5.5c the symbol timing of the signal of the control channel was correctly individuated.

Another experimental test shown in Fig.5.6 was executed by using different measurement station. This was made up of:

- Signal Generator (SG), Agilent E4435C,
- Data Acquisition board (DAQ) on PCI bus, Signatec PDA 1000,
- control and processing unit, implemented on a Personal Computer (PC) Compaq Evo W4000 at 1.8 GHz,
- interconnecting interface bus IEEE 488.2.

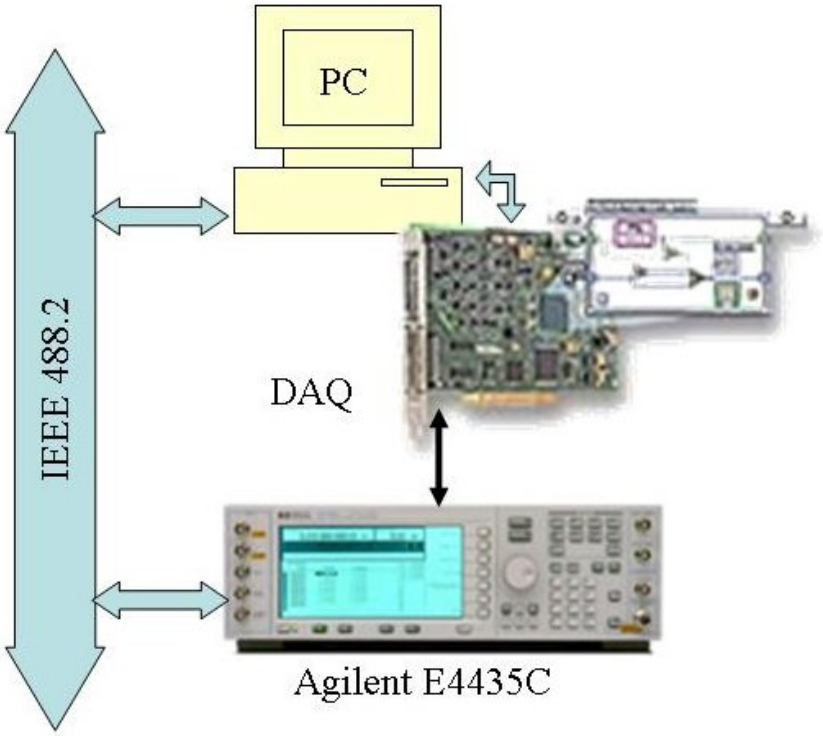

Fig. 5.6. Measurement station for experimental test on FSK digital modulated signals.

With this station was generated and acquired the 2-FSK signal with a carrier frequency equal to 20MHz, and a sampling rate equal to 250MS/s. Differently from the simulation environment, this measurement station is capable to generate modulated signals characterized by whole number of carrier period per each symbol. By imposing the symbol rate equal to 2,4 kS/s, and

the shorter symbol timing $T_{Symbmin}$ equal to 46.30μs, the symbol timing was measured and the error does not exceed the value of the $T_{Symbmin}$.

Successively two modems U.S. Robotics Courier 56k Business Modem were used, both connected to the wired telecommunication public network. One modem was programmed and controlled by Compaq Evo W4000 at 1.8 GHz and used as sender. Another was used as receiver able to negotiate the selected communication conditions according to the standard V.92 and V.90. The processed digital modulated signals were acquired at the input of receiver modem where the signal is degraded by both the noise and the interferences of the network operating in actual conditions.

Tab.5.3 shows the influence of the choice of both the symbol minimum frequency, $f_{Symbmin}$, and the sampling frequency f_s on the measure of the symbol frequency, once the operating conditions at the sender are:

- 16-QAM modulated signal,
- carrier frequency equal to 2000Hz,
- assigned symbol rate equal to 8400 Symb/s.

Fig.5.7 shows the trend of the measured symbol frequency versus the sampling frequency fs, once the operating conditions at the sender are:

- 16-QAM modulated signal,
- carrier frequency equal to 2000Hz,
- symbol rate equal to 8400 Symb/s.

These results highlight that the sampling frequency weakly influences the method accuracy.

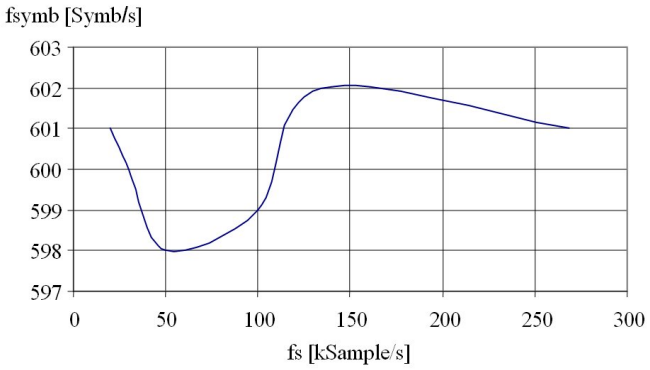

Fig. 5.7. trend of the measured symbol frequency versus the sampling frequency fs for a modem signal.

Table 5.3. Influence of f_s and $f_{Symbmin}$ in the symbol time estimation for 16-QAM modem signals with fc=2kHz, fsymb=8400 Symb/s.

$f_{symbmin}$ [Symb/s]	$f_s = 134400Hz$	$f_s = 268800Hz$
67200	8400	8400
33600	8400	8400
16800	8400	8400
$f_{symbmin}$ [kSymb/s]	$f_s = 100kHz$	$f_s = 200kHz$
50	8333,33	8333,33
25	8333,33	8333,33
20	10000,00	10000,00

5.4 Conclusion

The method is presented to measure the symbol timing in the modulated signals:

- M-ary Quadrature Amplitude Modulation,
- M-ary Amplitude Shift Keying,
- M-ary Phase Shift Keying,
- M-ary Frequency Shift Keying.

The approach followed is based on the statistical analysis in the base band of the digital modulated signal. The symbol timing is evaluated by determining the maximum occurrence of the symbol classes.

This approach is particular convenient and permits to realise very fast, reliable and accurate measurement. Numerical and experimental tests were performed on modulated signals according to the telecommunication standard GSM 900 Burst, UMTS and modem V.90, V.92. The results permit to highlight the robustness of the method and the high accuracy.

In all the tests the maximum error in determining the symbol timing was equal to one unit of the trial symbol timing used in the signal demodulation and showing the higher occurrence of the consecutive repetition.

The method, the result of the numerical and experimental tests are published in the paper [12].

6

ANN based demodulator for UMTS signal measurements

The field of Artificial Neural Networks (ANNs) has made greath progress in terms of theory, algorithms, and applications. Compared to conventional signal processing algorithms that are mainly based on linear models, ANN offer an attractive alternative by providing nonlinear parametric models with universal approximation power, as well as adaptive training algorithms. The availability of such powerful modeling tools justifies numerous research efforts to explore new signal processing applications of ANN [71].

The advantageous use of the ANNs in measurement instrumentation and, in particular, to process the modulated signals for telecommunication has been shown in [72]-[73]. In [72] the ANN based decoder is shown for Dual Tone Multi Frequency signals. The comparison with the traditional ones permits to highlight the advantageous performances of the ANN based demodulator beyond the limits given by the international recommendations. In [73] the ANN based demodulator of signals of the GSM telecommunication standard was designed, discussed and metrological characterised. Also in this case, numerical tests confirm that the use of this demodulator permits to reduce the measurement error of the carrier frequency in both the case of static and dynamic propagation of the signals.

These results confirm that the ANNs show interesting properties to efficiently process the input signals affected by high level of both noise and distortion that characterize the telecommunication networks. In particular, the parallel architecture of the ANNs permits:

- to process the signals in very fast way,
- to overcome the limits of the traditional approach to the signal processing.

According to this interesting properties the ANN is taken into account in order to realise innovative decoder of the UMTS signals. This decoder must ensure the correct demodulation beyond the noise and alterations with values greater than the values defined in the international recommendations [40]. To this scope in the following the characteristics of the ANN are analysed. Successively, the ANN based demodulator is designed and tested.

6.1 Basic characteristics of ANNs

The nonlinear nature, the ability to learn from their environments in supervised or unsupervised ways, and the approximation property of ANN make them highly suited for solving both complex and hard signal processing problems.

From a signal processing perspective, it is imperative to develop a proper understanding of basic ANN structures and how they impact on signal processing algorithms and applications. A challenge in surveying the field of ANN paradigms is to identify those ANN structures that have been successfully applied to solve real world problems from those that are still under development or have difficulty scaling up to solve realistic problems. When dealing with signal processing applications, it is critical to understand the nature of the problem formulation so that the most appropriate ANN paradigm can be applied. In addition, it is also important to assess the impact of ANN on the performance, robustness, and cost-effectiveness of signal processing systems and develop methodologies for integrating ANN with other signal processing algorithms. Another important issue is how to evaluate ANN paradigms, learning algorithms, and ANN structures and identify those that do and do not work reliably for solving signal processing problems [71].

6.1.1 McCullochand Pitts Neuron Model

Among numerous ANN models that have been proposed, all share a common building block known as a neuron and a networked interconnection structure. The most widely used neuron model is based on McCulloch and Pitts work and it is shown in Fig.6.1.

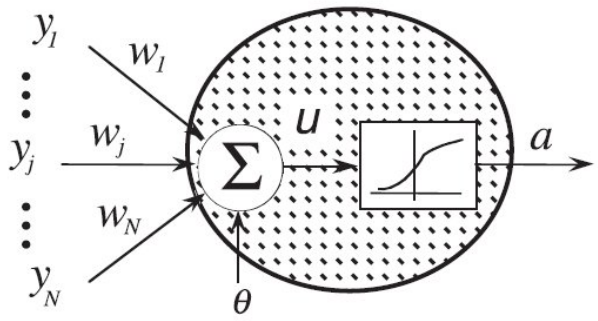

Fig. 6.1. McCulloch and Pitts neuron model.

Each neuron consists of two parts: the net function and the activation function. The net function determines how the network inputs $\{y_j; 1 \leq j \leq N\}$ are

combined inside the neuron. In the Fig.6.1, the weighted linear combination is adopted:

$$u = \sum_{i=1}^{N} w_j y_j + \theta \tag{6.1}$$

$\{w_j; 1 \leq j \leq N\}$ are parameters known as synaptic weights. The quantity θ is called the bias (or threshold) and is used to model the threshold. In the literature, other types of network input combination methods have been proposed as well [71].

The output of the neuron, denoted by a_i, is related to the network input u_i via a linear or nonlinear transformation called the activation function:

$$a = f(u) \tag{6.2}$$

In various ANN models, different activation functions have been proposed.

6.1.2 ANN Topology

In a ANN, multiple neurons are interconnected to form a network to facilitate distributed computing. The configuration of the interconnections can be described efficiently with a directed graph. A directed graph consists of nodes (in the case of a ANN, neurons, as well as external inputs) and directed arcs (in the case of a ANN, synaptic links).

The topology of the graph can be categorized as either acyclic or cyclic. ANN with acyclic topology, Fig.6.2a, consists of no feedback loops. Such an acyclic ANN is often used to approximate a nonlinear mapping between its inputs and outputs. As shown in Fig.6.2b, ANN with cyclic topology contains at least one cycle formed by directed arcs. Such a ANN is also known as a recurrent network. Due to the feedback loop, a recurrent network leads to a nonlinear dynamic system model that contains internal memory.

Recurrent ANNs often exhibit complex behaviors and remain an active research topic in the field of artificial ANNs.

6.1.3 Multilayer Perceptron (MLP) Model

The multilayer perceptron [74] is by far the most well known and most popular ANN among all the existing ANN paradigms. To introduce the MLP, let us first discuss the perceptron model.

Perceptron Model

In the perceptron model, a single neuron with a linear weighted net function and a threshold activation function is employed. The input to this neuron

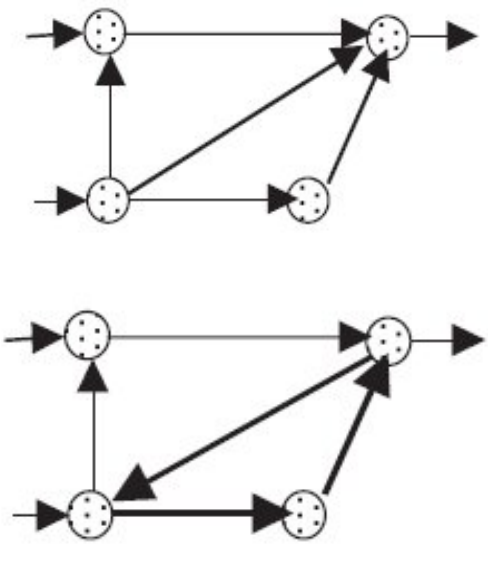

Fig. 6.2. a) acyclic graph and b) cyclic graph.

$x = (x1, x2, x3, ..., x_n)$ is a feature vector in an n-dimensional feature space. The net function u(x) is the weighted sum of the inputs:

$$u(x) = w_0 + \sum_{i=1}^{n} w_i x_i \tag{6.3}$$

and the output y(x) is obtained from u(x) via threshould activation function:

$$y(x) = 1 \quad u(x) \geq 0 y(x) = 0 \quad u(x) < 0 \tag{6.4}$$

6.1.4 Multilayer Perceptron

A multilayer perceptron (MLP) ANN model consists of a feed-forward, layered network of McCulloch and Pitts neurons. Each neuron in the MLP has nonlinear activation function that is often continuously differentiable. Some of the most frequently used activation functions for MLP include the sigmoid function and the hyperbolic tangent function.

Weights determination of a Single Neuron MLP

If it's considered a simple example consisting like is shown in Fig.6.3 that represents the neuron in two separate parts: a summation unit to compute

the net functions u, and a nonlinear activation function $z = f(u)$, the output z is to be compared with a desired target value d, and their difference, the error $e = d - z$, will be computed. There are two inputs [x1 x2] with corresponding weights w_1 and w_2. The input in the figure labeled with a constant 1 represents the bias term θ shown in Fig.6.4. The bias term is labeled w_0. The net function is computed as:

$$u = \sum_{i=0}^{2} w_i x_i = Wx \tag{6.5}$$

where $x_0 = 1$, $W = [w_0, w_1, w_2]$ is the weight matrix, and $x = [1, x_1, x_2]^T$ is the input vector.

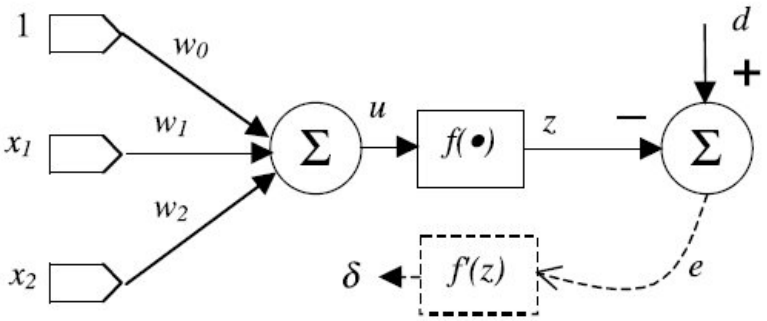

Fig. 6.3. MLP for back-propagation the training of a single neuron ANN.

Given a set of training samples $(x(k), d(k)); 1 \leq k \leq K$, the error back-propagation training begins by feeding all K inputs through the MLP network and computing the corresponding output $z(k); 1 \leq k \leq K$. Here we use an initial guess for the weight matrix W. The objective is to adjust the weight matrix W to minimize the error. This leads to a nonlinear least square optimization problem. There are numerous nonlinear optimization algorithms available to solve this problem. Basically, these algorithms adopt a similar iterative formulation:

$$W(t+1) = W(t) + \Delta W(t) \tag{6.6}$$

where $\Delta W(t)$ is the correction made to current weights W(t). Different algorithms differ in form of $\Delta W(t)$. Some important algorithm are:

- Steepest descend gradient method,
- Newtons method,
- Conjugate-Gradient method.

The complexity of the problem increases with the number of the layer present into the network.

A typical MLP configuration is depicted in Fig.6.4. Each circle represents an individual neuron. These neurons are organized in layers, labeled as the hidden layer 1, hidden layer 2, and the output layer. While the inputs at the bottom are also labeled as the input layer, there is usually no neuron model implemented in that layer. The name hidden layer refers to the fact that the output of these neurons will be fed into upper layer neurons and, therefore, is hidden from the user who only observes the output of neurons at the output layer. Fig.6.4 illustrates the configuration of MLP where interconnections are provided only between neurons of successive layers in the network. In practice, any acyclic interconnections between neurons are allowed. An MLP provides a nonlinear mapping between its input and the output.

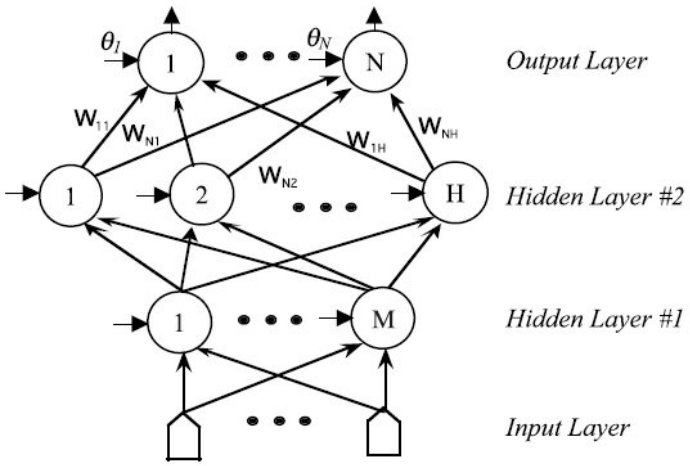

Fig. 6.4. Three-layer multilayer perceptron configuration.

Error Back-Propagation Training of MLP

A key step in applying the MLP model is to choose the weight matrices. Assuming a layered MLP structure, the weights feeding into each layer of neurons form a weight matrix of that layer (the input layer does not have a weight matrix as it contains no neurons). The values of these weights are found using the error back-propagation training method.

There are two parameters that must be chosen: the learning rate, and the momentum constant m. The learning rate is a parameter used to determine the

influence of the error in the new weight. The momentum provides a mechanism to adaptively adjust the step size. When the gradient vectors in successive epochs point to the same direction, the effective step size will increase. When successive gradient vectors form a zigzag search pattern, the effective gradient direction will be regulated by this momentum term so that it helps minimize the mean-square error. Both of these parameters should be chosen from the interval of [0 1].

6.2 ANN based demodulator architecture for GMSK signal measurements

In [73] is presented an interesting demodulator for GMSK signal based on ANN.

Demodulation of the GMSK signal is very difficult in real cases. The transmitted signal is corrupted by channel noise, by Doppler effect and by multipath propagation so that bit decoding is not easy.

GMSK modulation has been widely used in several wireless telecommunication systems, i.e. for GSM cellular telephone system in Europe, for CDPD (Cellular Digital Packet Data) system in the USA.

The GMSK modulation belongs directly from continuous-phase Frequency Shift Keying (FSK) with a modulation index (h=0.5) that will produce orthogonal signaling.

In the GMSK signal, the information is carried out by the phase of the modulated signal. In particular, the slope of the signal depends on the transmitted bit. A positive slope means a binary "1" has been transmitted, while a negative slope means a binary "0' has been transmitted as is shown in Fig.6.5 and Fig.6.6. The GMSK demodulator must extract the phase from the modulated signal and, by using a slope classifier, decode the transmitted bits.

In the GMSK modulation, the phase modulated signal is:

$$s(t) = S_M cos[2\pi f_c t + \varphi_i(t)] \tag{6.7}$$

where f_c, is the carrier frequency and $\varphi(t)$ is the information carrying phase.

Before being sent to the ANN demodulator, the phase signal is preprocessed according to the following rules:

1. the baseband phase signal is sampled;
2. synchronisation is performed by detecting the first change to the signal slope;
3. the different phase shifts of the incoming modulated signal are detected and organized to send to the demodulator;
4. 18 samples for each transmitted bit are stored;
5. four samples, selected from the central zone of the 18 samples, are fed into the modulator.

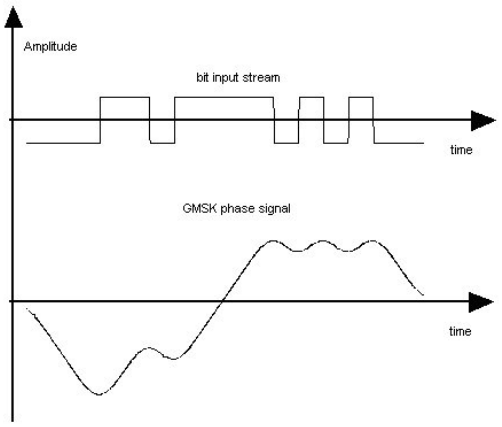

Fig. 6.5. GMSK phase signal and corresponding bit input stream.

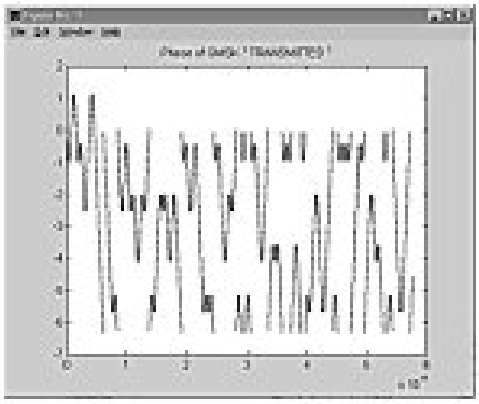

Fig. 6.6. GMSK modulated signal.

The GMSK slope classifier is based on the Learning Vector Quantization (LVQ) ANN. The LVQ ANN is able to decode the input signal by classifying the phases slope which depends on the transmitted bit.

The number of both the input neurons and codebooks is set during the initialisation phase. The number of input neurons depends on

- satisfying the international recommendations GMSK signal demodulation,
- the sampling frequency of the incoming signal.

By taking into account these problems, and in order to make the demodulator robust, less sensitive to the noise, the sampling frequency of the realised prototype has been set equal to 4.5MHz so as to obtain 18 samples for symbol when the signal is acquired in the base band. Only 4 samples, selected in the

central zone of each symbol, are sent to neural demodulator. In this manner the problems depending on the sample leakage at the end of the symbol are avoided.

The number of the codebooks is fixed equal to 4, two for each slope.

In the output layer, the minimum of the Euclidean distance between the codebooks and the output of the net, is evaluated and the decoded bit is determined.

The training set is constituted by the phase slope of 5 random bursts of a GSM signal for a total of 151x5 random The ANN is trained by using an evolution of LVQ algorithm (LVQ2) and the Fig.6.7 shows the block scheme of the learning phase.

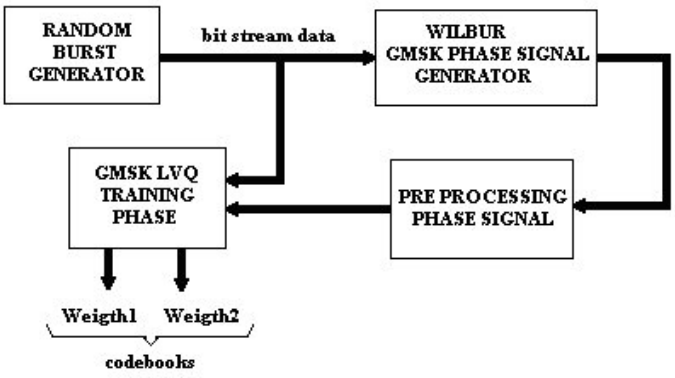

Fig. 6.7. Block scheme of the learning phase

The neural demodulator has been tested according to the European Telecommunication Standard Institute (ETSI) recommendation [38]. In order to execute estimation of the Bit Error Rate (BER), several channel models have been simulated.

The models, as established by the ETSI recommendation, are:

- the Rural Area characterised by maximum speed 250km/h(RU 250),
- Total Urban maximum speed 50km/h (TU 50),
- Hilly Terrain maximum speed 100km/h (HT 100).

These tests are called dynamic because the receiver is in motion. Moreover, static test has been carried out and shown in Fig.6.8 in which the channel is assumed to be characterised by Additive White Gaussian Noise (AWGN) and the receiver is motionless.

The test results show the good performance of the demodulator for high degradated sigals.

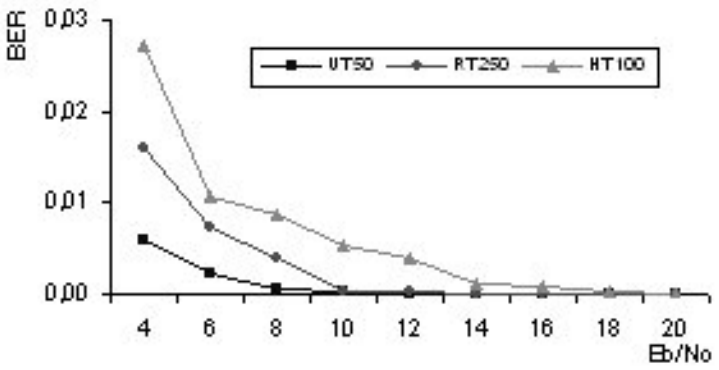

Fig. 6.8. BER for the neural based demodulator for different condition of propagation versus Eb/N0.

6.3 ANN based demodulator architecture for UMTS signal

The ANN based demodulator pointed out works into the input block of the non-intrusive instrument designed for measurements on modulated signals according to the Universal Mobile Telecommunications System (UMTS) Terrestrial Radio Access (UTRA) standard. Important aspect taken into account in the design of the ANN based demodulator is that the UMTS standard imposes:

- the scrambling code in order to realize the transmission with frame Wideband Code Division Multiple Access (W-CDMA),
- the spreading code in order to realize the multi-user transmission.

Therefore, beside to be able to operate in substitution of the traditional demodulator block, others assigned functions to the proposed demodulator regard to both the descrambling and the despreading operations of the input signal. Then, the operations that the ANN are required to perform in one shot are:

- the descrambling of the input signal according to the used code by the transmitter, previously down converted in base band,
- the despreading in order to recovery the transmitted symbols,
- the symbol extraction.

Fig.6.9 shows the block schemes of both the traditional and the ANN based demodulator in the case four output channels are considered. In both the schemes:

1. the signal is down converted in base band at the input section,
2. the two components, the in-phase signal component I and the quadrature component Q, are extracted,

3. the symbols are recovered,
4. the symbols are reconstructed for each channel.

Nevertheless, the two schemes of Fig.6.9 differ because the ANN based demodulator works so as to perform in parallel way the operations of descrambling, despreading, and symbol extraction. Differently, the traditional demodulator performs the previous processing operations by means of three successive steps.

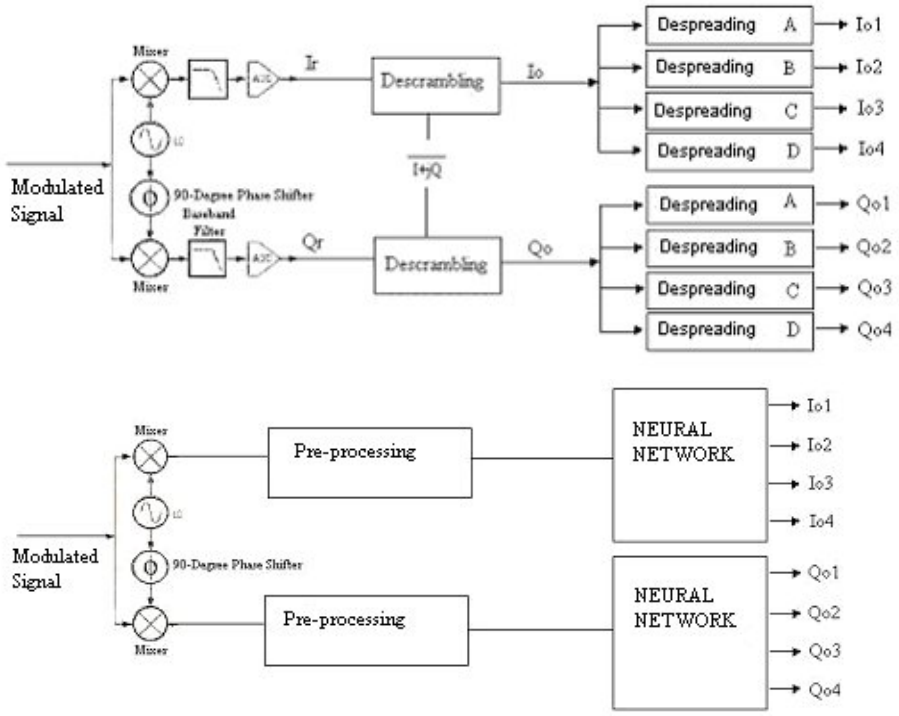

Fig. 6.9. Block schemes of the traditional receiver (up) and of the ANN based receiver (down).

The pre-processing block, before the ANN block of Fig.6.9, operates to adapt the signal to the requirements of the successive block. The proposed demodulator is constituted by ANN with two layers and two outputs. One output corresponds to the in-phase signal component I and another to the quadrature component Q. The ANN architecture showing the best performances and, consequently, used in the proposed demodulator is the MLP.

In the following, both the design and the training phase of the MLP ANN based demodulator are presented in the case of the Frequency Division Duplex (FDD) functioning modes. Successively, the preliminary results of the numer-

ical tests on modulated signals, generated according to the international recommendations of the standard UMTS [75]-[80], are given and compared with that of the traditional demodulator.

6.3.1 ANN based demodulator training

In order to recovery the transmitted symbol, the ANN is trained according to the following relations for the I and the Q components, respectively:

$$Symb(n) = \frac{\sum_{i=(n-1)SF+1}^{nSF}((L_r(i)I_s(i) + Q_r(i)Q_s(i))(-C(i)))}{2SF} \tag{6.8}$$

$$Symb(n) = \frac{\sum_{i=(n-1)SF+1}^{nSF}((Q_r(i)I_s(i) - I_r(i)Q_s(i))(-C(i)))}{2SF} \tag{6.9}$$

where: $I_r(i)$ and $Q_r(i)$ are the in-phase and quadrature components, respectively, of the modulated signal after the filtering and sampling process, $I_s(i)$ and $Q_s(i)$ are the in-phase and quadrature components of the scrambling code, respectively, C(i) is the spreading code of the selected channel, SF is the spreading factor identifying the selected channel.

In order to reduce the computational complexity, the ANN training refers to four channels, only. Therefore, the input vector is constituted by 20 components, four for each of $I_r(i)$, $Q_r(i)$, $I_s(i)$, $Q_s(i)$ and C(i). The ANN is trained by using modulated signals generated according to the UMTS standard [75], [77] and [79] in the following operating conditions:

- assigned scrambling code,
- assigned channel set [0, 1, 5, 7].

Therefore, the trained ANN can work in the following operating conditions:

- channels included in the standard,
- signals with scrambling code corresponding to that used in the training phase.

6.3.2 The ANN design

The ANN design mainly consists of defining the topology (i.e., the arrangement of neurons, connections, and patterns into the ANN) and the architecture (i.e., the selection of the number of neurons, layers, and number of neurons for each layer necessary for the specific application of the topology) of the network.

Among the digital ANN topologies, the MLP shows interesting characteristics according to the advantageous application given in literature for the signal demodulation [72], [73]. The lack of any a-priori evidence about the better

suitability of the architecture imposes assessing experimentally the characteristics in order to minimize the ANN error.

In the MLP networks, the neurons in a layer are connected to all the neurons in the following layer through unidirectional links represented by connection weights [81]. Therefore, the MLP requires the determination of the activation functions and the thresholds of the neurons, as well as of the connection weights. First, the activation functions and the thresholds are defined by a recursive optimization procedure [81]. Then, the connection weights are computed by means of a learning algorithm. The simplest and most widespread learning algorithm is the Back-Propagation (BP) [81]. However, its classical version suffers problems of slow convergence speed and local minima in training. Enhanced versions exploit the method of the Momentum parameter in order to avoid oscillation problems, and to speed up and made less sensitive to small error the network training phase. On the basis of this method, the new weights are determined by the sum of a fraction of the last weight change and the new change suggested by the BP rule. The magnitude of the change is allowed by the momentum constant, m_c, which is a number in the interval [0, 1]. The lack of any a-priori evidence about the better suitability of the value of this constant for the current problem imposes an experimental performance assessment. In learning phase is assumed m_c=0.05.

In order to reduce the convergence problems, the resilient back-propagation algorithm is implemented, also. The learning rate was set equal to 0.5.

The optimal network parameters are heuristically found. In particular, the training tests allow the number of hidden layer and neurons to be selected experimentally according to the ANNs performance in terms of accuracy and operating speed.

Moreover, the over training of the MLP ANN and local minimum trap of the network parameters impose to experimental assess the optimal network parameters. Therefore, the learning of the network is repeated by changing the training data set.

After numerous tests, the best configuration of the ANN based demodulator consists of the MLP architecture with:

- 20 neurons in the input layer,
- 210 neurons in the hidden,
- 2 neurons in the output layer.

The training phase is performed by assuming the sigmoid transfer function of each neuron. The training data set is constituted by the normalized input signal modulated according to the UMTS standard, and the output signal constituted by sequences of the discrete values [-1, 1], according to the symbol levels.

The trend of the percentage error, defined as difference between the assigned symbol and the detected one, is shown in Fig.6.10 versus the epochs of the training phase.

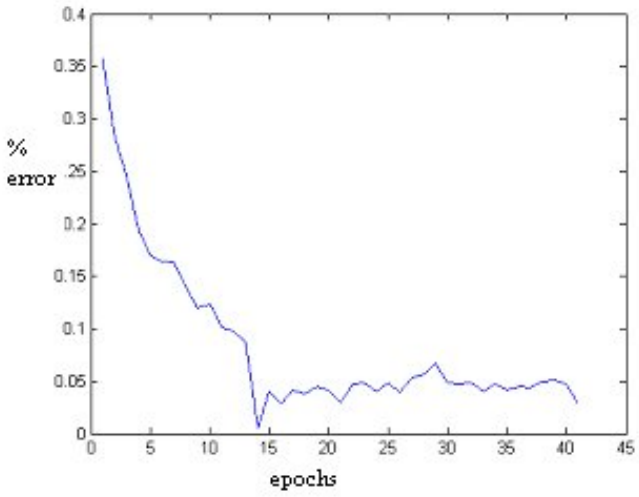

Fig. 6.10. Trend of the percentage error during the training phase of the MLP ANN.

In the validation phase, the MLP ANN is forced to demodulate the signal different from that used in the training phase.

The considered ANN architecture is particularly robust. Indeed, tested by signals not included in the training set, the error is 0.8%.

6.3.3 Numerical tests of the ANN based demodulator

Numerical tests are performed to assess the errors of the MLP ANN based demodulator in the following actual operating conditions:

1. signal affected by clipping,
2. carrier frequency error,
3. carrier phase error,
4. burst synchronisation error,
5. transmission noise,
6. signal affected by multi-path interferences.

The modulated signals occurring in these operating conditions are degraded and they can differ from the theoretical ones on the basis of the different causes. Therefore, the numerical generation of these degraded signals is performed in accordance to the limit conditions given in the ETSI recommendations [77]-[80], and to both the rules and the simulation models presented in literature [82]-[85]. In the previously considered operating conditions, the MLP ANN based demodulator is compared with the traditional one in order to highlight:

- the advantages,
- the disadvantages,
- to detect the limit operating conditions.

The parameter used in the comparison is the Bit Error Rate (BER) according to the ETSI recommendation [76], [77]. In the following the comparison between the neural demodulator and the tradition one is shown by examining each of the actual operating conditions taken into account.

Signal affected by clipping

The clipping occurs when the signal amplitude overcomes the dynamical range of the integrated components. The consequent signal degradation causes the frequency distortion out the assigned band, and the Error Vector Magnitude variation. The clipping level, defined as the ratio between the clipped signal and the original one, in the UMTS system can rice the value of 64%. Fig.6.11 shows that the ANN based demodulator is characterised by BER values lower than the traditional demodulator for clipping level greater than the value of 14 dB, corresponding to the values of the clipping level of the usual functioning conditions of the UMTS system.

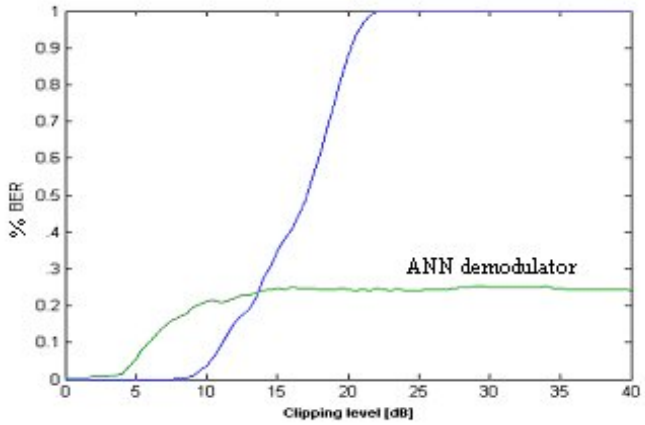

Fig. 6.11. BER evaluated in the case of traditional and MLP ANN based demodulator in the operating conditions characterised by clipping.

Carrier frequency error

The carrier frequency error occurs as consequence of the non correct down conversion of the modulated signal. Fig.6.12 shows that the ANN based de-

modulator is characterised by BER values lower than the traditional demodulator for frequency error greater than 100 Hz, corresponding to 4.17 ppm of the carrier frequency equal to 2.4 GHz.

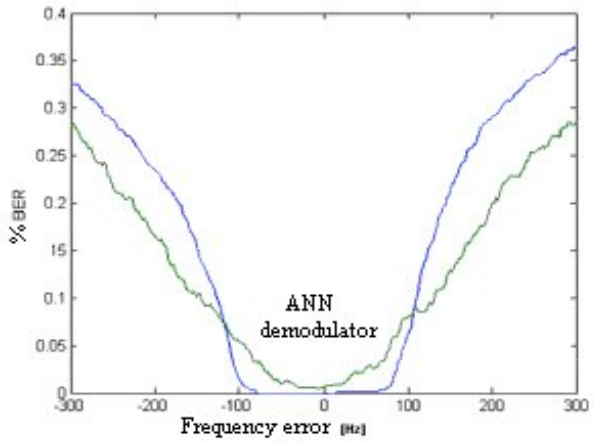

Fig. 6.12. BER evaluated in the case of traditional and MLP ANN based demodulator in the operating conditions characterised by carrier frequency error.

Carrier phase error

The carrier phase error occurs as consequence of the non correct synchronization during the demodulation. Fig.6.13 shows that the ANN based demodulator is characterised by BER values lower than the traditional demodulator for phase error greater than 5 rad.

Burst synchronisation error

In the case the burst synchronisation error occurs, Fig.6.14 shows that the ANN based demodulator is characterised by BER values lower than the traditional demodulator for synchronisation error greater than 30 samples.

Transmission noise

The noise superimposed to the modulated signal is the Average White Gaussian Noise (AWGN). Fig.6.15 shows the original signal and the corrupted one characterised by SNR=20dB. It can be noted as the original signal is deteriorated and the corrupted one has shape almost different from the original signal. Fig.6.16 shows that the ANN based demodulator is characterised by BER lower than the traditional demodulator for SNR greater than 0 dB.

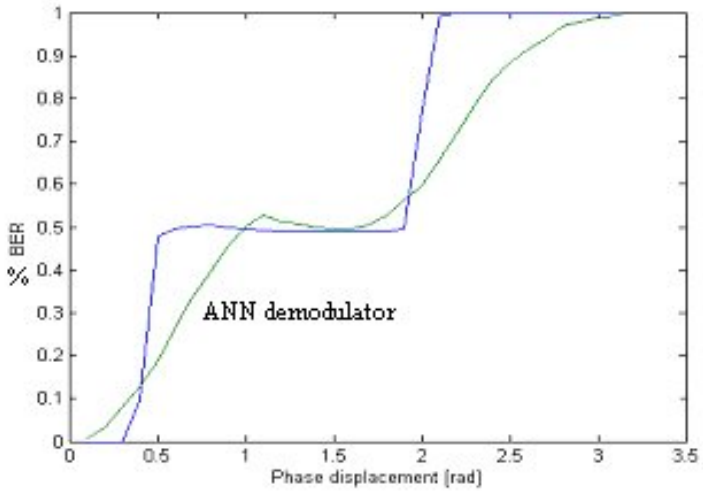

Fig. 6.13. BER evaluated in the case of traditional and MLP ANN based demodulator in the operating conditions characterised by carrier phase error.

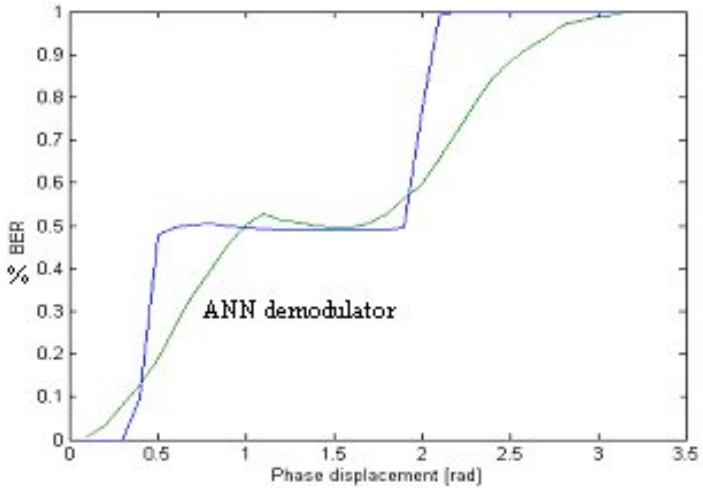

Fig. 6.14. BER evaluated in the case of traditional and MLP ANN based demodulator in the operating conditions characterised by burst synchronisation error.

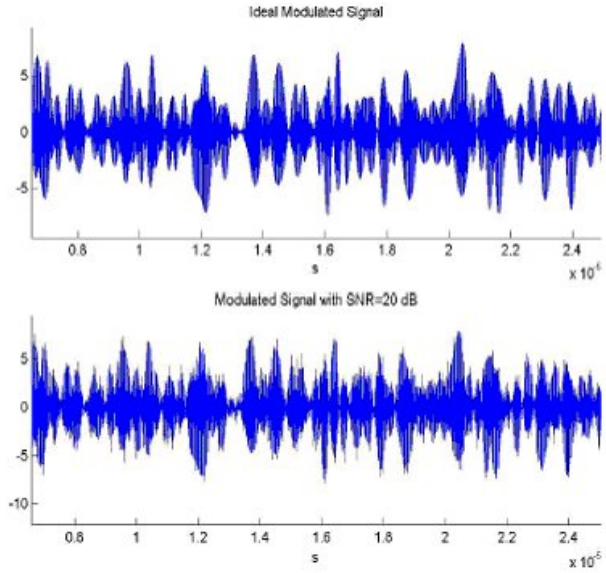

Fig. 6.15. Modulated signal affected by AWGN: the original signal (upper), the modulated signal with SNR equal to 20dB (down).

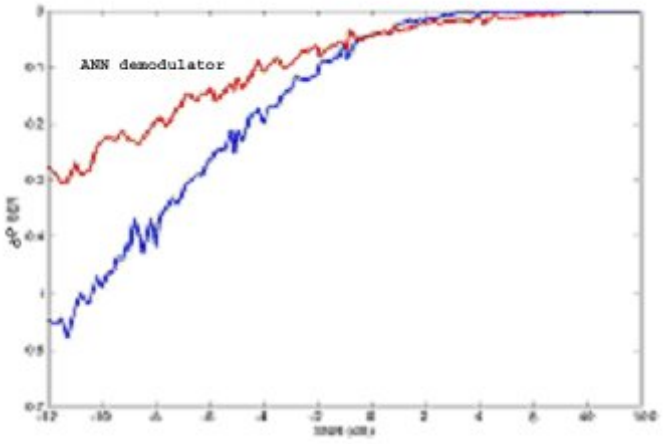

Fig. 6.16. BER evaluated in the case of traditional and MLP ANN based demodulator in the operating conditions characterised by transmission noise.

Multi-path interferences

The multi-path propagation is produced by reflection of the transmitted signal from obstacles and, consequently, a lot of signals, instead of only one, with different time delay and attenuation are received. Moreover, the variety of paths causes, also, the phase changes, which are frequency dependent. In addition, the speed of the mobile station causes Doppler effect on the received signal. All these effects are very difficult to model. The method presented in [85] permits to realize the adequate modelling of the multi-path fading for mobile radio. This model is based on the assumption that the amplitude of the complex envelope of the received signal at the antenna is characterised by Rayleigh distribution.

Fig.6.17 shows the modulated signal and the corresponding signal affected by multi-path interferences simulated according to the model given in [85]. It can be noted as the signal affected by multi-path interferences is substantially degraded and the waveform shape is far different from that of the original modulated signal. Therefore, both the ANN based and the traditional demodulators work in very cumbersome operating conditions.

In the case only one channel is taken into account and the signal is affected by multipath interferences, Fig.6.18a , and Fig.6.18b show that the ANN based demodulator is characterized by BER lower than the traditional demodulator. Moreover, Fig.6.18c shows the trend of the BER evaluated for the ANN based demodulator, in the case two channels are contemporary working and the signal is affected by fade interferences with delay equal to 0, 0.1 Ts and 0.2 Ts, where Ts is the chip time defined in the UMTS standard [40]. Also in this working condition the values of the BER are low.

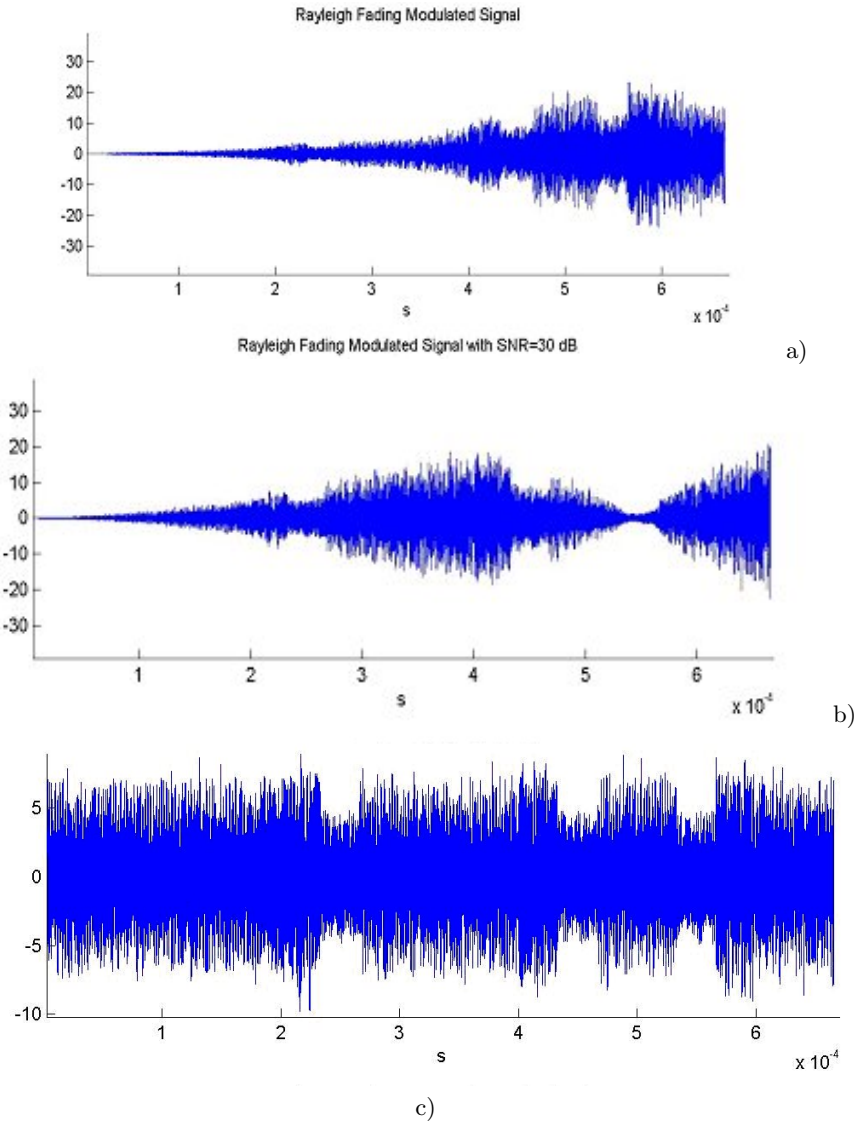

Fig. 6.17. Rayleigh fading modulated signal (a), Rayleigh fading modulated signal and noise (b), original modulated signal (c).

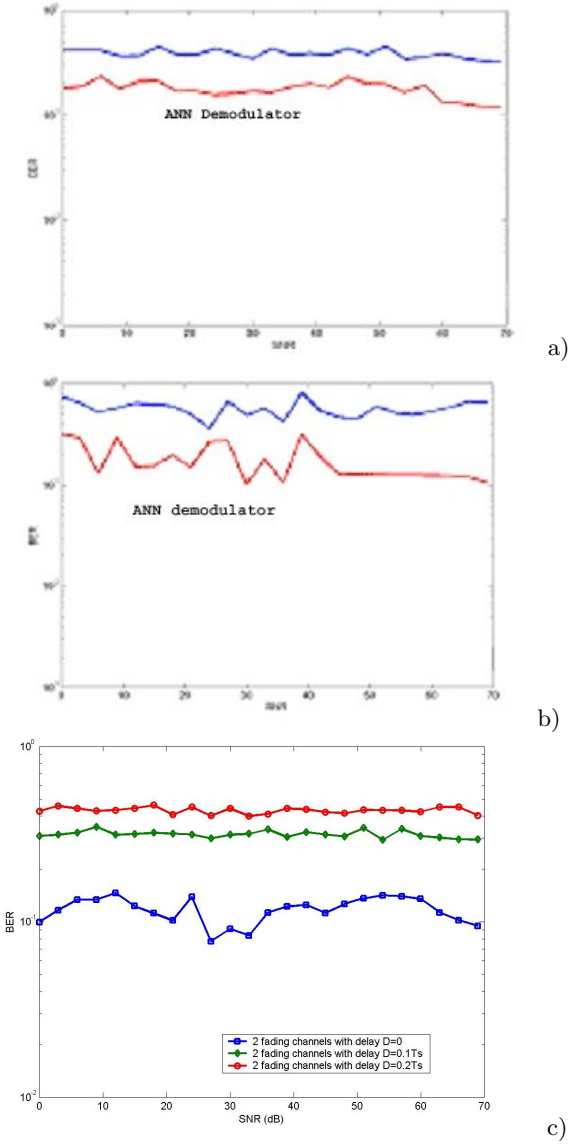

Fig. 6.18. BER evaluated in the case of traditional and MLP ANN based demodulator in the operating conditions characterised by: a) one channel with signal affected by multipath interferences and speed 90 km/h, b) one channel with signal affected by multipath interferences and speed 5 km/h, c) two channels.

6.4 Conclusion

The new demodulator architecture for telecommunication signals is proposed by using the Multi Layer Perceptron (MLP) Artificial Neural Network (ANN). This demodulator is designed to be employed into the measurement instrument for the third generation mobile telecommunication systems.

The operating characteristics of the MLP ANN based demodulator were evaluated in the following conditions:

- input signal affected by clipping,
- carrier frequency error,
- carrier phase error,
- burst synchronisation error,
- transmission noise,
- input signal affected by multi-path interferences.

The numerical tests have pointed out that the MLP ANN based demodulator is more robust than the traditional demodulator and it candidates to be used in the measurement instruments. Indeed, the MLP ANN demodulator can guaranty greater accuracy in the case the modulated signal is affected by high level of both noise and distortion.

The method, the result of the numerical and experimental tests are published in the paper [64].

7

Architecture implementing the carrier frequency error measurement

More functions of the radio systems are implemented in software, leading towards the Software Radio (SR). In the receiver of the SR, the incoming signal is translated into the digital domain by the Analog to Digital Converter (ADC) and is demodulated by using software techniques [35].

The benefits of this approach consist in using single general-purpose platform to perform different functions by simply running different programs. The main effort is to get the hardware architecture able to support the SR [86], by taking into account the strong diversity of existing and future communication systems.

The common architecture of the SR proposed in literature and generating widespread interest in the telecommunication industry [35], [86] is constituted by three main functional blocks, shown in Fig.7.1. They are :

1. the Radio Frequency (RF) section realised by the analog hardware module,
2. the Intermediate Frequency (IF) section realised by the cascade of the ADC and the Digital Down Converter (DDC),
3. the base band processing section realised by the Digital Signal Processor (DSP).

The current research trend is addressed to perform the digital conversions right to the antenna [87].

Both the feasibility and the adaptability made this architecture interesting to efficiently implement the method pointed out to measure the carrier frequency error of the single carrier digital modulations for telecommunication systems [88]. This method requires to process the incoming signal according to the following steps:

1. to down convert the signal in base-band,
2. to determine both the in-phase (I) and in quadrature (Q) components of the signal,
3. to compute the phase from the ratio of these two components.

These three steps well match the functional blocks of the SR architecture.

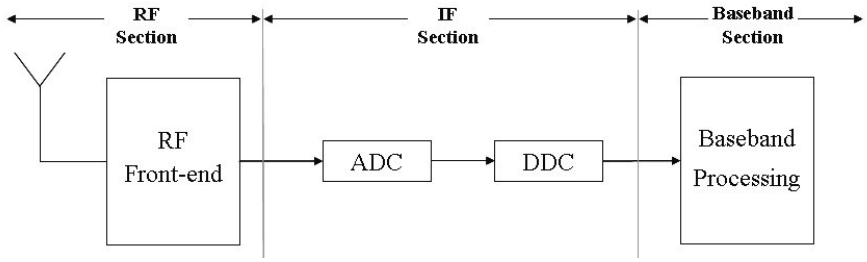

Fig. 7.1. Block scheme of the receiver of the software radio constituted by the cascade of the RF section, the IF section and the base band section.

Looking to the method implementation in the architecture of SR, the design of the ADC architectures is taken into account. This architecture is a trade-off between the availability of the technologies and both the accuracy and the sensitivity of the frequency error measurement. These last are important aspects to be taken into account and to be investigated before the realization of the ADC by the available technology.

In particular, the effects of the ADC architecture on the carrier frequency error measurement is investigated. Indeed, given the high cost of prototyping new ADC, the results from simulation of different architectures is a realistic solution for addressing the choise of the right architecture. The attention is restricted to the ADC architectures used into the SR [89]-[95] and realizable with the existing technologies at that time. In particular they are:

1. the Pipeline ADC,
2. the Sigma-Delta ($\Sigma\Delta$) Band-Pass (BP) ADC. Among them, the $\Sigma\Delta$ BP ADC based on :
   - the Single Quantizer Loop (SQL) BP,
   - the Multistage Noise Shapers (MASH) BP

These two architectures of $\Sigma\Delta$ BP ADCs influence in different way the carrier frequency error measurement because the quantization noise and the noise shaping are different according to the different architectures.

In the following the block scheme of the ADC architectures designed to be implemented into the IF section of the SR is discussed. The ADC architectures taken into account are that realizable with the existing technologies at that time. At the end, the results of the numerical tests carried out to investigate on the effects of the ADC architectures on the carrier frequency error measurement are given.

7.1 Functional block architecture for frequency error measurement

7.1.1 Functional block architecture

The implementation of the method for the frequency error measurement on the measurement instrument requires the fulfillment of the following steps:

1. down converter in base band of the input signal;
2. evaluate the I and Q components of the modulated signal in order to permit the computation of the argument of the base-band signal;
3. estimate the slope of the phase trend in order to determine the carrier frequency error f_{sh}.

The previous three steps match with the fundamental steps performed in the SR architecture. As a consequence, Fig.7.2 shows the cascade of the ADC, the DDC and the Digital Signal Processor (DSP), extracted from the SR architecture, to implement the method to carrier frequency error measurement.

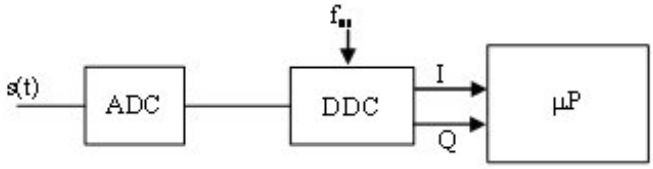

Fig. 7.2. Block scheme of the cascade of the ADC, the DDC and the DSP implementing the method to carrier frequency error measurement.

Since the signal processing is always simpler and more efficiently performed at the base band, the digitized signal is down converted first. The advantages of the DDC after the ADC [35], compared to the analog down conversion before the ADC, are that the perfect IQ matching can be obtained, and the image rejection can be easily realized. The IQ components at the output of the DDC, which are determined by means of the digital mixer of the input signal, depend mainly on:

- the symbol transmitted,
- the channel noise,
- the carrier frequency error.

These two IQ components are the input to the following block devoted to the computation of the phase. If this block is realised by the DSP, the DDC can be implemented by software and, consequently, modification can be made easily to adapt new requirements. The hardware implementation can be

conveniently used when high level of decimation must to be performed. The digitization by the ADC and the IF processing performed by the DDC can be realized on common hardware according with the technologies available today.

In the past, the ADC architecture able to provide both high dynamic range and high linearity is confined to low input bandwidth. Today, new technologies of integrated components increase in speed and in conversion rates up to several megasamples/s. Nevertheless, the current state of the art shows the difficulty to support the RF bands. In fact, the carrier frequency of the modulated signal is of the order of gigahertz and, consequently, the ADC must to operate at the very high sampling frequency, hundreds or thousands times of the carrier frequency. With respect to this limit, the critical functionality of the block architecture of Fig.7.2 is investigated. In particular the effect of the ADC on the carrier frequency error measurement is analyzed and the architecture of the ADC is suggested that is realizable with the existing technologies.

The characteristic aspects of the input signal s(t) in Fig.7.2 are:

- carrier frequency into the range of the IF according to the available technologies at that time,
- digital modulation according to the schemes M-ASK, M-QAM and M-PSK.

According to the recent research given in literature [89]-[92], three different architectures of ADC can be taken into account. The first is the pipeline architecture shown in Fig.7.3a [94]. This architecture uses the pipeline stage of 1 bit in order to optimizes the speed.

The second architecture is the $4-th$ order $\Sigma\Delta$ BP based on SQL modulator shown in Fig.7.3b [93]. This modulator has Multiple Feedback (MFB) structures with a single bit quantizer. The resonator in the loop filter is implemented by the Double Delay (DD) topology. The DD resonator consists of two delay elements in series, with a feedback term of one.

The third architecture is the $\Sigma\Delta$ BP based on the MASH modulator [95] shown in Fig.7.3c. This operates with two $\Sigma\Delta$ modulators. The MASH architecture consists of the stages in cascade each one constituted by a SQL. Each stage is feed by the quantizer error arising from the previous one. This configuration increases the performance in band of the converter and permits to increase the Effective Number Of Bits (ENOB). As a result, the increasing of the bit resolution contributes to increase the accuracy in the frequency error estimation. Both the BP $\Sigma\Delta$ modulators architecures have a central frequency [93] equal to fs/4, with fs sampling frequency.

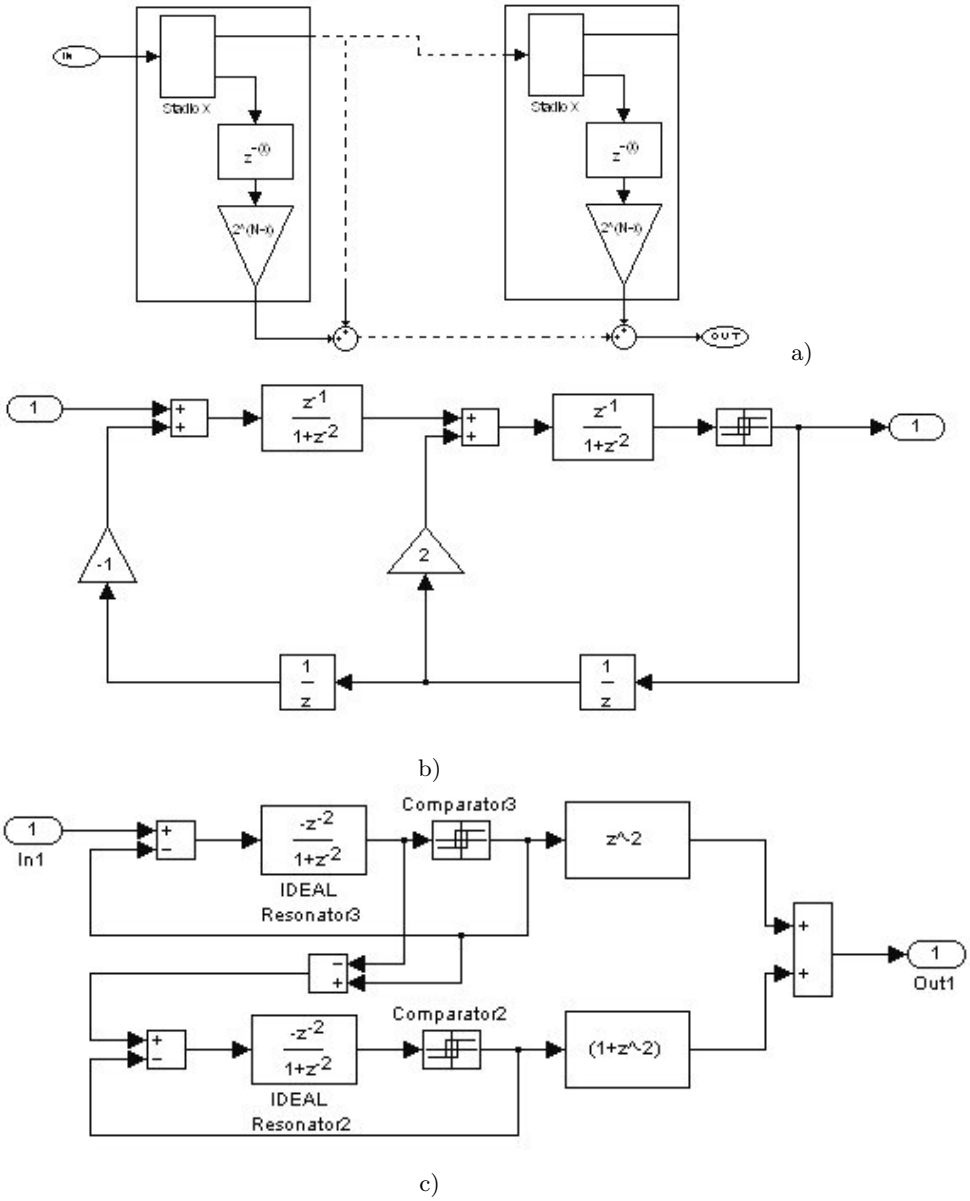

Fig. 7.3. Block scheme of a) Pipeline ADC, b) $\Sigma\Delta$ Band-Pass based on second order SQL modulator, and c) $\Sigma\Delta$ BP MASH modulator.

The common structure of the DDC is shown in the block scheme in Fig.7.4. It operates the multiplication by using the digital sinusoidal signal with frequency equal to f_o. In the case of the $\Sigma\Delta$ BP modulator the signal must be translated by taking into account the central band frequency (f_w). Because this last is related to f_s by the relation $f_w = f_s/4$, the relation $f_o = f_s/4$ must be respected in the structure of Fig.7.2. Therefore, it can be assumed that the carrier frequency error is evaluated by the distance between the central band frequency of the $\Sigma\Delta$ BP modulator and the real carrier frequency of the modulated signal.

To obtain the IQ components of the input signal base band translated, the output of both the $\Sigma\Delta$ BP modulator and the Pipeline ADC is multiplied by the sequence 1,0,-1,0,1,..., for the components I, and by 0,1,0,-1,0,1,..., for the component Q. These two sequence are orthogonal and are obtained as follows:

- the sequence 1,0,-1,0,1,... is obtained from $cos(\pi n/2)$, n=0, 1,..., N and corresponds to the sampling at the frequency f_s of the unitary function cos(.), defined in the time domain at the frequency $f_s/4$ equal to the central band frequency of the modulator;
- the sequence 0,1,0,-1,0,1,...is obtained from $sin(\pi n/2)$, n=0, 1,..., N and corresponds to the sampling at the frequency f_s of the unitary function sin(.), defined in the time domain at the frequency $f_s/4$.

Because the output of the $\Sigma\Delta$ BP modulators taken into account is constituted by only one bit, as shown in Fig.7.5, the multiplication is simpler respect to that of the Pipeline ADC. Indeed, this last is characterized by multi-bit resolution output.

Moreover, the decimator FIR filter in the DDC [96] is used to remove the high frequency components, and to modify the digital output resolution.

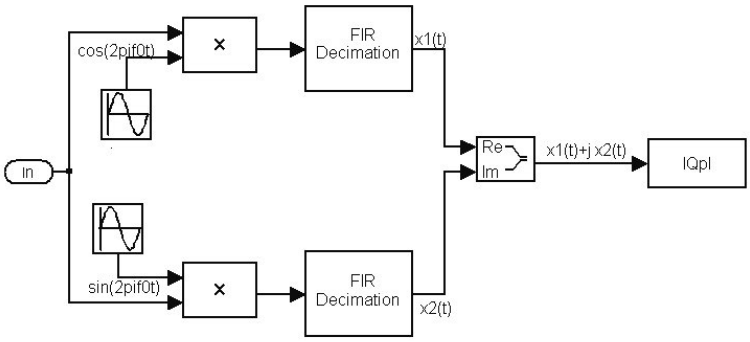

Fig. 7.4. Block scheme of the Digital Down Converter.

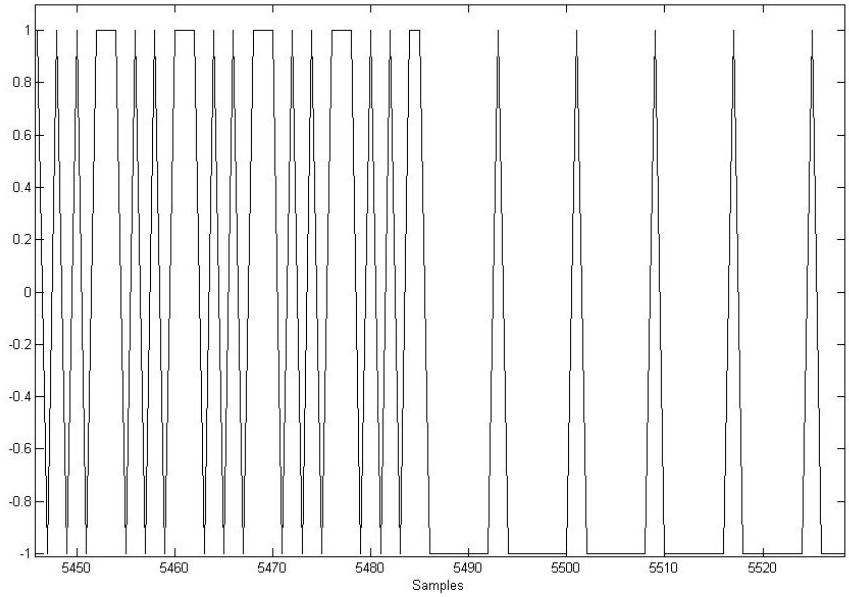

Fig. 7.5. Output signal of the $\Sigma\Delta$ BP SQL modulator corresponding to the input signal generated according to the modulation 4-PSK. The modulator central frequency is equal to 19.98MHz, the sampling frequency is equal to 79.92MHz, and the carrier frequency error is 40Hz.

7.2 Effects of the ADC Architecture on the frequency error measurement

The effects of the previous considered architectures of the ADC upon the carrier frequency error measurement are investigated by means of the simulations performed in the MATLAB and Simulink environment.

A particular interest is devoted to the ADC architectures because they determine more the over all behaviour of the proposed structure.

Therefore, the measurement error (e_m), defined by the difference between the assigned shift of the carrier frequency and the measured carrier frequency error, is evaluated and taken into account as performing index.

The investigation is performed by assuming basic common characteristics to design the ADC architectures, and by evaluating the trend of the measurement error (e_m) in different operating conditions.

7.2.1 Design characteristics of the ADC architectures

The block schemes of Fig.7.3 furnish the useful information for the simulation.

The design parameters characterising each block are established by imposing the agreement among the three architectures of the Signal to Noise Ratio (SNR), the ENOB, and the pass band of the frequency response.

The values of the SNR and the ENOB evaluated for each architecture of the Fig.7.3 are given in Tab.7.1.

In contrast to the Pipeline ADC, whose quantization noise is uniformly distributed in frequency, the $\Sigma\Delta$ BP modulator is characterised by the noise shaping. Therefore, the evaluation of both the SNR and ENOB is influenced by the width of the pass band following from the noise shaping effect.

The fundamental problem is that the pass band of the $\Sigma\Delta$ modulator cannot be defined a priori in a traditional way.

In general, the pass band is defined according to the employment of the $\Sigma\Delta$ modulator in the communication channel, and the band of the modulated signal to be processed. As a consequence, the values of the Tab.7.1 must to be considered as the trend values for each architecture taken into account.

Owing to the quite correspondence among the trend values of Tab.inseriscimi, the effects of the three ADC architectures can be compared.

In order to investigate about the passband of the frequency response, the Power Spectral Density (PSD) can be analysed conveniently. Fig.7.6 shows the PSD of

- the Pipeline ADC,
- the $\Sigma\Delta$ BP SQL modulator,
- the $\Sigma\Delta$ BP MASH modulator.

The comparison among the PSD portraits highlights that these architectures can operate in the same frequency range, characterised by band width $f_{wd} = 270kHz$ and central band frequency $f_w = 19.98MHz$.

Table 7.1. SNR and ENOB for the Pipeline ADC, $\Sigma\Delta$ BP SQL modulator, and $\Sigma\Delta$ BP MASH modulator.

Converter	SNR	ENOB
Pipeline ADC	86.80 dB	14.12 bit
$\Sigma\Delta$ BP SQL	90.10 dB	14,68 bit
$\Sigma\Delta$ BP MASH	95,10 dB	15,51 bit

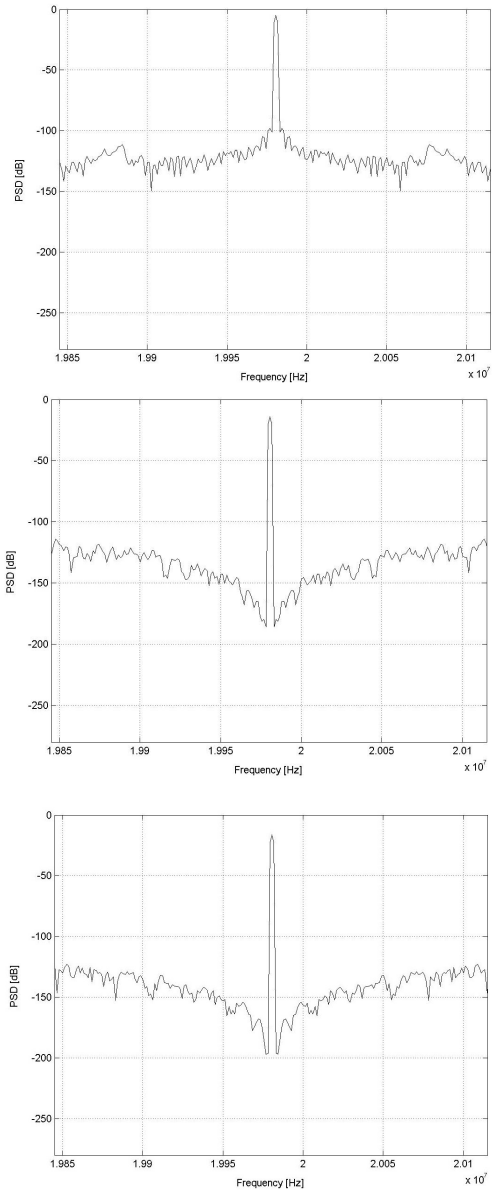

Fig. 7.6. Power Spectral Density of the pipeline ADC (upper), the $\Sigma\Delta$ BP SQL modulator (center), and the $\Sigma\Delta$ BP MASH modulator (lower).

7.2.2 Measurement error trend

In order to preliminary assess the correctness of the operation mode of the proposed structure numerous tests are performed. Fig.7.7 shows the evaluated phase trend in the third block of the Fig.7.2. The results refer to:

1. input modulated signal according to the 16-QAM,
2. $\Sigma\Delta$ BP SQL modulator,
3. modulator central band frequency $f_w = 19.98MHz$,
4. carrier frequency error $f_{sh} = 40Hz$.

The phase slope denotes that the carrier frequency differs from the central frequency of the $\Sigma\Delta$ modulator.

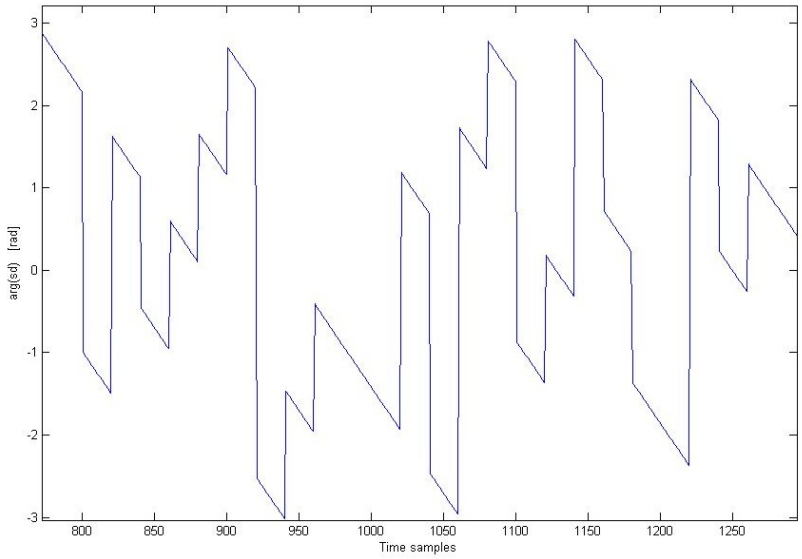

Fig. 7.7. Trend of the phase at the output of $\Sigma\Delta$ BP SQL modulator for 16-QAM input signal. The modulator central frequency is equal to 19.98MHz, and the carrier frequency error is equal to 40Hz.

The investigation about the trend of the measurement error e_m in different operating conditions is fundamental to highlight the metrological characteristics of the ADC architecture, and to detect the influencing parameters.

The tests are performed by examining 100 different test signals for each digital modulation, and by assuming the symbol frequency $f_{symb} = 4Msymbol/s$. In all the tests the measurement error e_m is evaluated versus the assigned shift of the carrier frequency.

In the following the results of the performed tests are discussed to highlight the performances of the three ADC architectures, to evaluate the effects of

the sample number on the carrier frequency error measurement, and to define the acceptable lower bound of the SNR.

Fig.7.8 shows the trend of the measurement error in the case of the Pipeline ADC and $\Sigma\Delta$ BP SQL based ADC, respectively. The input is the 4-PSK modulated signal, and 100ksamples are processed for each test signal. Fig.7.9 shows the trend of the measurement error in the case of the $\Sigma\Delta$ BP MASH based ADC. The input is always the 4-PSK modulated signal and the samples processed for each test signal are:

- 50ksamples,
- 100ksamples,
- 150ksamples.

The interesting performance of the $\Sigma\Delta$ BP MASH based ADC can be highlighted. Indeed, the measurement error is reduced if compared to other two architectures. Similar conclusions can be deduced by analyzing the tests performed by using the other modulated signals.

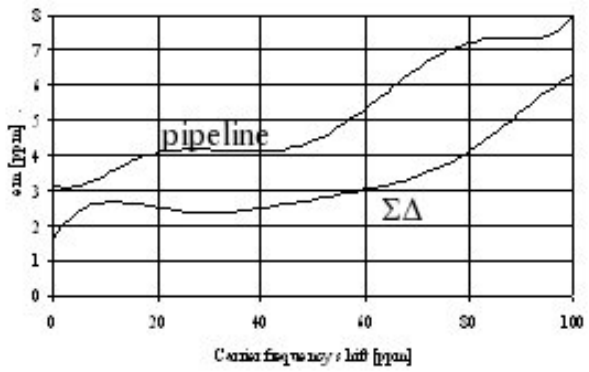

Fig. 7.8. Trend of the measurement error in the case of $\Sigma\Delta$ BP SQL modulator and Pipeline ADC for the 4-PSK modulation signal. 100ksamples are processed.

Moreover, Fig.7.9 shows that the measurement error trend weakly dependents on the number of the processed samples. Also for the $\Sigma\Delta$ BP SQL based ADC the measurement error trend weakly dependents on the number of the processed samples, as shown in Fig.7.10. Nevertheless, the measurement error is always greater than the error in the case of the $\Sigma\Delta$ BP MASH based ADC if the assigned shift of the carrier frequency is lower than 200ppm.

On the basis of the results of the previous considered tests, the architectures employing the $\Sigma\Delta$ BP modulators show interesting performance if compared to the Pipeline ADC architecture. Both the $\Sigma\Delta$ architectures are characterized by the property of the noise shaping in the pass band, as shown

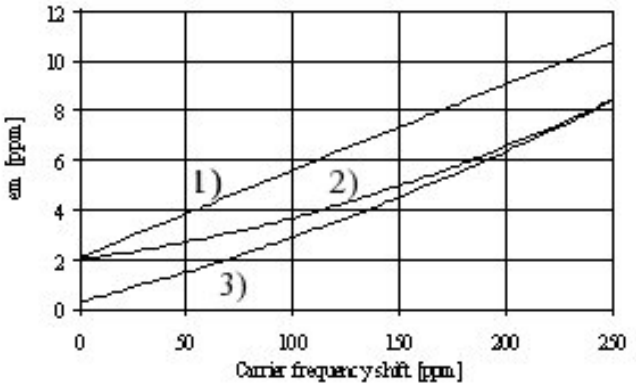

Fig. 7.9. Trend of the measurement error in the case of $\Sigma\Delta$ BPMASH modulator for the 4-PSK modulation signal by processing 1) 50ksamples, 2) 100ksamples, and 3) 150ksamples, respectively.

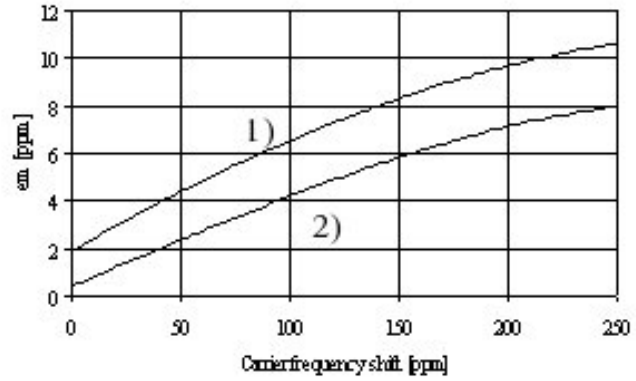

Fig. 7.10. Trend of the measurement error in the case of $\Sigma\Delta$ BP SQL modulator for the 4-PSK modulation signal by processing 1) 50ksamples, and 2) 150ksamples, respectively.

in the PSD portrait of Fig.7.3. This property is of great interest and advantages for application to the telecommunication signals.

Successive investigation is devoted to evaluate the effects of the noise on the measurement error e_m.

Fig.7.11 shows the trend of the measurement error in the case of $\Sigma\Delta$ BP SQL modulator. The inputs are the 16-QAM modulated signal, the 4-PSK modulated signal, and the 4-ASK modulated signal. Moreover, Gaussian noise is superimposed to the modulated signal and the value of the SNR is equal to:

1. 100 dB,
2. 50 dB,
3. 30 dB.

In particular, the measurement error increases as decreases the SNR. The lower bound of the SNR can be assumed equal to 30dB. Indeed, lower value of SNR increases the error to not acceptable values.

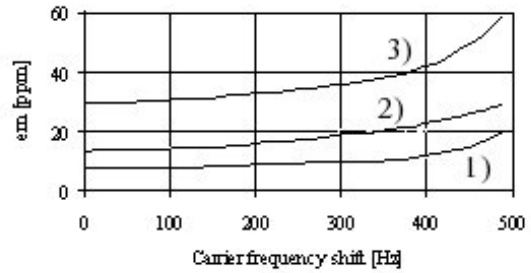

a)

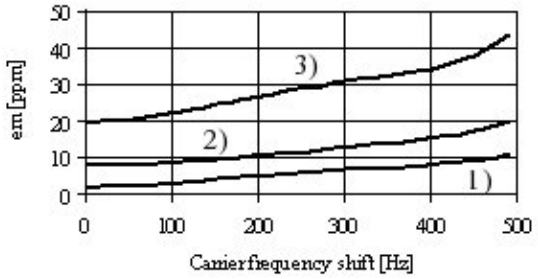

b)

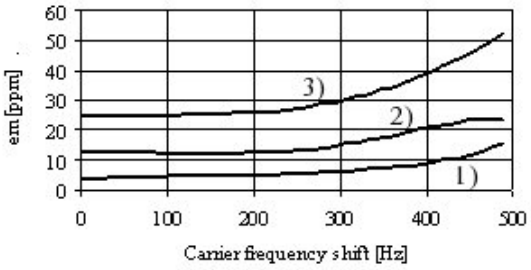

c)

Fig. 7.11. Trend of the measurement error in the case of $\Sigma\Delta$ BP SQL modulator. The input is a)16-QAM modulated signal, b) 4-PSK modulated signal, and c) 4-ASK modulated signal. Gaussian noise is superimposed with SNR equal to 1) 100 dB, 2) 50 dB, and 3) 30 dB.

Other tests are performed to investigate on the influence of the noise superimposed to the signal in the case of the BP MASH modulator. The inputs

are always the 16-QAM modulated signal, the 4-PSK modulated signal, and the 4-ASK modulated signal. As shown in Fig.7.12, the error is near the error of the $\Sigma\Delta$ BP SQL modulator in the following condition: Gaussian noise superimposed to the modulated signal and value of the SNR equal to 25 dB. Therefore, the lower bound of the SNR can be assumed equal to 25dB for the $\Sigma\Delta$ BP MASH modulator.

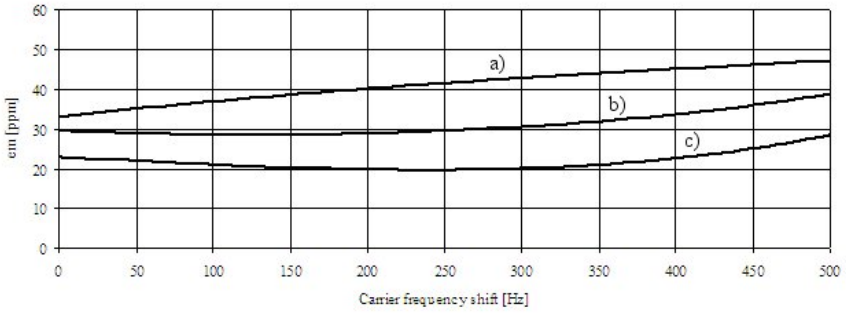

Fig. 7.12. Trend of the measurement error in the case of $\Sigma\Delta$ BP MASH modulator. The input is a) 16-QAM modulated signal, b) 4-PSK modulated signal, and c) 4-ASK modulated signal. Gaussian noise is superimposed with SNR equal to 25dB

These last tests confirm the interesting performance of the $\Sigma\Delta$ BP MASH modulator based ADC to the carrier frequency error measurement on digital modulated signals of the schemes M-ASK, M-PSK and M-QAM.

7.3 Conclusions

The functional block architecture implementing the method to measure the carrier frequency error of the single carrier digital modulations is presented. It is able to operate on the single carrier digital modulated signals M-ASK, M-QAM and M-PSK.

The functional block architecture, obtained from the Software Radio architecture, is based on the cascade of the Analog to Digital Converter (ADC), the Digital Down Converter and the base band processing. The performance of this cascaded architecture is analyzed by considering three different ADC architectures based on: the pipeline, the single quantizer loop $\Sigma\Delta$ modulator, and the Multistage Noise Shaper (MASH) $\Sigma\Delta$ modulator.

Numerical tests confirm the important role of the ADC in this architecture, and highlight that the $\Sigma\Delta$ Band Pass MASH modulator based ADC offers interesting performances. Consequently, it candidates to be implemented in hardware and to be used in advanced measurement instrument.

The results of research given to pointed out the functional block implementing the method for the carrier frequency error measurement are presented in [97].

Conclusion

Nowadays, the telecommunication systems show heterogeneous scenario. Different telecommunications standards are commonly used, each one with its particular modulation scheme. With the developing of these systems is growing up the necessity to characterize the digital modulated signals generated. A problem of the usually method for the digital modulated signal characterization is the necessity of a lot of a-priory information about the signal to be characterized.

To overcome this limit a new method is proposed in this thesis. In particular, this method is able to operate on the single carrier digital modulated signals M-ASK, M-QAM, M-FSK and M-PSK. The parameters that can be evaluated are:

- Carrier frequency measurement;
- Phase offset Measurement;
- Phase noise;
- Amplitude noise;
- Symbol time.

The carrier frequency is evaluated by means of the mean value of the instantaneous frequencies. The instantaneous frequency could be evaluated on the basis of the time interval between two consecutive zero crossing. This is an incorrect evaluation of the carrier frequency. In order to overcome this inconvenient, two different procedures are pointed out. The former is used in the case of the M-FSK modulation, the later in the case of M-ASK, M-PSK and M-QAM modulations, according to their different characteristic properties. For M-FSK modulation, in the histogram the M central frequencies are selected. For M-ASK, M-PSK and M-QAM modulations the initial trial frequency is detected, successively the corrective factor is evaluated. This is evaluated from the base-band signal.

Particular interest is devoted in developing the method to process the modulated signals of the UMTS standard.

Experimental tests performed on actual signal generated according to the UMTS standard, M-PSK and M-QAM according to V.92 and V.90 standards confirm the robustness and the accuracy of the measurement method. To perform these tests, the measurement station is implemented by using signal generator and acquisition board.

For the phase offset estimation the method creates a grid G on the basis of the theoretical constellation to be examined. The grid is rotated and the number of the points included into the grid are evaluated. The rotation angle, corresponding to the maximum number of the points in the grid proximity, is the phase offset.

For the amplitude and phase noise parameter estimation the method create a Virtual Symbol (VS) from the knowledge of the theoretical modulation scheme of the input signals.

The amplitude and the phase noise are estimated by means of the excursion of the module and of the phase of the VS respect to the theoretical point. The numerical tests support the theoretical developments. Moreover, these tests denote that the method is particularly attractive, robust, and accurate if compared with the method based on the frequency domain analysis. To use the method with digital standard modulated signal are necessary some preliminary step, but the tests confirm the possibility to use the same method for every standard taking into consideration.

The symbol time parameter is estimated using the demodulation of the input signal with a very short symbol timing. After this operation, the consecutive symbol repetition length is used to build the histogram. The maximum value of the occurrences permits to select the length of the symbol time respect to the measurement unit taken into account. Numerical and experimental tests are performed on modulated signals according to the telecommunication standard GSM 900 Burst and UMTS. The results permit to highlight the robustness of the method and the high accuracy. In all the tests the maximum error in determining the symbol timing was equal to one unit of the trial symbol timing used in the signal demodulation and showing the higher occurrence of the consecutive repetition.

In the method proposed and in other method present in literature for the parameters estimation on digital modulated signal is evident the importance of the demodulation process. When the input signal is affected by high level of noise and distortion it's possible that the demodulator don't recognize the real information transmitted. This error decreases the accuracy of the measure. To overcome this problem the use of the ANNs is analysed. In particular, the ANN based demodulator is implemented to efficiently process the input signals affected by high level of both noise and distortion that characterize the telecommunication networks. The demodulator proposed is based on the Multi Layer Perceptron (MLP) ANN. This demodulator is designed to be employed into the measurement instrument of signals of the third generation mobile telecommunication systems (UMTS).

The operating characteristics of the MLP ANN based demodulator are evaluated in the following conditions:

- input signal affected by clipping,
- carrier frequency error,
- carrier phase error,
- burst synchronisation error,
- transmission noise,
- input signal affected by multi-path interferences.

The numerical investigation has pointed out that the MLP ANN based demodulator is more robust than the traditional demodulator and it candidates to be used in the measurement instruments. Indeed, the MLP ANN demodulator can guaranty greater accuracy in the case the modulated signal is affected by high level of both noise and distortion.

It has been verified that the hardware architecture that best fit the characteristics of the method based on the unified approach for measurement on digital modulated signal is the Software Radio (SR) architecture. This permits to obtain an flexible an adaptable architecture that can efficiently implement the method pointed out for the characterization of digital modulated signals.

The functional block architecture is based on the cascade of the Analog to Digital Converter (ADC), the Digital Down Converter (DDC) and the base band processing. The performance of this cascaded architecture is analyzed by considering three different ADC architectures based on: the pipeline, the single quantizer loop $\Sigma\Delta$ modulator, and the Multistage Noise Shaper (MASH) $\Sigma\Delta$ modulator. Numerical tests confirm the important rule of the ADC in this architecture, and highlight that the $\Sigma\Delta$ Band Pass MASH modulator based ADC offers interesting performances. Consequently, it candidates to be implemented in hardware.

References

1. D. Grimaldi, S. Rapuano, G. Truglia, "An automatic digital modulation classifier for measurement on telecommunication networks", to be appear on IEEE Trans. on Instrum. and Measur.
2. J.G. Proakis, "Digital comunications", McGraw-Hil, 2nd edition 1989.
3. A. S. Tanenbaum, "Computer networks", Prentice-Hall, 4th edition 2003.
4. E. Conte, "Lezioni teoria dei segnali", Liguori.
5. K. Feher, Telecommunications measurements, analysis, and instrumentation, Noble Publishing Corp., 1997.
6. F. Rice, B. Cowley, B. Moran, M. Rice, "Cramr-Rao lower bounds for QAM phase and frequency estimation", IEEE Trans. Commun., vol. 49, Sept. 2001, pp. 1582-1591.
7. E. Serpedin, P. Ciblat, G.B. Giannakis, P. Loubaton, "Performance analysis of blind carrier phase estimators for general QAM constellation", IEEE Transaction on Signal Processing, vol.49, n.8, August 2001, pp.1816-1823.
8. H. Xu, Q. Huang, H. Zheng, "On the blind carrier phase estimation for large QAM constellation", Proc. of 17th Intern. Conf. on Adv. Inform. Netw. and Applic. (AINA'03), Xi'an (China), March 27-29, 2003, pp.551-556.
9. K.V. Cartwright, "Blind phase recovery in general QAM communication systems using alternative higher order statistics", IEEE Signal Processing Letters, vol. 6, n. 12, Dec 1999, pp.327-329.
10. G.N. Karystinos, D.A. Pados, "Supervised phase correction of blind space-time DS/CDMA channel estimates", Proc. of Conf. on Inform. Scien. and Syst., Princeton Univ., March 16-17, 2000.
11. W. Cowley, "Phase and frequency estimation for PSK packets: bounds and algorithms", IEEE Trans. Comm., vol. 44, Jan. 1996, pp. 1-3.
12. Carni' D.L., Grimaldi D., "Unified Approach to Parameter Measurements of Single Carrier Digital Modulations", Measurement, vol.39, N.5, 2006, pp. 440-446.
13. A.A. Abidi, Analog Circuit Design-RF Analog-to-Digital Converters; Sensor and Actuator Interfaces; Low-Noise Oscillators, PLLs and Synthesizers, Kluwer Acad. Publis., Boston, 1997.
14. L. D. Cosart, L. Peregrino, and A. Tambe, "Time domain analysis and its practical application to the measurement of phase noise and jitter", IEEE Trans. on Instr. and Measur., vol. 46, N.4, pp. 1016-1019, Aug. 1997.

15. S. Bregni, "Clock stability characterization and measurement in telecommunication", IEEE Trans. on Instrum. and Measur., vol. 46, N.6, pp.1284-1294, Dec. 1997.
16. L. Angrisani, A. Baccigalupi, M. D'Arco, "A new method for phase noise measurement" IEEE Instrum. and Measurement Technology Conference, Anchorage, AK, USA, 21-23 May 2002.
17. K. Korcz, B. Paczynska, L. Spiralski, "Digital measurement of noise parameters of communication receiver", 12th IMEKO TC4 International Symposium Electrical Measurements and Instrumentation, September 25-27, 2002, Zagreb, Croatia, pp.502-505.
18. I. Viscor, J. Halmek, "Phase noise measurement", Proc. of the Rad., 2001, Brno, Czech Rep., pp. 131-134.
19. P. Ciblat, P. Loubaton, E. Serpedin, G.B. Giannakis, "Asymptotic analysis of blind cyclic correlation-based symbol-rate estimators, IEEE Trans. on Information Theory, vol. 48, No.7, July 2002, pp.1922-1934.
20. L.P Sabel, W.G. Cowley, "Block processing feedforward symbol timing estimator for digital modems", Electronics Letters, vol. 30, No. 16, 4 August 1994, pp.1273-1274.
21. Y. Wang, P. Ciblat, E Serpedin, P Loubaton, "Performance analysis of a class of nondata-aided frequency offset and symbol timing estimators for flat-fading channels", IEEE Transactions on Signal Processing, vol. 50, No.9, September 2002, pp. 2295-2305.
22. J.L. Seung, "A new non-data-aided feedforward symbol timing estimator using two samples per symbol", IEEE Communications Letters, vol. 6, No.5, May 2002, pp.205-207.
23. Y. Wang, E Serpedin, P. Ciblat, "An alternative blind feedforward symbol timing estimator using two samples per symbol", IEEE Trans. on Com.s, vol. 51, No. 9, Sept. 2003, pp. 1451-1455.
24. Y. Yang, C. H.Liu, "An asymptotic optimal algorithm for modulation classification", IEEE Comm. Letters, vol. 2, No. 5, May 1998, pp.117-119.
25. A. Polydoros, K. Kim, "On the detection and classification of quadrature digital modulations in broad-band noise", IEEE Trans. on Communication, vol. 38, No. 8, August 1990, pp. 1199-1211.
26. S.Z. Hsue, S.S. Soliman, "Signal classification using statistical moments", IEEE Trans. on Communications, vol. 40, No. 5, May 1992, pp. 908-916.
27. S. Reichert, W. Schreygg, "Modulation classification of QAM schemes using the DFT of phase histogram combined with modulus information", Proceedings of IEEE MILCOM '97, vol. 3, Nov. 1997, pp. 1372-1376.
28. J.A. Sills, "Maximum-likelihood modulation classification for PSK/QAM", IEEE MILCOM '99 Proceedings, vol. 1, 1999, pp. 217-220.
29. A. Swami, B. M. Sadler, "Hierarchical digital modulation classification using cumulants", IEEE Trans. on Comm., vol. 48, No. 3, March 2000, pp. 416-429.
30. A. K. Nandi, E. E. Azzouz, "Algorithms for automatic modulation recognition of communication signals", IEEE Transa.s on Comm., vol. 46, No. 4, April 1998, pp.431-436.
31. K.R. Farrel, R.J. Mammone, "Modulation classification using a neural tree network", Proc. of Milit. Comm. Conf., MILCOM '93, vol. 3, 1993, pp.1028-1032.
32. K.C. Ho, W. Prokopiw, Y.T. Chan, "Modulation identification of digital signals by wavelet transform", Proc. of Milit. Comm. Conf., 1998, pp. 325-330.

33. Carni' D.L., Grimaldi D., "Amplitude and phase noise measurement in single carrier digital modulations", IEEE Transaction on Instrumentation and Measurement, under press.
34. D.L. Carni', D. Grimaldi, "Symbol timing measurement for single carrier digital modulations", IEEE IMTC/2004, Como (Italy), May 19-21, 2004.
35. T. Hentschel, G. Fettweis, "Software radio receivers", in CDMA Techniques for Third Generation Mobile Systems, vol. 487, Kluwer International Series in Engineering and Computer Science, ch. 10, pp. 257-283, 1999.
36. C. Heegard, J. A. Heller and A. J. Viterbi, "A Microprocessor-Based PSK Modem for Packet Transmission over Satellite Channels", IEEE Trans. Commun., vol. COM-26, pp. 552-564. May 1978.
37. H. Meyr, M. Moeneclay et S. A. Fechtel, "Digital Communication Receivers: Synchronization, Channel Estimation, and Signal Processing.", Wiley Series in Telecommunications and Signal Processing, 1998.
38. ETSI TR 101 290, "Digital Video Broadcasting; Measurement guideline for DVB systems", May 2001.
39. ETSI EN 300 421, "Digital Video Broadcasting; Framing structure, channel coding, and modulation for 11/12 GHz satellite services", August 1997.
40. ETSI TS 125.104, "(UMTS): UTRA (BS), FDD, Radio transmission and reception, v3.5.0", Dec. 2000.
41. B. E. Paden, "A matched nonlinearity for phase estimation of a PSK-modulated carrier", IEEE Trans. Inform. Theory, vol. IT-32, pp. 419-422, May 1986.
42. A. J. Viterbi and A. M. Viterbi, "Nonlinear estimation of PSK-modulated carrier phase with application to burst digital transmissions", IEEE Trans. Inform. Theory, vol. IT-29, pp. 543-551, July 1983.
43. F. Classen, H. Meyr, and P. Sehier, "Maximum likelihood open loop carrier synchronizer for digital radio", in Conf. Rec. ICC'93, Geneva, Switzerland, 1993, pp. 493-497.
44. G. D. Jonghe and M. Moeneclaey, "Optimal averaging filter length of the Viterbi and Viterbi carrier synchronizer for a given frequency offset", in Conf. Rec. GLOBECOM'94, San Francisco, CA, 1994, pp. 1363-1368.
45. U. Mengali and A. N. D'Andrea, "Synchronization Techniques for Digital Receivers", New York: Plenum, 1997.
46. S. Bellini, C. Molinari, and G. Tartara, "Digital frequency estimation in burst mode QPSK transmission", IEEE Trans. Commun., vol. 38, pp. 959-961, July 1990.
47. C. Bergogne, P. Sehier, M.Bousquet, "Reduced complexity frequency estimator applied to burst transmission", in Proc. 4th IEEE Int. Conf. Universal Personal Communications, 1995, pp. 231-235.
48. S. N. Crozier, "Low complexity frequency estimator with close-to-optimum performance", in Conf. Rec. PIRM'93, vol. 1, 1993, pp. 426-430.
49. J. P. Seymour and M. P. Fitz, "Nonlinear digital phase estimation for mobile communications", in Conf. Rec. PIMRC'92, Boston, MA, 1992, pp. 194-198.
50. M. P. Fitz, "Nonlinear digital carrier synchronization for Rician fading channels", in Conf. Rec. GLOBECOM'90, San Diego, CA, 1990, pp. 623-628.
51. F. Mazzenga and G. E. Corazza, "Blind least-squares estimation of carrier phase, Doppler shift, and Doppler rate for MPSK burst transmission", IEEE Commun. Lett., vol. 2, pp. 73-75, Mar. 1998.
52. M. K. Simon and D. Divsalar, "Doppler-Corrected Differential Detection of MPSK", IEEE Trans. Commun., vol. COM-37, pp. 99-109, Feb. 1989.

53. "PN9000 Automated Phase Noise Measurement System Application Note", Aeroflex.
54. Dr. Kamilo Feher "Telecommunications Measurements, Analysis and Instrumentation", Noble Publ. Corp., Atlanta, 1997.
55. K.W. Wan, J. Austin, E. Vilar, "A novel approach to the simultaneous measurement of phase and amplitude noise of oscillators", Proc. of IEEE forty-fourth Ann. Symp. on Freq. Control, Baltimore, MD ,USA, May 1990, pp.140-144.
56. J. Li, E. Ferre-Pikal, F.L. Walls, "Review of PM and AM noise Measurement systems", Microwave and Millimeter Wave Technology Proceedings ICMMT, Beijing China , Aug. 1998, pp.197-200.
57. L. D. Cosart, L. Peregrino, and A. Tambe, "Time domain analysis and its practical application to the measurement of phase noise and jitter", IEEE Trans. on Instrum. and Meas., vol. 46, N.4, Aug. 1997, pp. 1016-1019.
58. S. Bregni, "Clock stability characterization and measurement in telecommunication", IEEE Trans. on Instrum. and Meas., vol. 46, N.6, 1997, pp.1284-1294.
59. L. Angrisani, A. Baccigalupi, M. D'Arco, "A new method for phase noise measurement", Proc. of IEEE Instrumentation and Measurement Technology Conference, Anchorage, AK, USA, 21-23 May, 2002, pp.663-670.
60. K. Korcz, B. Paczynska, L. Spiralski, "Digital measurement of noise parameters of communication receiver", Proc. of 12th IMEKO TC4 International Symp. on Electrical Measur. and Instrum., Sept. 25-27, 2002, Zagreb, Croatia, 2002, pp.502-505.
61. Viscor, J. Halmek, "Phase noise measurement", Proc. of the Radioelektronika, Brno, Czech Rep., 2001, pp. 131-134.
62. D. L. Carni', D. Grimaldi, "Phase Noise Measurement in Single Carrier Digital Modulations", Proc. of 13th IMEKO TC4 International Symp. on Measur. for Research and Industry Applic., Athens, Greece, September 29- October 1, 2004, pp.51-56.
63. D. L. Carni', D. Grimaldi, "Carrier frequency and phase measurement for general single carrier digital modulations", Proc. of IEEE IMTC/2004, Como (Italy), May 19-21, 2004, pp. 413-418.
64. Carni' L., Grimaldi D., "ANN based demodulator for UMTS signal measurements", Measurement, Vol . 39, N. 10, pp. 877-883.
65. P. Ciblat, P. Loubaton, E. Serpedin, G.B. Giannakis, "Asymptotic analysis of blind cyclic correlation-based symbol-rate estimators, IEEE Transaction on Information Theory, vol. 48, No.7, July 2002, pp.1922-1934.
66. L.P Sabel, W.G. Cowley, "Block processing feedforward symbol timing estimator for digital modems", Electronics Letters, vol. 30, No. 16, 4 August 1994, pp.1273-1274.
67. Y. Wang, P. Ciblat, E Serpedin, P Loubaton, "Performance analysis of a class of nondata-aided frequency offset and symbol timing estimators for flat-fading channels", IEEE Transactions on Signal Processing, vol. 50, No.9, September 2002, pp. 2295-2305.
68. J.L. Seung, "A new non-data-aided feedforward symbol timing estimator using two samples per symbol", IEEE Communications Letters, vol. 6, No.5, May 2002, pp.205-207.
69. Y. Wang, E Serpedin, P. Ciblat, "An alternative blind feedforward symbol timing estimator using two samples per symbol", IEEE Transactions on Communications, vol. 51, No. 9, September 2003, pp. 1451-1455.

70. ETSI TS 125.104, (UMTS): UTRA (BS), FDD, Radio transmission and reception, v3.5.0, Dec. 2000.
71. Yu Hen Hu, Jenq-Neng Hwang, "Handbook of neural network signal processing", crc press .
72. P. Daponte., D. Grimaldi, L. Michaeli, "A neural network and DSP based decoder for DTMF signals", IEE Proceedings - Science, Measurement and Technology, vol.147, No.1, January 2000, pp.34-40.
73. A. aiello, D. Grimaldi, S.Rapuano "GMSK neural network based demodulator", Intelligent Data Acquisition and Advanced Computing Systems: Technology and Applications, International Workshop on, 2001. 1-4 July 2001, pp:2-6
74. D.E. Rumelhart, J.L.MacClelland, "Parallel Distributed Processing: Explorations in the Microstructure of Cognition", vol. I, MIT Press, Cambridge, MA, 1986.
75. ETSI TS 125.201, (UMTS), Physical layer-General Description, v3.1.0, June 2000.
76. Agilent Application Note n 1355, "Designing and Testing 3GPP W-CDMA Base Stations".
77. ETSI TS 125.211, (UMTS); Physical Channel and mapping of transport channels onto physical channels (FDD), v3.5.0, Dec. 2000.
78. ETSI TS 125.212, (UMTS): Multiplexing and channel coding (FDD), v3.5.0: Dec. 2000
79. ETSI TS 125.213, (UMTS): Spreading and modulation (FDD), v3.4.0, Dec. 2000.
80. ETSI TS 125.104, (UMTS): UTRA (BS), FDD, Radio transmission and reception, v3.5.0, Dec. 2000.
81. F. L. Luo and R. Unbehauen, Applied Neural Networks for Signal Processing. Cambridge, U.K.: Cambridge Univ. Press, 1997.
82. M. E. Xamani: "Hybrid, Phase Shift Keying (HPSK) Proposed for 3G System", Wireless Application, Jan. 2000.
83. F. Alam, Simulation of third generation CDMA system, Master of science in Electrical Engineering, 15 Dec. 1999.
84. R. Prasad, "An Overview of CDMA Evolution toward wideband CDMA", IEE Comun. Surveyes.Vol 1, N 1, 1998.
85. J. I. Smith, "A computer generated multipath fading simulator for mobile radio", IEEE Transaction on Vehicular Technology, vol. VT-24, August 1975, pp. 39-40.
86. Wipro Technologies, "Software-defined radio", White Paper, August 2002.
87. Maloberti, "High-speed high-resolution data converters for base stations: technologies, architectures and circuit design", Proc. of Workshop on ADC Modelling and Testing, Prague, Czech Republic, June 2002, pp.1-6.
88. D.L. Carni', D. Grimaldi, "Carrier frequency and phase offset measurement for general single carrier digital modulations", Proc. of IMTC/2004, Como (Italy), May 19-21, 2004.
89. Grimaldi, L. Serratore, "Effect of Pipeline ADC architecture and modulator on DDC", Proc. of IWADC, Perugia, It., Sep.8-10, 2003, pp.193-196.
90. W. Yang, "A 3-V 340-mW 14-b 75-MSample/s CMOS ADC with 85-dB SFDR at Nyquist input", IEEE J. S.-St. Circ., vol.36, pp.1931-1936, Dec.2001.
91. Q. Huang, C. Hammerschmied, T. Burger, "Meeting the challenge of high dynamic range, high speed A/D Conversion for Software-Defined Radio (SDR)", http://www.wireless-world-research.org

92. Chon-In Lao, Ho-Ieng Ieong, Kuai-Fok Au, Kuok-Hang Mok Seng-Pan U, R.P.Martins, "A 10.7-MHz Bandpass Sigma-Delta Modulator Using Double-Delay Single-opamp SC Resonator with Double-Sampling".
93. Don Orofino, "Fixed-point GSM digital down converter in Simulink", http://www.mathworks.com/matlabcontrol/ fileexchange
94. P. Yu, "A 14b 40MSample/s Pipelined ADC with DFCA", Proc. of ISSCC Dig. Tech. Papers, San Francisco, CA, Feb. 2001, pp. 136-137.
95. Kuo, C.J.; Liu, C.T.; Hou, C.J. "Sigma-delta modulator for bandpass signal"; Circuits and Systems, 1996. ISCAS '96., 'Connecting the World'., 1996 IEEE Inter. Symposium on Volume 1, 12-15 May 1996 Page(s):29 - 32 vol.1
96. B. Hogenauer, "An economical class of digital filters for decimation and interpolation", IEEE Trans. ASSP, April 1981, 155-162.
97. Carn D.L., Grimaldi D., " ADC based frequency error measurement in single carrier digital modulations", IEEE Transaction on Instrumentation and Measurement, vol.55, No.5, February 2006, pp.1523-1529.